National Library of Canada
Bibliothèque nationale du Canada

Canadian Theses Service
Service des thèses canadiennes

Ottawa, Canada
K1A 0N4

NOTICE

The quality of this microform is heavily dependent upon the quality of the original thesis submitted for microfilming. Every effort has been made to ensure the highest quality of reproduction possible.

If pages are missing, contact the university which granted the degree.

Some pages may have indistinct print especially if the original pages were typed with a poor typewriter ribbon or if the university sent us an inferior photocopy.

Reproduction in full or in part of this microform is governed by the Canadian Copyright Act, R.S.C. 1970, c. C-30, and subsequent amendments.

AVIS

La qualité de cette microforme dépend grandement de la qualité de la thèse soumise au microfilmage. Nous avons tout fait pour assurer une qualité supérieure de reproduction.

S'il manque des pages, veuillez communiquer avec l'université qui a conféré le grade.

La qualité d'impression de certaines pages peut laisser à désirer, surtout si les pages originales ont été dactylographiées à l'aide d'un ruban usé ou si l'université nous a fait parvenir une photocopie de qualité inférieure.

La reproduction, même partielle, de cette microforme est soumise à la Loi canadienne sur le droit d'auteur, SRC 1970, c. C-30, et ses amendements subséquents.

NL-339 (r. 88/04) c

Canada

National Library of Canada
Bibliothèque nationale du Canada

Canadian Theses Service
Service des thèses canadiennes

Ottawa, Canada
K1A 0N4

The author has granted an irrevocable non-exclusive licence allowing the National Library of Canada to reproduce, loan, distribute or sell copies of his/her thesis by any means and in any form or format, making this thesis available to interested persons.

L'auteur a accordé une licence irrévocable et non exclusive permettant à la Bibliothèque nationale du Canada de reproduire, prêter, distribuer ou vendre des copies de sa thèse de quelque manière et sous quelque forme que ce soit pour mettre des exemplaires de cette thèse à la disposition des personnes intéressées.

The author retains ownership of the copyright in his/her thesis. Neither the thesis nor substantial extracts from it may be printed or otherwise reproduced without his/her permission.

L'auteur conserve la propriété du droit d'auteur qui protège sa thèse. Ni la thèse ni des extraits substantiels de celle-ci ne doivent être imprimés ou autrement reproduits sans son autorisation.

ISBN 0-315-55318-9

Canada

THE UNIVERSITY OF ALBERTA

ISENTROPIC ANALYSIS OF SEVERE CONVECTIVE WEATHER

by

DENNIS E. DUDLEY

©

A THESIS

SUBMITTED TO THE FACULTY OF GRADUATE STUDIES AND RESEARCH

IN PARTIAL FULFILMENT OF THE REQUIREMENTS FOR THE DEGREE OF

MASTER OF SCIENCE

in

METEOROLOGY

DEPARTMENT OF GEOGRAPHY

EDMONTON, ALBERTA

Fall, 1989

THE UNIVERSITY OF ALBERTA

RELEASE FORM

NAME OF AUTHOR: Dennis E. Dudley

TITLE OF THESIS: Isentropic Analysis of Severe Convective Weather

DEGREE: Master of Science

YEAR THIS DEGREE GRANTED: 1989

Permission is hereby granted to THE UNIVERSITY OF ALBERTA LIBRARY to reproduce single copies of this thesis and to lend or sell such copies for private, scholarly or scientific research purposes only.

The author reserves other publication rights, and neither the thesis nor extensive extracts from it may be printed or otherwise reproduced without the author's written permission.

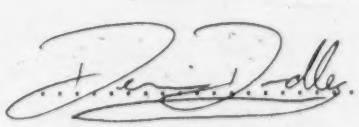

529 Hegler Crescent
Edmonton, Alberta
T6R 1C4

Date: 1 September, 1989

UNIVERSITY OF ALBERTA

FACULTY OF GRADUATE STUDIES AND RESEARCH

The undersigned certify that they have read, and recommend to the Faculty of Graduate Studies and Research, for acceptance, a thesis entitled ISENTROPIC ANALYSIS OF SEVERE CONVECTIVE WEATHER submitted by DENNIS E. DUDLEY in partial fulfilment of the requirements for the degree of MASTER OF SCIENCE in METEOROLOGY.

E. Reinelt

.....

Supervisor

.....

.....

Date 1 September 1989

Abstract

Convection within the atmosphere produces vital rain needed to sustain life on Earth. However, severe convection can cause wide spread destruction and death. Increasing public awareness of the latter has become evident in Alberta since the infamous "Edmonton Tornado" of 31 July, 1987, which killed 27 people and caused over 250 million dollars damage. Since then, Albertans have become more aware of severe storms and also, perhaps, of the weather forecasts that warn of such calamitous events. The demand for better severe weather forecasts is ever increasing and, to this end, isentropic analysis offers a unique tool to help supplement the current operational methods.

In this study, isentropic analysis is used to diagnose the threat of convective weather in Alberta six to eighteen hours before onset. The pre-convective environment is assessed using 1200 UTC isentropic data from which key atmospheric parameters, specific to the isentropic framework, are deduced. Particular attention is given to the diagnosis of severe convective potential. Differential temperature and moisture advection juxtaposed with strong upper-level winds were found synonymous with strong, well organized convective outbreaks.

To help evaluate the utility of these charts, several case studies along with statistical analysis were used. The study is restricted to the period June 1st to August 31st, 1988.

With the aim of using isentropic data to best advantage, a simple nomogram has been developed for estimating the type of severe weather that may be expected in a severe storm threat area. Heavy rain, large hail or tornadic potential is estimated by assessing the moisture, instability and relative humidity values in the area of severe weather threat.

Results based on these initiatives are encouraging, suggesting that isentropic methods can not only be useful for depicting the place and strength of convective weather, but also for estimating severe weather types up to 18 hours prior to occurrence. Isentropic analysis offers a different view of the atmosphere and provides deeper insight into the mechanisms that drive severe convection in Alberta.

It is hoped that these investigations will provide further impetus for the operational implementation of isentropic analysis techniques in Canadian weather offices.

Acknowledgements

I am greatly indebted to Professor Emeritus E.R. Reinelt, who agreed to supervise this program, despite his retirement in 1987. His dedication to synoptic meteorology, his thorough reviews of this rather lengthy dissertation, and his moral support are gratefully acknowledged.

I appreciate the time and helpful comments given by Dr. R.B. Charlton and Dr. G.E. Swaters who served on my examination committee. Many thanks goes to Dr. K.J. Fairbairn who saw that funding was made available for part of this research. Also, gratitude is due Laura Smith for typing the equations and greek symbols found in this manuscript.

I wish to acknowledge the Atmospheric Environment Service (AES) for allowing the free access to data. Also, the help of several Western Region employees of AES deserve particular mention. John Linton is acknowledged for providing the impetus for this research. Gary Schram, Yves Gendron, Ron Goodson, and Pat McCarthy are all acknowledged for their insightful comments. They all felt that this work was worthwhile and provided encouragement to complete this field of study.

Each chapter begins with a quotation from a key author whose published research has been valuable to this study. These quotations serve to recognize the contributions of earlier work and emphasize the main concepts being discussed.

Finally, I am indebted to my family whose love and support I could not have done without. The encouragement from my Mother and Father is especially acknowledged along with the constant support and help from my best friend, Susan.

Table of Contents

Chapter		Page
1.	INTRODUCTION	1
	1.1 Isentropic Analysis - Review and Preview	1
	1.2 Purpose of Present Study	6
2.	STABILITY ANALYSIS - REVIEW	9
	2.1 The Tephigram	9
	2.2 Potential Temperature	19
	2.2.1 The Adiabatic Assumption	23
	2.3 Cross Section Analysis	25
	2.3.1 Stability	26
	2.3.2 Moisture	29
	2.3.3 Thermal Wind	30
3.	THE OPERATIONAL ISENTROPIC CHARTS	33
	3.1 How they are Produced	33
	3.2 Station Plot	35
	3.3 Upper Left Panel - Height Field	41
	3.4 Upper Right Panel - Moisture Field	49
	3.5 Lower Left Panel - Static Stability Field	54
	3.6 Lower Right Panel - Relative Humidity Field	60
	3.7 Summary - The Isentropic Package	63
4.	THE ANALYSIS PROCEDURE	65
	4.1 Choosing the Isentropic Levels	65
	4.2 Checking the Data	68
	4.3 Parameter Analysis	69
	4.4 Verification	70
	4.4.1 Lightning Data	71

4.4.2 Severe Weather Reports 73
4.5 Summary 75
5. CASE STUDIES 77
5.1 Introduction 77
5.2 Case Studies 79
5.2.1 07 July, 1988 79
5.2.2 09 August, 1988 85
5.2.3 11 August, 1988 92
5.2.4 22 June, 1988 98
5.2.5 20 July, 1988 105
5.2.6 11 July, 1988 112
5.2.7 21 July, 1988 121
5.2.8 04 August, 1988 130
5.2.9 16 August, 1988 137
5.2.10 29 August, 1988 144
5.3 Discussion 153
6. STATISTICAL ANALYSIS 155
6.1 Introduction 155
6.2 Lightning 156
6.3 Severe Weather 159
6.3.1 Tornadoes 160
6.3.2 Large Hail 163
6.3.3 Heavy Rain 165
6.3.4 04 August, 1988 169
6.3.5 16 August, 1988 172
6.3.6 29 August, 1988 175
6.4 Summary 178

7. CONCLUSIONS AND FUTURE WORK 180

7.1 Conclusions 180

7.2 Future Work 184

7.3 Final Remarks 187

BIBLIOGRAPHY 188

APPENDIX A
Equations of Motion in Isentropic Coordinates 193

Set A - Isentropic Relations 194

Set B - Isobaric Relations 195

APPENDIX B
Isobaric and Surface Analysis Charts 199

APPENDIX C
Cross-Section Plots 209

APPENDIX D
Alberta Forecast Regions 214

List of Tables

Table		Page
4.1	Parameter Analysis Decode	69
4.2	Lightning Plot Color Code	72
6.1	Lightning Statistics	157

List of Figures

Figure		Page
2.1	Tephigram with labelled curves	11
2.2	Sounding with latent instability	14
2.3	Sounding with latent and potential instability	16
2.4	Vertical cross-section illustrating forces resisting vertical displacements	22
2.5	Isentropic cross-section for 1200 UTC, 23 August, 1988	27
3.1	Base chart for 1200 UTC, 17 April, 1989	36
3.2	Isentropic analysis station plot decode	37
3.3	Tephigram sounding for 1200 UTC, 17 April, 1989	40
3.4	Four-panel isentropic chart for 1200 UTC, 05 September, 1988	42
3.5	Upper level (308K) height panel for 0000 UTC, 01 August, 1987	43
3.6	Three dimensional chart of upper level (308K) surface for 0000 UTC, 01 August, 1987	44
3.7	12 hour development of lower level (298K) surface height field from 0000 UTC, 22 October, 1988 to 1200 UTC, 22 October, 1988.	47
3.8	Lower level (298K) moisture panel for 1200 UTC, 29 August, 1988	50
3.9	24 hour development of lower level (298K) moisture field from 0000 UTC, 22 October, 1988 to 0000 UTC, 23 October, 1988	51
3.10	Lower level (298K) static stability panel for 1200 UTC, 23 August, 1988	55
3.11	Isentropic cross-section for 1200 UTC, 23 August, 1988	57
3.12	Lower level (298K) relative humidity panel for 1200 UTC, 29 August, 1988	61

4.1 Isentropic cross-section for 1200 UTC, 04 August, 1988 67

4.2 Lightning plot for 27 June, 1988 74

5.1 Upper level (308K) isentropic chart for 1200 UTC, 07 July, 1988 81

5.2 Lower level (298K) isentropic chart for 1200 UTC, 07 July, 1988 82

5.3 Composite chart for 1200 UTC, 07 July, 1988 ... 83

5.4 Lightning plot for 07 July, 1988 84

5.5 Upper level (308K) isentropic chart for 1200 UTC, 09 August, 1988 88

5.6 Lower level (298K) isentropic chart for 1200 UTC, 09 August, 1988 89

5.7 Composite chart for 1200 UTC, 09 August, 1988 . 90

5.8 Lightning plot for 09 August, 1988 91

5.9 Upper level (308K) isentropic chart for 1200 UTC, 11 August, 1988 94

5.10 Lower level (298K) isentropic chart for 1200 UTC, 11 August, 1988 95

5.11 Composite chart for 1200 UTC, 11 August, 1988 . 96

5.12 Lightning plot for 11 August, 1988 97

5.13 Upper level (308K) isentropic chart for 1200 UTC, 22 June, 1988 101

5.14 Lower level (298K) isentropic chart for 1200 UTC, 22 June, 1988 102

5.15 Composite chart for 1200 UTC, 22 June, 1988 .. 103

5.16 Lightning plot for 22 June, 1988 104

5.17 Upper level (308K) isentropic chart for 1200 UTC, 20 July, 1988 108

5.18 Lower level (298K) isentropic chart for 1200 UTC, 20 July, 1988 109

5.19 Composite chart for 1200 UTC, 20 July, 1988 .. 110

5.20 Lightning plot for 20 July, 1988 111

5.21 Upper level (308K) isentropic chart for 1200 UTC, 11 July, 1988 116

5.22 Lower level (298K) isentropic chart for 1200 UTC, 11 July, 1988 117

5.23 Composite chart for 1200 UTC, 11 July, 1988 .. 118

5.24 Lightning plot for 11 July, 1988 119

5.25 Upper level (308K) isentropic chart for 1200 UTC, 12 July, 1988 120

5.26 Upper level (308K) isentropic chart for 1200 UTC, 21 July, 1988 124

5.27 Lower level (298K) isentropic chart for 1200 UTC, 21 July, 1988 125

5.28 Composite chart for 1200 UTC, 21 July, 1988 .. 126

5.29 Lightning plot for 21 July, 1988 127

5.30 Mid level (303K) isentropic chart for 0000 UTC, 22 July, 1988 128

5.31 Infrared satellite image from NOAA-10 at 02:58 UTC, 22 July, 1988 129

5.32 Upper level (308K) isentropic chart for 1200 UTC, 04 August, 1988 133

5.33 Lower level (298K) isentropic chart for 1200 UTC, 04 August, 1988 134

5.34 Composite chart for 1200 UTC, 04 August, 1988. 135

5.35 Lightning plot for 04 August, 1988 136

5.36 Upper level (308K) isentropic chart for 1200 UTC, 16 August, 1988 140

5.37 Lower level (298K) isentropic chart for 1200 UTC, 16 August, 1988 141

5.38 Composite chart for 1200 UTC, 16 August, 1988. 142

5.39 Lightning plot for 16 August, 1988 143

5.40 Upper level (308K) isentropic chart for 1200 UTC, 29 August, 1988 148

5.41 Mid level (298K) isentropic chart for 1200 UTC, 29 August, 1988 149

5.42 Lower level (293K) isentropic chart for 1200 UTC, 29 August, 1988 150

5.43 Composite chart for 1200 UTC, 29 August, 1988. 151

5.44 Lightning plot for 29 August, 1988 152

6.1 Severe weather nomogram for evaluating severe weather type 168

6.2 Severe weather nomogram for 1200 UTC, 04 August, 1988, Edmonton region 171

6.3 Severe weather nomogram for 1200 UTC, 16 August, 1988, Calgary region 174

6.4 Severe weather nomogram for 1200 UTC, 29 August, 1988, High Level region 177

B1 CMC 00 hour objective analysis for 1200 UTC, 07 July, 1988 200

B2 CMC 00 hour objective analysis for 1200 UTC, 09 August, 1988 201

B3 CMC 00 hour objective analysis for 1200 UTC, 11 August, 1988 202

B4 CMC 00 hour objective analysis for 1200 UTC, 22 June, 1988 203

B5 LFM 00 hour objective analysis for 1200 UTC, 20 July, 1988 204

B6 CMC 00 hour objective analysis for 1200 UTC, 11 July, 1988 205

B7 CMC 00 hour objective analysis for 1200 UTC, 21 July, 1988 206

B8 CMC 00 hour objective analysis for 1200 UTC, 04 August, 1988 207

B9 CMC 00 hour objective analysis for 1200 UTC, 16 August, 1988 208

C1 Isentropic cross-section for 1200 UTC, 22 June, 1988 210

C2 Isentropic cross-section for 1200 UTC, 11 July, 1988 211

C3 Isentropic cross-section for 1200 UTC, 21 July, 1988 212

C4 Isentropic cross-section for 1200 UTC, 04 August, 1988 213

D1 The Alberta forecast regions 214

"The study of isentropic flow patterns in the atmosphere represents a fruitful synthesis of thermodynamic and hydrodynamic methods in air mass analysis."

C.-G. Rossby (1937)

CHAPTER 1

INTRODUCTION

1.1 Isentropic Analysis - Review and Preview

Isentropic analysis, that is the depiction and analysis of meteorological variables on a surface of constant entropy, originated in the early 1900's. Sir Napier Shaw (1933) formally outlined its significance in his "Manual of Meteorology," where he included a chart showing the distribution of isotherms on an isentropic surface. He pointed out that isotherms, isobars and lines of constant density coincide on surfaces of constant potential-temperature, a variable closely related to entropy. However, due to the lack of upper air data and the fact that the conservation of specific humidity was not recognized as a significant air mass indicator, Shaw's emphasis on the isentropic motion of the free atmosphere did not receive the recognition it deserved.

Several years later, Rossby (1937) and Namias (1938) leading a group of meteorologists at the Massachusetts Institute of Technology (MIT), supported the operational implementation of isentropic analysis in the early 1940's. Rossby advocated worldwide adoption of isentropic coordinates, knowing that a potential-temperature surface represents the flow in the free atmosphere more accurately than either a constant pressure or constant height analysis.

> *"It can hardly be doubted that the isentropic charts represent the true motion of the air more faithfully by far than synoptic charts for any fixed level in the free atmosphere. At a fixed level in the middle of the troposphere entire air masses may, as a result of slight vertical displacements, appear or disappear in the time interval between two consecutive charts, making the entire method of representation futile."*
>
> *Rossby et al., (1937)*

But with the increase in aviation activity during war-time and the lack of high computing power, isentropic analysis fell out of favor and pressure was adopted as the standard vertical coordinate for analysis. Also, errors as high as 20% in the calculation of the streamfunction introduced by Montgomery (1937) were providing forecasters with inaccurate analyses. In 1959, however, Danielsen re-evaluated this

function, negated these errors, and produced a useful wind relationship in isentropic coordinates. This discovery led to a resurgence of interest in isentropic analysis.

Many researchers demonstrated the advantages of an isentropic coordinate system during the 1950's and 1960's. Oliver and Oliver (1951) found that, since the adiabatic component of vertical motion is implicit on the 2-dimensional charts, unsaturated moisture transport is more coherent in space and time on isentropic charts than on conventional constant pressure charts. This was found to be of tremendous advantage to the forecaster whose predictions depended critically on the diagnosis of the moisture profile within the atmosphere. In the late 1950's, there was renewed interest in atmospheric transport because of radioactive fallout from nuclear tests. This prompted Danielsen and others, on behalf of the Atomic Energy Commission, to investigate the mixing of stratospheric and tropospheric air. Using isentropic analysis, the controversial concept of "tropopause folding" was born out of this research, suggesting that stratospheric air could penetrate deeply into the troposphere in frontal zones. Danielsen (1961) compared air parcel trajectories deduced from an isobaric analysis to those derived from an isentropic analysis. He found that the trajectories obtained from the isentropic coordinate system matched the actual air parcel paths more closely. Duquet (1964)

developed data processing techniques for isentropic analysis. A few years later, isentropic trajectories were used to explain many of the characteristic cloud patterns shown on satellite pictures (Danielsen, 1966; Danielsen and Bleck, 1967). Danielsen prepared a four-dimensional diagnosis of a cyclonic storm using isentropic analysis. Green et al. (1966) looked at isentropic relative flow analysis and investigated the Parcel Theory, showing that the adiabatic assumption is reasonable in synoptic-scale processes when the parcel flow time through a system is significantly less than the lifetime of the system.

The 1970's saw several researchers experiment with numerical models formulated in isentropic coordinates (Eliassen and Raustein, 1968; Bleck, 1973; Bleck and Shapiro, 1976; Petersen and Uccellini, 1979). During this time, several important isentropic characteristics were revealed. It was reestablished that isentropes paralleled frontal zones, eliminating the discontinuities found on conventional analyses. It was also found that isentropes are tightly packed in stable areas and near jet streams, resulting in high vertical and horizontal resolution. Isentropic "folding" was produced by superadiabatic lapse rates, and strong diabatic effects within the boundary layer greatly disturbed the isentropic surfaces. Hoskins and Bretherton (1972) showed that frontogenesis may occur in adiabatic flow, revealing the value of isentropic analysis

for modeling the generation of fronts. Uccellini (1976) then described operational diagnostic applications of isentropic analysis and proposed that it be used more readily within the operational community. Uccellini suggested that only a lack of familiarity along with the inexperience in interpreting the "new" charts were the major reasons why they were not used.

In the early 1980's, detailed studies exploited the use of isentropic techniques in diagnosing the threat of severe weather using various analysis procedures. Wilson, Sick, and Marios (1980) used isentropic analysis to assess the atmosphere's convective potential. They examined two particular case studies, both in Southern Ontario, and showed how several isentropic parameters revealed a potential for severe weather. They then used these parameters to "hindcast" the occurrence of severe storms in the Toronto and Montreal areas. They did suggest, however, that more research is required to realize the full potential of these techniques. Moore (1981) used a slightly different isentropic analysis package for delineating areas of severe weather threat in Texas and Oklahoma. Moore found that certain isentropic parameters were extremely useful in providing an assessment of the atmosphere's available potential energy. An analysis of this kind led him to the short-term prediction of severe weather outbreaks in the southern States.

In recent years, the main thrust of research has been in isentropic relative flow analysis (Carlson, 1980, Browning, 1986, Pearson and Blackwell, 1987). Using both dry adiabatic and moist adiabatic potential temperature surfaces, the motion of air parcels within a cyclonic system can be traced using relative flow techniques. The existence of many familiar cloud patterns observed on satellite pictures can be accounted for by this method.

1.2 Purpose of Present Study

Even today, with its advantages well established, isentropic analysis is not well known within the operational forecasting community, particularly in Western Canada. The only investigation to date in the Alberta region was that of Wilson (1981) who disscused isentropic analysis at an Alberta Weather Centre (ALWC) seminar. In response, attemps were made to incorporate this diagnostic tool into the local severe weather forecasting techniques. However, mainly due to the unfamiliarity of the charts, they were only used to a "very limited extent" and an evaluation of their utility was not performed.

Impetus for this present study is rooted with John Linton, operational meteorologist in charge of development and training at the Arctic Weather Centre (ARWC). As a

summer student (1987-1988) under his direction, the author began to assess the utility of the isentropic analyses produced at the ARWC. Preliminary results found that the charts were helpful in diagnosing the atmosphere's convective potential. Since this study is, in a sense, a pilot project, the goals of this research are rather modest. They are: 1)to evaluate the utility of isentropic analysis, particularly in assessing convective potential in the Alberta region, 2)to determine whether isentropic data can help delineate areas of severe weather threat, and, if so, estimate the probability of forecasting the particular type of severe weather event i.e. heavy rainfall (>25mm/hr), destructive hailsize (>20mm), or tornadoes.

To this end, an isentropic analysis procedure was developed to "hindcast" the occurrence of convective storms in Alberta, Northeastern British Columbia, and the Southern Mackenzie Valley region. This procedure was tested daily during June, July, and August 1988 using lightning data, satellite pictures, and severe weather reports as verification. Simple statistical methods were also used to evaluate the utility of the isentropic charts. It is appreciated, of course, that a larger data sample with the inclusion of further verification techniques and more complex statistical analysis would be desirable. However, as a preliminary investigation, it was thought preferable to keep the analysis of data as simple as possible.

Though elementary, it is worthwhile to review stability analysis, since convective potential is largely a function of atmospheric stability, not considering at this stage what are sometimes referred to as convective "triggers". To this end, Chapter 2 reviews tephigram and cross-section analysis techniques. A description of the isentropic charts used in this text is given in Chapter 3, followed by a discussion of the analysis methodology presented in Chapter 4. The application of procedures for deducing convective potential, using isentropic techniques is given in Chapter 5 by way of several case studies, with particular emphasis on the diagnosis of severe convective weather. Chapter 6 provides a statistical analysis of the isentropic chart's utility, including a discussion on how isentropic data can be used to forecast the potential for tornado, large hail or heavy rain threat. Finally, conclusions and recommendations for future isentropic research is discussed in Chapter 7. The fundamental equations of motion in isentropic coordinates can be found in Appendix A. Appendix B contains conventional surface and isobaric charts corresponding to each case study in Chapter 5. Selected cross-sections also related to the case studies are given in Appendix C. A map displaying Alberta's forecast regions is given in Appendix D.

"The problem of shower and thunderstorm forecasting, therefore, revolves chiefly about the determination of the lapse rate and the source and availability of moisture."

J. Namias (1938)

CHAPTER 2

STABILITY ANALYSIS - REVIEW

2.1 The Tephigram

The tephigram (T-θ, temperature-entropy) is a thermodynamic chart in which area is proportional to energy or work. In this section, a brief review of the main uses of the tephigram relevant to this research will be given. With emphasis on stability analysis (static, latent, and potential), this section provides motivation for the procedures developed in later chapters.

"Aside from the surface weather chart, the tool most commonly used at present in forecasting thunder showers is the tephigram, or some similar diagram, which enables one to obtain an estimate of the energy available through overturning of the atmosphere."

J. Namias, (1938)

The tephigram is composed of five sets of curves useful for depicting the thermodynamic state of an air column. Figure 2.1 shows a tephigram with typical curves labelled, and a plot of a temperature profile plotted from radiosonde ascent data.

The static stability of an air column is dependent upon the slope of its temperature curve (i.e. "lapse-rate"). If the temperature within a layer decreases with height faster than the dry-adiabatic lapse rate, then that layer is "absolutely unstable" or superadiabatic. This condition is rarely observed through any great depth, since a superadiabatic layer would quickly overturn and mix with the surrounding atmosphere, because the buoyancy forces brought into play would lead to vertical acceleration and displacement of the air parcels.

> *"Overturning is Nature's attempt to bring about equilibrium in the atmosphere"* *Namias, (1938).*

However, absolute instability is readily set up within a shallow boundary layer where radiational heating raises the temperature of the air in contact with the earth's surface.

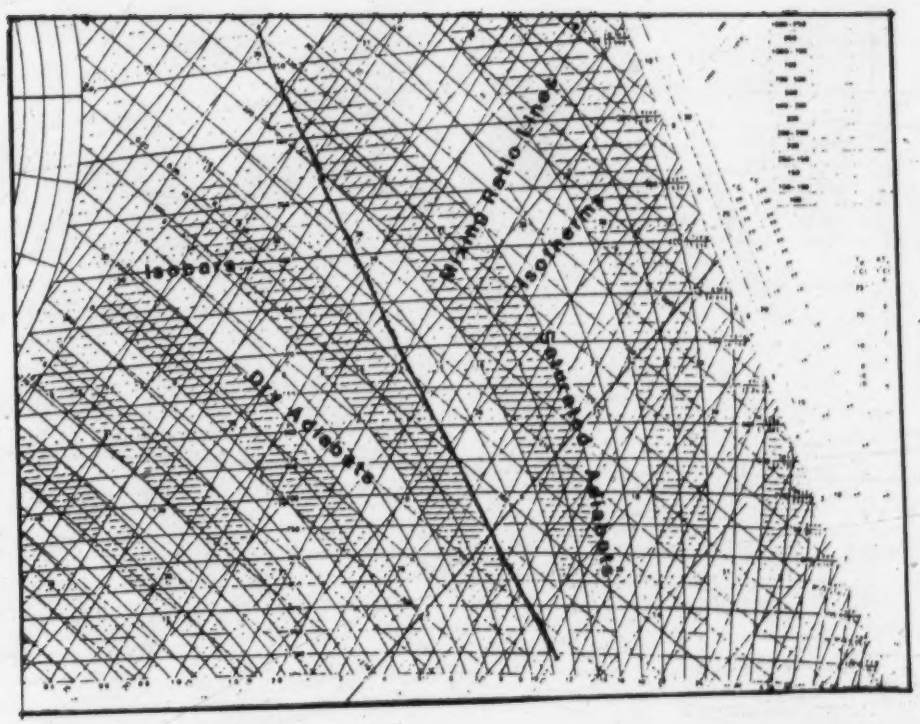

Figure 2.1: Tephigram with labelled curves and a (typical) temperature profile plotted from radiosonde ascent data.

If a layer has a temperature lapse-rate less than saturated adiabatic then the layer is said to be "absolutely stable" with respect to vertical displacements. On the other hand, a layer is "conditionally unstable" if its temperature lapse-rate is between the dry adiabatic and saturated adiabatic rate. If a parcel is saturated within this layer, it will be unstable with respect to its environment. An unsaturated parcel, however, is stable in this conditionally unstable layer. Finally, neutral stability prevails when the temperature lapse-rate of an unsaturated layer equals that of the dry adiabat. An unsaturated parcel within such a layer will neither assist nor hinder vertical perturbations. It should be noted that potential temperature does not change with height in neutrally stratified layers.

The concept of static stability will frequently be used also in a relative sense. For example, a certain region of the atmosphere may be referred to as being "more unstable" than another. This terminology only suggests that a particular area has a steeper lapse-rate than an adjacent one or that its "static stability" is less. This will become important in Chapter 3 which considers the analysis of actual static stability values. It will be shown that static stability varies considerably throughout the atmosphere. Regions having the lowest static stability values will be conveniently referred to as "unstable". This

static stability analysis, however, reveals little about the available buoyant energy of an air column, and thus little about the potential strength of the vertical accelerations. Other stability analysis classifications must be considered to further diagnose the thermodynamic properties of the atmosphere, such as the latent instability and the potential instability.

The extent and degree of latent instability, unlike static instability, depends upon the atmosphere's entire thermodynamic profile. Figure 2.2 shows a parcel ascent curve ("updraft" curve) to the right of the temperature curve of the environment. These two curves enclose an area (A+) proportional to the buoyant energy available to a representative parcel rising vertically through the undisturbed column of the surrounding air. This "positive area" is directly related to the maximum vertical velocity obtainable by a parcel rising through its environment. A large positive area will produce strong updrafts, supporting bigger and more vigorous storm complexes. By inspection, it is easily seen that temperature advection decreasing with height will alter the positive area, and thus change the column's convective potential. For example, warm air advection decreasing with height will increase the positive area at a rapid rate. Conversely, warm air advection increasing with height will stabilize the atmosphere, damping out any vertical accelerations.

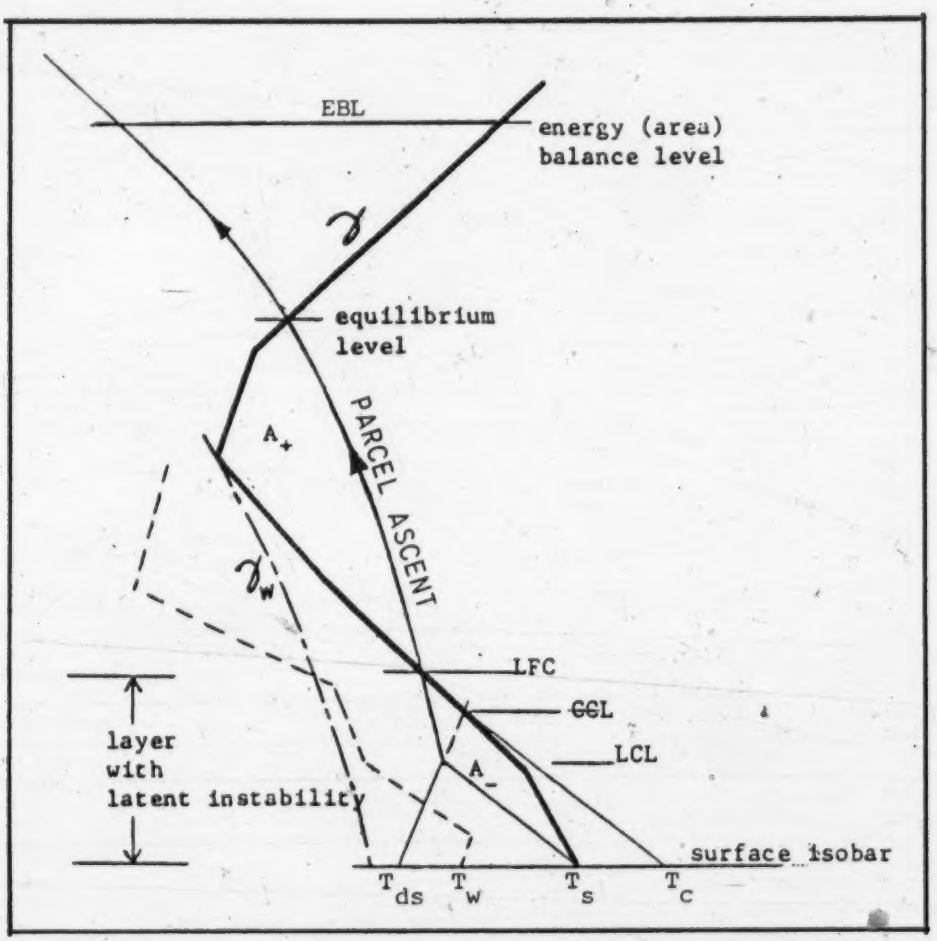

Figure 2.2: Sounding with a layer of latent instability. Dark solid curve denotes temperature profile, dashed curve indicates wet-bulb temperature curve, and dot-dashed curve denotes wet-adiabatic lapse-rate. A+ denotes positive area. (adapted from Environment Canada, Summer Severe Weather Correspondence Course, 1982)

"For a thunderstorm to become energetic and produce considerable amounts of precipitation it must have available an ample supply of moisture." Namias, (1938)

Latent instability also depends on the moisture stratification in the atmospheric column. Large amounts of moisture are needed in the boundary layer to support lower condensation levels and stronger updrafts (see Figure 2.2). It will be noted that the buoyant energy is reduced as the low-level moisture supply decreases. On the other hand, the absence of moisture above the boundary layer often enhances storm severity (Kamburova and Ludlam, 1966; Weisman and Klemp, 1986). This moisture deficit produces strong vertical gradients in the moisture profile, producing another type of instability called convective or potential instability.

An atmospheric layer is classified as potentially unstable if its wet-bulb potential temperature decreases with height. Figure 2.3 shows a sounding with a potentially unstable layer, as well as low-level layer with latent instability. If the layer with potential instability were given sufficient lift, its base would become saturated before the top. Further lifting would destabilize the

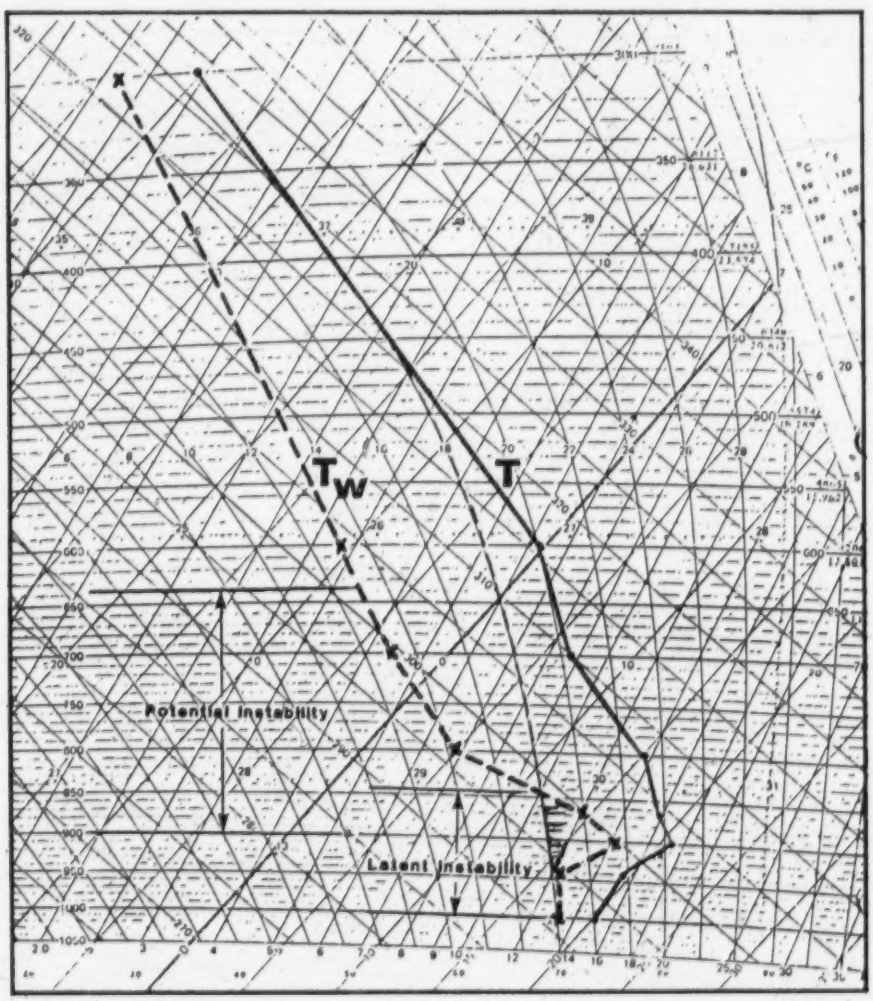

Figure 2.3: Sounding with a mid-level layer of potential instability along with a low-level layer of latent instability.

layer, since it would cool faster at the top than at the bottom. Potential instability is again increased when warm, moist air is underlying cold, dry air.

To summarize, both latent and potential instabilities play an integral part in the convective potential of the atmosphere. They have an intimate relationship with one another, since latent instability is generated as potential instability is realized. Also, if there is no potential instability throughout the air column, there can be no latent instability. In short, to produce strong convective potential (i.e strong updrafts and downdrafts within convective cells), the atmosphere has to be stratified with a deep layer of latent instability in the low levels and a mid-level layer of pronounced potential instability. This can be achieved with warm, moist air near the surface and cooler, drier air aloft.

A radiosonde can measure air mass characteristics only in the immediate vicinity of the ascent and at a specific time. It is well known that mesoscale environments are not resolvable with the current upper-air network. However, using various interpolation techniques, radiosonde data can produce reasonably detailed atmospheric analyses on the synoptic scale. A single tephigram plot, however, reveals only a "snap-shot" of the state of an air column.

"There are advectional and thermodynamic changes taking place in the overlying atmosphere after the soundings are made, which appreciably alter their characteristics." *Namias, (1938).*

To this end, it is common practice for a forecaster to simply replace the current sounding with a sounding representative of the upstream flow. In this way the convective potential of a column of air may be estimated by using the speed of the mean flow and prognostic surface charts. When convective potential is very high, however, associated low-level winds normally veer strongly with height and thus modify parcel trajectories. In these conditions, it is poor practice to simply "exchange" a sounding with one upstream. Instead, a three-layer isentropic model should be used to assess the "tephigram's" changes.

"The greatest advantage of the isentropic chart for thunderstorm forecasting lies in its peculiar adaptation to fore-telling the changes likely to occur in individual soundings. Thus, though the tephigram may offer definite indications, one should use the isentropic chart to take any likely changes into account." *Namias, (1938)*

In a practical, operational setting, it being desirable to know the potential energy in the lower half of the troposphere, it is most useful to choose one isentropic surface within the boundary layer, say near 900mb, a second, higher surface near 800mb, and a third surface at about 600mb. Such a three-level analysis leads to a better depiction of the organizing storm environment. It has been well documented (Danielsen, 1966; Green, 1966; Danielsen and Bleck, 1967; Carlson, 1980; Browning, 1986; Pearson and Blackwell, 1987), that synoptic-scale cyclones are composed of many different air-streams, with associated vertical wind shears and thermal instabilities. Apart from terrain effects and "trigger" mechanisms, a mesoscale storm environment, able to support strong convection, shows similar characteristics. Severe storm forecasting provides the motivation for using an isentropic coordinate system as a diagnostic aid in assessing convective potential.

2.2 Potential Temperature

Before cross-section analysis is discussed, it is useful to review its vertical ordinate, the potential temperature.

Since potential temperature is an atmospheric variable that cannot be measured directly like pressure and temperature, for example, it is not immediatly useful to the

operational meteorologist. Defined as the temperature a parcel of dry air would have if brought adiabatically from its initial state to 1000mb, it has by itself little meaning to a forecaster who has deadlines to meet. It is only when potential temperature is used in stability analysis that it comes into its own, as a fundamental thermodynamic variable.

Mathematically, potential temperature is defined as

$$\theta = T\left(\frac{p_o}{p}\right)^{R/c_p} \quad , \qquad (2.1)$$

where;

θ = potential temperature

T = temperature in degrees Kelvin

p = pressure in millibars

R = gas constant for dry air

c_p = specific heat of dry air at constant pressure

It is easily seen from Equation 2.1 that when potential temperature is held constant, as on a potential-temperature surface, the temperature of a parcel is a function only of its pressure. This fact is very useful, since the height of a potential temperature surface can reveal much about the temperature distribution of the atmosphere.

"The elevation of a potential-temperature surface is an indication of the mean temperature of the air column below the surface, a high elevation implying low mean temperature, and a low elevation implying high mean temperature." *Beers, (1938)*

The following equation relates potential temperature to entropy;

$$S = c_p \log\theta + \text{constant} \quad , \qquad (2.2)$$

where S is the entropy and c_p is defined as above (Namias, 1940). A surface of constant potential temperature, then, is also a surface of constant entropy called an *isentropic surface*. However, because natural processes are not reversible, a constant potential-temperature surface is not exactly equivalent to an isentropic surface, since constant entropy implies reversibility.

Since the atmosphere is normally stable with respect to unsaturated displacements, that is the temperature lapse-rate is less than neutral, potential temperature normally increases with height. It is convenient, then, to consider the atmosphere consisting of an infinite number of isentropic sheets of constant theta. In the free atmosphere, unsaturated air parcels are confined to move adiabatically along these sheets as long as unsaturated conditions prevail. Figure 2.4 helps to illustrate this

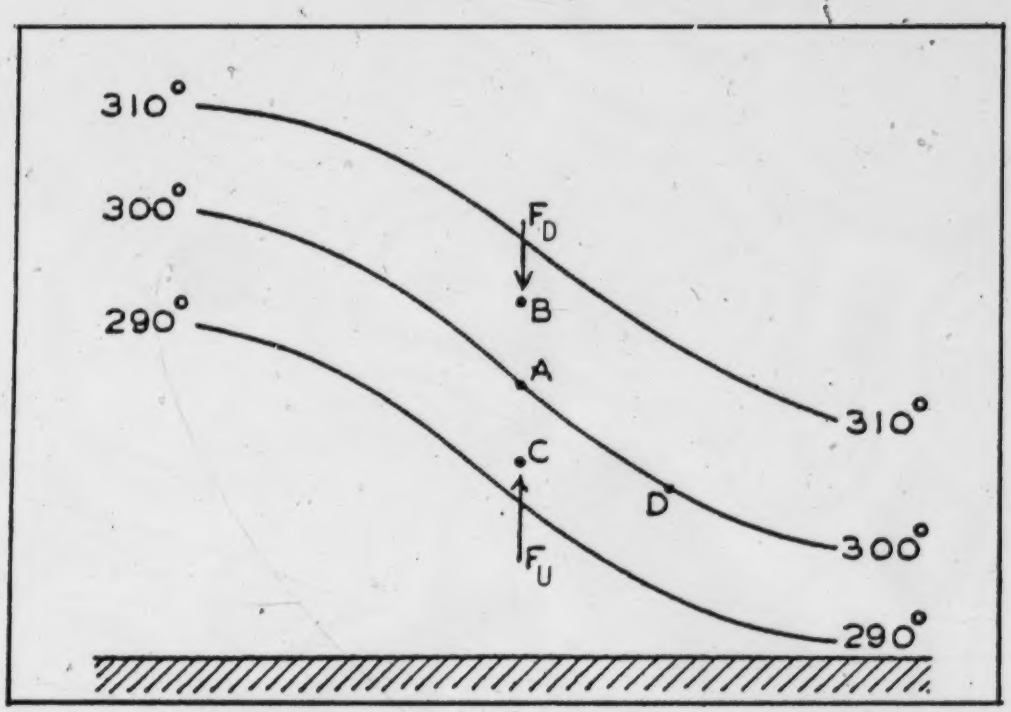

Figure 2.4: Vertical cross-section of potential temperature illustrating the forces resisting displacements from isentropic sheets. (adapted from Namias, 1940)

"confinement" by showing a vertical cross-section of a typical atmospheric layer. If a parcel at A were displaced to B, it would find itself colder than its environment and hence be subjected to a downward restoring force, Fd. If, on the other hand, the parcel were displaced from A to C, an upward force Fu would act to resist this displacement. It is important to note that the strength of these restoring forces is proportional to the vertical gradient of potential temperature. It is in this way that potential temperature is extremely useful in assessing atmospheric stability. If the parcel at A were displaced along the isentropic surface to D, however, no restoring force would be exerted, since the parcel would always have the same temperature as its environment. This restricted movement exhibits the conservative property of potential temperature, one of the key advantages of an isentropic coordinate system. That is, neglecting diabatic effects, an air parcel in the free atmosphere will retain its potential temperature throughout its course, unless it becomes saturated. In that case, the latent heat of condensation is realized and the parcel will follow the saturated adiabat.

2.2.1 The Adiabatic Assumption

"The assumption of adiabatic motion implies that each element of air remains in its proper isentropic layer.

C.-G. Rossby, (1937)

There has been much discussion about the validity of the adiabatic assumption during the past several decades. Many authors have made the assumption that flow in the free atmosphere tends to follow along surfaces of constant potential temperature over short time scales (Rossby, 1937; Namias, 1938; Oliver and Oliver, 1951; Danielsen, 1961; Green, 1966; Carlson and Ludlam, 1966; Carlson, 1980; Iskenderian, 1987).

> *"Adiabatic changes of state of particles in the free atmosphere can justifiable be assumed, because non-adiabatic temperature changes are so slow and uniformly distributed that they do not appreciably affect a relatively rapid phenomenon such as cyclogenesis." Oliver and Oliver, (1951)*

Of course, diabatic effects such as radiation, condensation and evaporation are important when tracing parcel trajectories through a mesoscale environment or over large time intervals. But because the procedures used in this investigation only depend on the diagnosis of actual atmospheric data and the short term (<12hrs) estimated motion of selected analysis fields, the adiabatic assumption will be considered to be valid here as well.

Potential temperature is a convenient variable for describing the stability of the atmosphere. By way of example, the following section presents a cross-section which displays the vertical distribution of potential temperature.

2.3 Cross-Section Analysis

> *"...to serve as a helpful link between the isentropic chart and the surface map, vertical cross-sections showing the arrangment of the various isentropic surfaces from the ground up to 5 or more kilometers are useful."* *C.H Pierce, (1938)*

In addition to providing a different "view" of the atmosphere, a vertical cross-section clearly reveals many important thermodynamic properties not easily seen on any other atmospheric diagram. It is the purpose of this section to illustrate these properties and familiarize the reader with basic cross-section analysis techniques. In this investigation, cross-sections are not explicitly used to forecast convective potential, but rather considered only as aids to help conceptualize the isentropic framework developed in the course of this research.

Often the meteorologist would like a more detailed picture of the upper air than that given by a four-level isobaric analysis or even by a three-layer isentropic model. To this end, vertical cross-sections help to link the standard isobaric and isentropic levels, by showing the arrangement of potential-temperature surfaces (isentropes) from the ground level up to beyond the tropopause. Figure 2.5 shows a cross-section produced at the Arctic Weather Centre (ARWC).

2.3.1 Stability

One of the main uses of a vertical cross-section is in stability analysis. As mentioned above, the spacing between isentropes reveals the local stability within an air column. In regions where the isentropes are packed together there is strong resistance to vertical displacement. Such packing reveals small temperature lapse-rates usually found near inversions, in frontal zones and at the tropopause (see Figure 2.5).

Ultimately, it is the temperature profile that determines the vertical spacing of the isentropes. As mentioned earlier, the height of a particular potential-temperature surface is also a measure of the temperature of the environmental air near that surface, i.e. the ambient atmospheric temperature. As the height of a

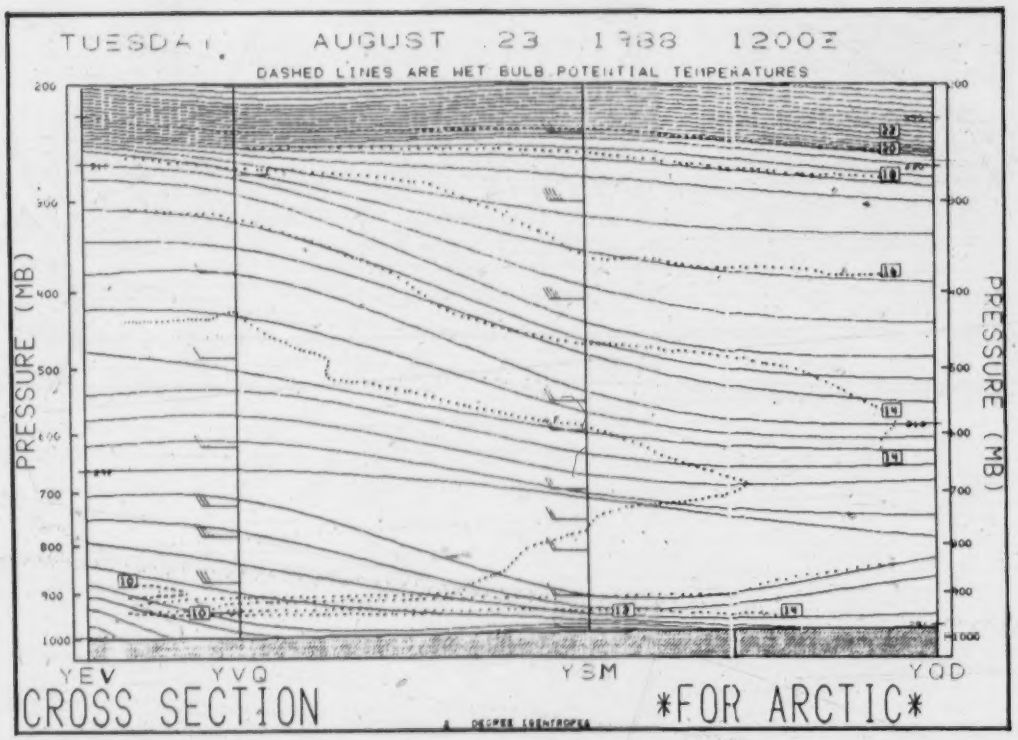

Figure 2.5: Isentropic cross-section for 1200UTC, 23 August, 1988. In the examples presented, solid lines are drawn through equal potential temperatures at intervals of two degrees Kelvin. The dash lines are isopleths of wet-bulb potential temperature spaced at two-degree Kelvin intervals, and the wind barbs indicate the component of the wind tangential to the plane of the cross-section. One full barb denotes 10 Km/hr.

particular isentrope increases, its ambient temperature decreases. Conversely, as an isentrope "sags" or decreases in height, the environmental air temperature correspondingly increases. The shape of an isentropic surface as seen on a cross-section then is due solely to the distribution of cold or warm air, pooling at different places in the troposphere. For example, a relatively cool air "pocket" will show up on a cross-section as a bowing up of the isentropes in that area. This bowing process stretches the isentropes, indicating a destabilization of the local environment. Clearly, any incursions of air creating a horizontal temperature gradient will tend to destabilize the environment. Unfortunately, such temperature "anomalies" are not normally resolvable using the conventional isobaric analysis. One needs the vertical resolution of an isentropic cross-section in order to reveal these vertical temperature variations, and thus the local stability variations in an air column.

Since this investigation deals with the assessment of convective potential, it is important to determine the magnitude as well as the changes of instability within the air column. As noted above, convective potential can be assessed by means of a tephigram, and the concepts of latent and potential instabilities. A cross-section, however, can also provide an estimate of these instabilities by superimposing the vertical moisture profile onto the plane.

Since it displays the tangential wind speeds as well, it can also provide an estimate of the advection of potential-temperature and the moisture field, possibly revealing an increase or decrease in convective potential in a particular region.

2.3.2 Moisture

The moisture profile is provided by the isopleths of wet-bulb potential temperature. Potential instability is revealed through the vertical distribution of this atmospheric variable. Profiles which show decreasing wet-bulb potential temperature with height indicate air columns having potential instability and a higher convective potential. Combining a decreasing wet-bulb lapse-rate with a weak vertical isentrope gradient will produce regions of strong convective potential. Isopleths of wet-bulb potential temperature are a function of both temperature and moisture. A differential increase in either temperature, moisture or both with height will destabilize the environment at a rapid rate. This process can be demonstrated also on a tephigram, but a cross-section has the ability to indicate environmental changes more readily.

2.3.3 Thermal Wind

> *"The isobars at any point on the isentropic surface are approximately parallel to the vertical shear of the geostrophic wind (i.e., the thermal wind) at that point."* *Beers, (1945)*

While the spacing of potential-temperature lines reveals much of the thermal stratification, the actual slope of an isentrope is also very important, since it is directly related to the thermal wind.

It is well known that the thermal wind relationship links the geostrophic vertical wind shear to the horizontal temperature gradient. Since it is easy to determine the horizontal temperature gradient from the isentropes drawn on a vertical plane, it is also easy to deduce the strength of the thermal wind at any point on a cross-section. For example, Figure 2.5 shows a pool of warm air within the 900mb - 750mb layer over Fort Smith (YSM) appearing as a bowl-like depression of the isentropes. This depression produces a steepening of the isentropic surface on both sides of the temperature "anomaly". It is in these sloped regions that the highest thermal winds are located. As the horizontal temperature gradient increases between the adjacent air regimes, the slope and packing of the isentropes separating them will increase, denoting an

increase in the vertical wind shear. To summarize, zones containing a dense packing of sloping isentropes indicate strong vertical wind shears and possibly the location of jet streams.

The significance of vertical wind shear in producing severe storm environments has been realized for many years (Carlson and Ludlam, 1966; Miller, 1972; Weisman and Klemp, 1986; Rotunno, 1986).

> *"In the presence of a favorable wind shear the cumulonimbus convection becomes more organized."*
>
> *Carlson and Ludlam, (1966)*

Recently (Weisman and Klemp, 1986), it has been found that while the thermodynamic structure strongly effects the vertical accelerations within a convective storm, it is the vertical wind shear that dictates the storm severity. Tornadogenesis, in particular, is dependent on strong environmental wind shear (Rotunno, 1986). Since wind shear is proportional to the slope of an isentropic surface, an isentropic cross-section can alert a forecaster to the particular threat of tornadic activity. It should be noted that the diagnosis of clear air turbulence (CAT) associated with the strong vertical wind shears near jet streams and fronts is also made easier by means of these cross-sections.

To summarize, an isentropic cross section can be a useful supplement to help diagnose the atmosphere's convective potential. By revealing the local and potential instabilities and areas of strong vertical wind shear, an operational meteorologist can better assess the areas of severe storm threat.

A three-layered isentropic analysis with its surfaces below 600 mb can display all of these conditions as well. Of course, the vertical resolution above 600mb is compromised, but, as was noted, convective potential is mainly dependent on conditions below this level. The isentropic analysis has the advantage of being able to display the thermal and moisture distibutions horizontally, and estimate their propagation in a three-dimensional sense.

It is important to conveniently display isentropic data in a manner which maximizes the operational utility of such an analysis scheme. To this end, Chapter 3 describes the isentropic charts produced at the Arctic Weather Centre.

"Isentropic analysis goes further than merely supplementing the surface analysis of air masses and fronts; it brings to light much entirely new knowledge of the physical processes at work in the atmosphere."

Namias (1938)

CHAPTER 3

THE OPERATIONAL ISENTROPIC CHARTS

3.1 How they are Produced

These investigations are based on the isentropic products routinely produced at the Arctic Weather Centre (ARWC). These charts are produced in three stages. First, the RAOB data for up to four chosen isentropic levels are extracted. Using a program by Lord (1980), later modified by Linton (1986), the sounding data are processed with the following observed and derived parameters calculated and interpolated to each isentropic level, as required:

1) Temperature (degrees Celsius x 10)
2) Height of isentropic level (meters)

3) Montgomery stream function values referenced to zero by (value - 2731.6) in units of 10^6 $(cm/sec)^2$ or ergs/gram

4) Dew-point temperature (degrees Celsius x 10)

5) Relative humidity (percent)

6) Stability (mb), thickness of a five-degree isentropic layer above the isentrope at its base. This is a measure of the average static stability within the isentropic layer.

7) Specific humidity (grams/Kilogram x 10)

8) Pressure (mb)

9) Saturation value (mb), pressure difference to lifted condensation level.

The winds, obtained from the sounding data, are interpolated linearly with height.

The second stage of the procedure uses a standard objective analysis (Cressman) to analyze the above parameters. It should be noted that only the streamfunction objective analysis uses a 12-hour history as a first-guess field. The objective analyses of all the other fields are independent of their previous history. Finally, the analyzed data are then processed by the plotting and contouring programs. Using bi-quadratic interpolation and extrapolation techniques, the plots are contoured at the ARWC. This three-stage analysis and plotting of 1200 UTC

data is normally completed by 9:00AM local time. The following sections describe these operational isentropic products.

3.2 Station Plot

Just as it is standard practice to display surface data (temperature, dew point, etc.) using a station plot on a surface chart, it is convenient also to display isentropic data using an isentropic station plot. For this purpose, a chart containing only grid data and the streamfunction field is produced first. Figure 3.1 shows an example of such a chart which will be referred to as a "base" chart. As previously mentioned, the streamfunction lines (solid) are analogous to the surfaces isobars in that they represent the geostrophic wind field on an isentropic surface. The station data are decoded and plotted with the format given in Figure 3.2. Each isentropic level has its own base chart.

There are two main purposes of plotting this base chart.

1) When the temperature of a sounding is everywhere higher than the isentrope value, there will be no station data to process since the temperature curve and isentrope never intersect in these cases The operational meteorologist should be aware of these "no data" stations, since, in such

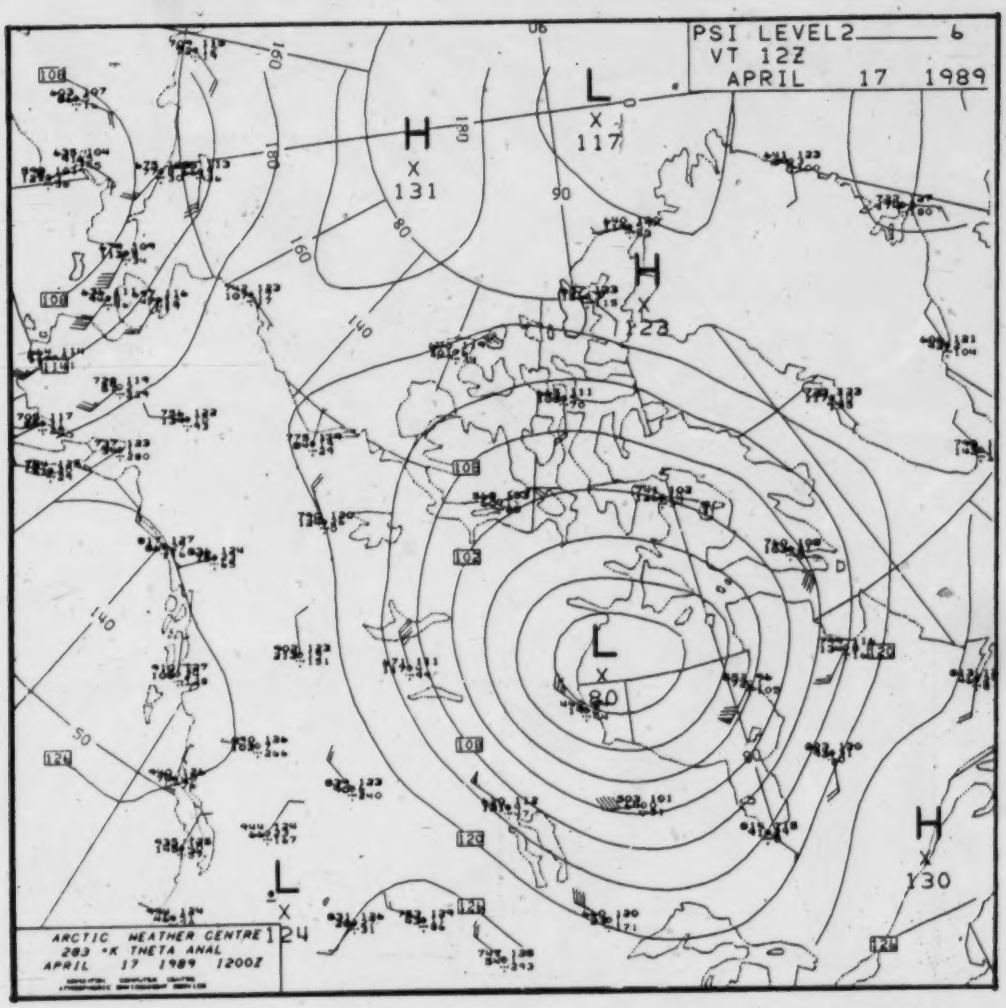

Figure 3.1: Base chart for 1200 UTC, 17 April, 1989. Displays station data and Montgomery Streamline contours for the 283K theta surface. "PSI LEVEL2_____ 6" denotes Montgomery Streamfunction for level 2 with 6 erg/gram contour spacing where level2 = 283K in this case. H = local Montgomery potential maximum, L = local Montgomery minimum. One full wind barb denotes 10 knots, a flag denotes 50 knots.

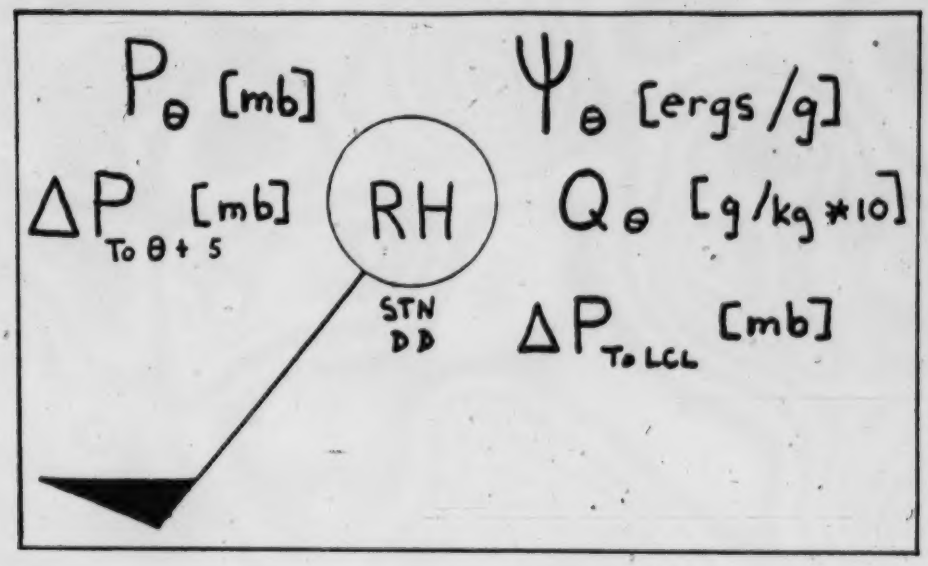

Figure 3.2: Isentropic analysis station plot decode. P=pressure of surface in mb, (deltaP "to" θ+5)=thickness in mb, Ψ =normalized Montgomery potential in ergs/gram, Q=specific humidity in g/Kg*10, and (deltaP "to" LCL)=adiabatic lift to saturation in mb.

areas, the resulting contoured parameter fields are not based on real data but rather on the extrapolations, used between stations with real data. Obviously the analysis will be less reliable in areas where the isentrope "goes below ground." By having a plot of the station data, the forecaster can easily see where there are no "real" data to support the accompanying analyses (see Figure 3.1. Note Spokane Washington (GEG) station plot with no data, denoted by X through station plot). It is important to chose the isentropic levels appropriately so as to minimize data loss. Further discussion in this regard will follow in Chapter 4.

2) The isentropic base chart provides a higher resolution of the isentropic flow where the actual wind barbs are plotted. Hence, the position and strength of the strongest winds (isentropic jet) can be more confidently delineated. Accurate placement of this "wind maximum" is important to improve the assessment of convective potential. The actual wind barbs can also be used to assess the ageostrophic component of the wind. Flow toward lower Montgomery function values implies a conversion of potential energy to kinetic energy (Wilson, 1980). Whenever there is an angle between the plotted wind vector and the streamline contours, the flow is ageostrophic and a conversion of energy is indicated.

It is worthwhile to illustrate the relationship between the station data and a tephigram sounding so that an appreciation of the plotted data can be developed. For instance, consider the sounding data for Edmonton, Alberta (WSE) from Figure 3.1. With reference to the station plot code (Figure 3.2), the tephigram displayed in Figure 3.3 illustrates the origin of the plotted station values.

By inspection the following simple relationships should be noted;

1) As p increases (decreases), height decreases (increases), temperature increases (decreases). i.e. temperature is inversely proportional to the height of surface.
2) As low-level q increases (decreases), potential buoyant energy increases (decreases).
3) As $dp/d\theta$ increases (decreases), the average static stability decreases (increases). Note that mid-tropospheric $dp/d\theta$ values greater than 115mb indicate conditionally unstable lapse-rates.
4) As dp-LCL decreases (increases), the relative humidity increases (decreases).

The utility of the isentropic analysis "package" becomes evident when these four parameters are contoured on their respective isentropic surface. To minimize clutter, a four-panel chart displaying each of these parameters

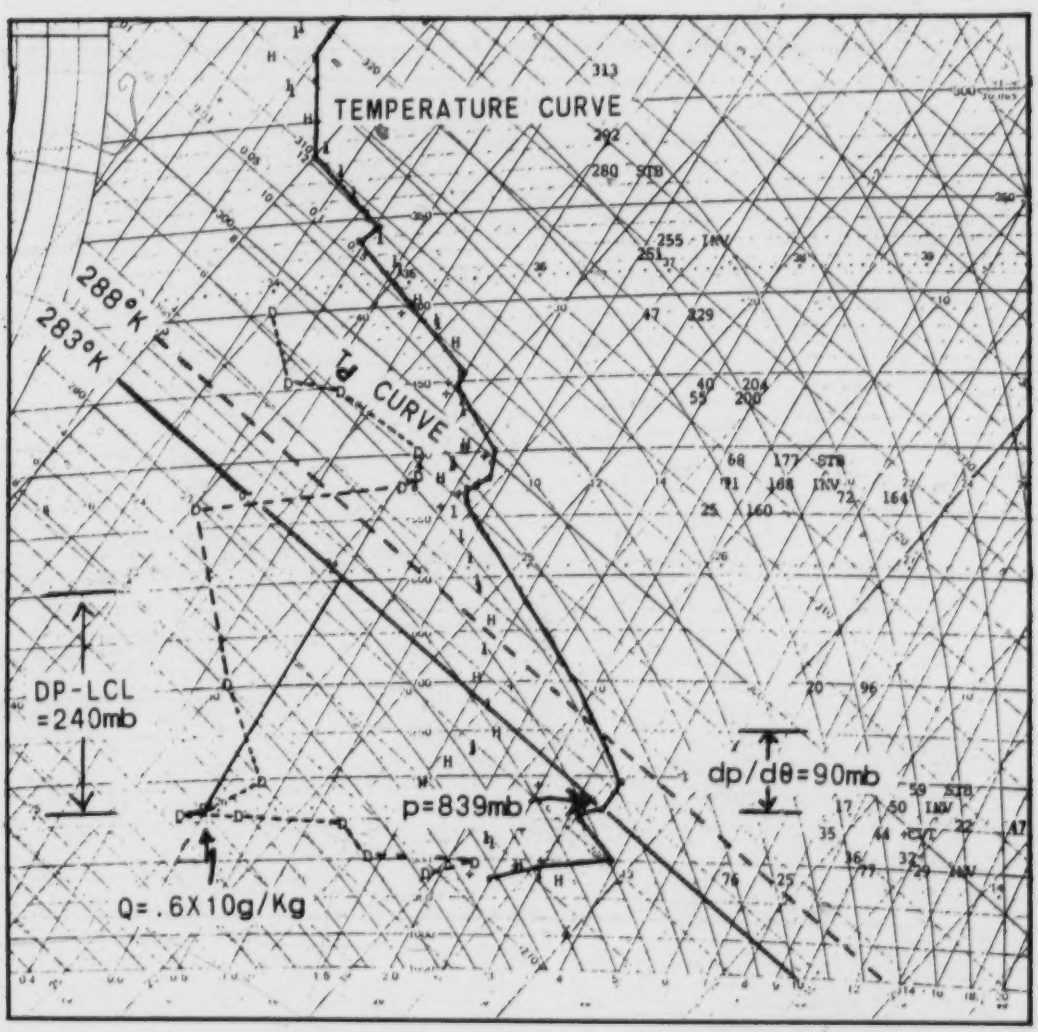

Figure 3.3: Tephigram sounding for 1200 UTC, 17 April, 1989, at Edmonton, Alberta (WSE). Illustrates isentropic data as seen on Figure 3.1.

separately is provided. The Streamfunction field is common to all panels, since it provides the flow field with which the parameters are advected. Figure 3.4 shows a typical four-panel chart whose format, though quite simple, is often confusing at first. It is important that the reader understand not only the different isopleths of each panel but also how each contributes to the diagnosis of convective potential. It is worthwhile, therefore, to discuss each of the panels separately in Sections 3.3 through 3.6.

3.3 Upper Left Panel - Height Field

The upper left panel contours the height (dashed lines) of the isentropic surface using pressure as the vertical coordinate. In addition, the streamlines (solid lines) are also plotted to provide the mean flow field on the theta surface. Figure 3.5 is an example of such a plot. It is important to note the strong pressure gradient in Central and Southern Alberta, with the mean flow perpendicular to this zone. Figure 3.6 illustrates the three-dimensionality of the isentropic surface in this area (boxed) which is the "picture" that should emerge after glancing at this panel. The areas of strong descent and ascent are marked by the superimposed arrow. These vertical motions correspond to areas where the isobars and streamlines are non-parallel (see Figure 3.5). Just as the isobaric flow is forced up the slope of a mountainside, the isentropic flow is forced

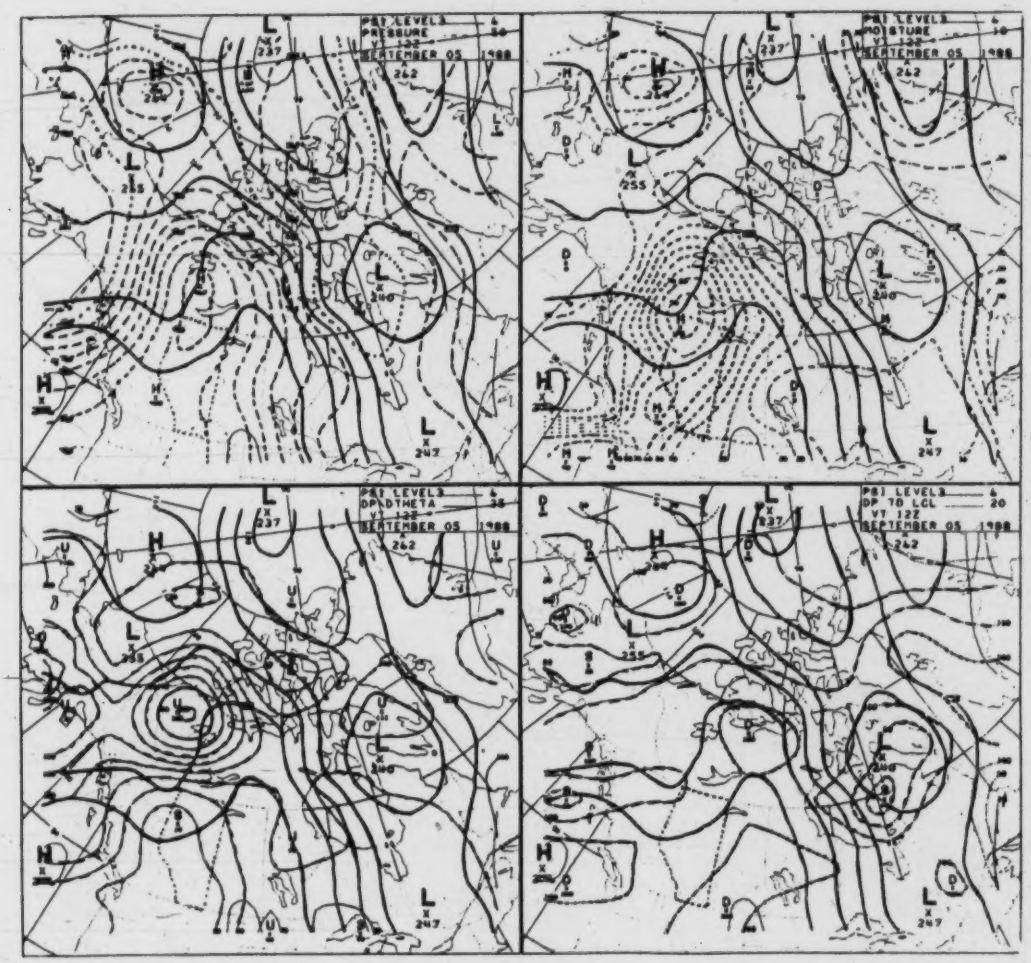

Figure 3.4: Four-paneled isentropic analysis chart for 1200 UTC, 5 September, 1988. Level 3 refers to the value of the isentropic surface. (i.e. Level 1 = X Degrees, Level 2 = Y Degrees, Level 3 = Z Degrees, Level 4 = W Degrees) in which X, Y, Z, W are the four different isentropic levels manually chosen for analysis.

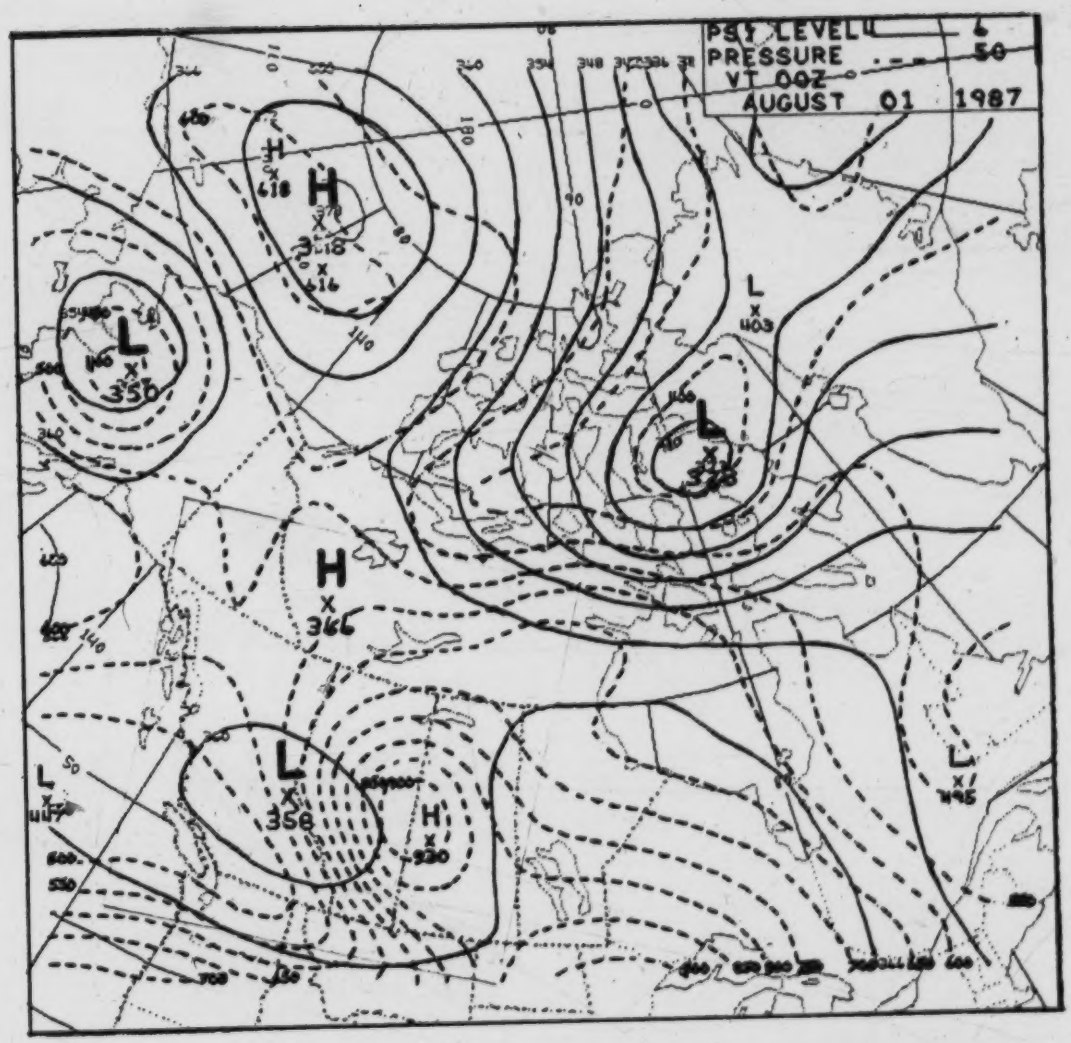

Figure 3.5: Height panel of Level 4 = 308K surface for 0000 UTC, 1 August, 1987. Montgomery Streamfunction values plotted in ergs/gram with a contour interval of 6ergs/gram. Large H denotes maximum of Montgomery potential and Large L denotes a minimum of Montgomery potential as on base chart. Plotted pressure values are in millibars with a 50 mb contour interval. Smaller H denotes High pressure local maximum (relatively high temperature), smaller L denotes Low pressure local minimum (relatively low temperature). Box denotes area of Figure 3.6.

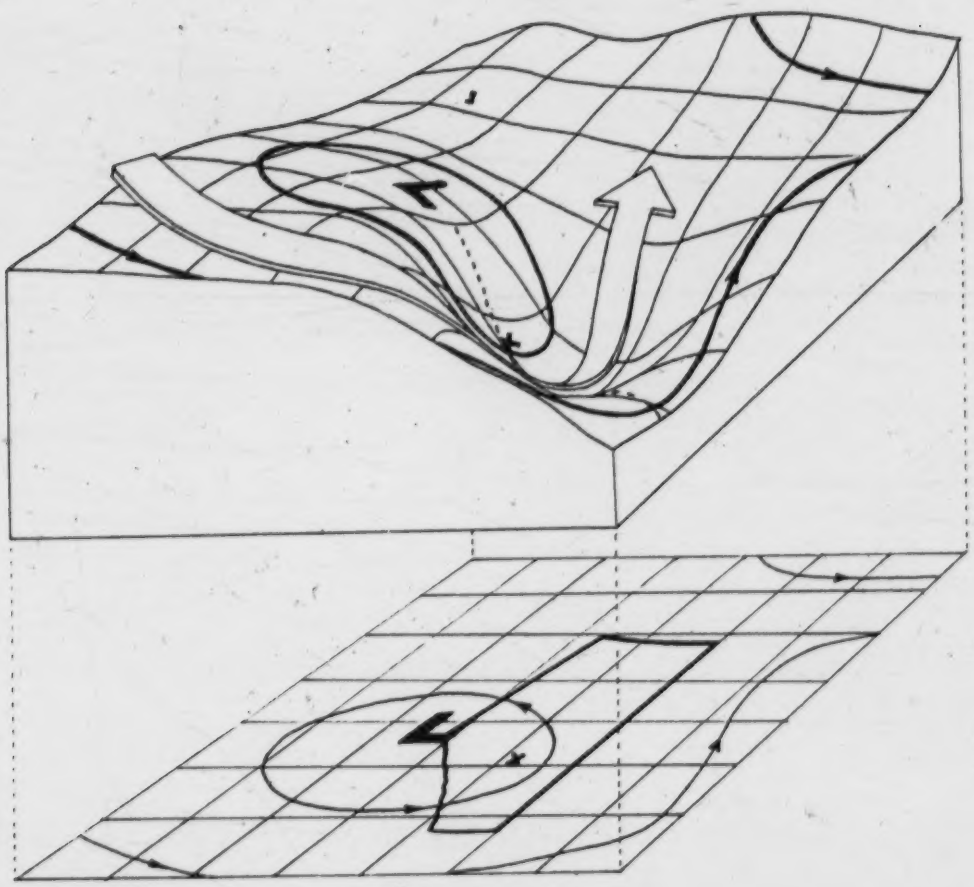

Figure 3.6: Three dimensional plot of 308K surface corresponding to Figure 3.5. – Arrow represents the mean flow on the isentropic surface. X denotes Edmonton, Alberta. (by Pat McCarthy)

adiabatically up or down the isentropic surface when the angle between these two isopleths is non-zero. In this way, the vertical component of the synoptic flow is implicit in this display. This property of the isentropic framework has been well explored (Green, 1966; Danielsen, 1966; Carlson, 1980; Browning,1986; Pearson and Blackwell,1987) to support the conveyer-belt theory of mid-latitude cyclones. In this study, the diagnosis of adiabatic vertical motion is not used explicitly as a main predictor of convective potential. However, temperature advection, a related process will be used extensively.

Temperature advection on the isentropic surface is indicated similarily by the streamline-height solenoidal field. Where the isotherms are not parallel to the streamlines, it is convenient to consider the mean flow advecting the temperature gradient (see Figure 3.5). The magnitude of this advection depends on the strength of the flow, the thermal gradient and the size of angle between them. Troughs in the height pattern (axes of large pressure values, see Figure 3.5) indicate axes of locally warmer air and conversely, ridges in the height pattern (axes of small pressure values) reveal relatively low temperatures. Cold advection is thus caused by the wind blowing toward higher pressures or lower heights. This property, resulting from height-streamline parallelograms, can be used to estimate the future positions of these thermal axes. Consider Figure

3.7 which shows the development of the thermal field on an isentropic surface over a 12 hour period. By quick inspection, a qualitative estimate of the surface's changing thermal structure can be obtained by assessing the solenoidal field (parallelograms) of the morning (12Z) plot. This thermal extrapolation is not exact since it only considers the adiabatic advective component, neglecting the diabatic displacement of the isentropic surface itself. For our purposes here, however, this technique provides a quick estimate as to the movement of thermal axes embedded in the flow. By preforming this analysis on several isentropic surfaces, a relatively detailed diagnosis of the differential temperature advection over an area can be made.

This panel also helps to delineate areas of severe storm potential, particularly the threat of tornadic activity. Earlier, it was mentioned that the slope of an isentropic surface is directly proportional to the strength of the thermal wind, which in turn is related to the vertical wind shear. It follows then, that tight pressure gradients plotted on an isentropic surface indicate areas with strong shearing winds. It was also noted that the most intense storms which support tornadic events are maintained in an environment containing strong wind shear veering with height at low levels. By the inspection of this panel then, areas with the strongest vertical wind shear can be clearly recognized. Referring again to Figure 3.5, the unusually

a)

b)

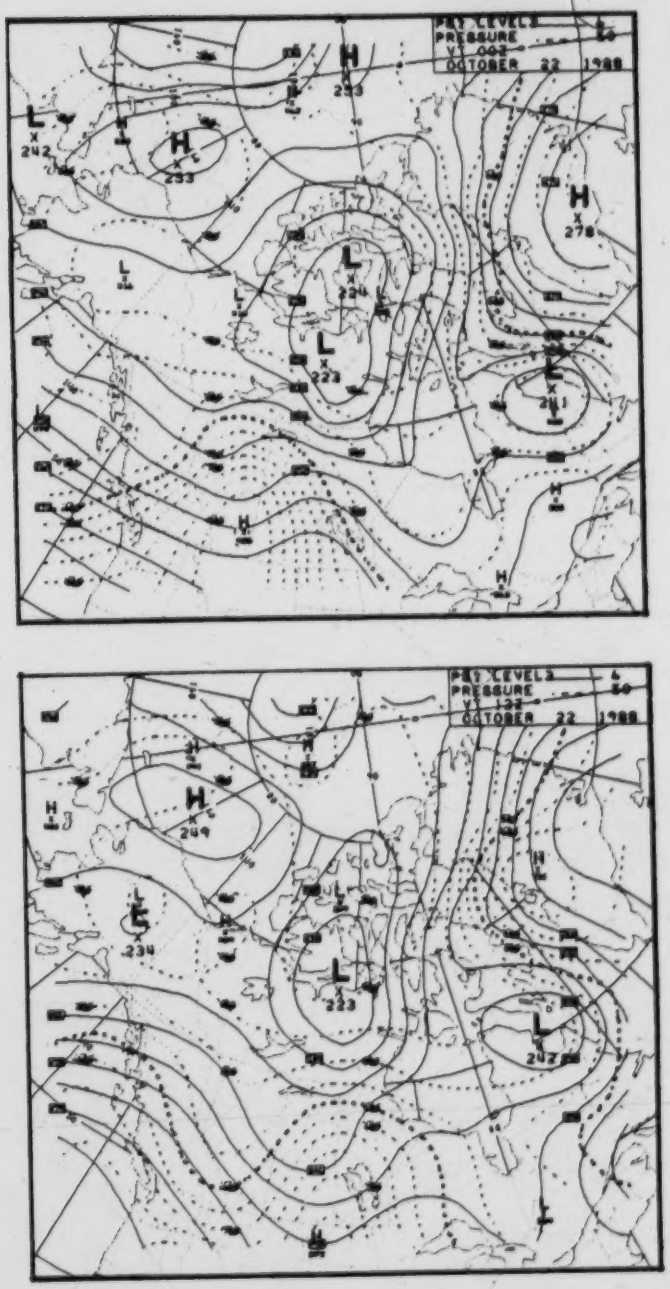

Figure 3.7: 12hr development of 298K surface height field. a) 0000 UTC, 22 October, 1988. b) 1200 UTC, 22 October, 1988. Illustrates relationship between temperature-streamline solenoidal field and propagation of thermal axis.

tight pressure gradient, as noted before, suggests unusually high values of vertical wind shear in the area. Three hours before, at 15:00 MDT, July 31, 1987, a violent tornado (F4) touched down in the Edmonton area, producing wide-spread and heavy damage. The 00Z plot is clearly indicative of an environment containing very strong horizontal temperature gradients and associated strong vertical wind shears in Central and Southern Alberta.

To summarize, the upper left panel can be used for delineating fronts, the adiabatic component of vertical motion, cold and warm air masses and other general tropospheric properties. In this study, however, emphasis is placed on the diagnosis of three features:

1) The location of thermal axes and centres implied by troughs in the height pattern.
2) The advection of thermal axes and centres with the mean isentropic flow, including differential temperature advection between two or more surfaces.
3) Areas of strong vertical wind shear indicated, by tight gradients in the pressure field.

3.4 Upper Right Panel - Moisture Field

> *"On an isentropic chart, the distribution of moisture is simply and vividly apparent and the analyst can, in general, validly follow a particular air particle in its day-to-day convolutions. Thus the isentropic chart is a potent addition to our tools for preparing optimum analyses."* *Oliver and Oliver, (1951)*

One of the major input elements needed for a more accurate diagnosis of the atmosphere's convective potential is the moisture profile below 600mb. In this regard, isentropic analysis is the best tool available, as it displays a coherent moisture pattern in space and time.

The upper right panel displays the distribution of moisture on the isentropic surface by means of "contours" of specific humidity deduced from the station data on the base chart. Figure 3.8 shows such a plot with the dashed lines denoting isopleths of specific humidity, the solid lines again being the streamlines on the theta surface. Analogous to the temperature advection found on the previous panel, moisture advection occurs in areas where the streamlines and moisture contours are non-parallel. A short-term forecast of the moisture field can then be made by analyzing the moisture-streamline solenoidal field. Figure 3.9 shows a 24 hour progression of the moisture field on the isentropic

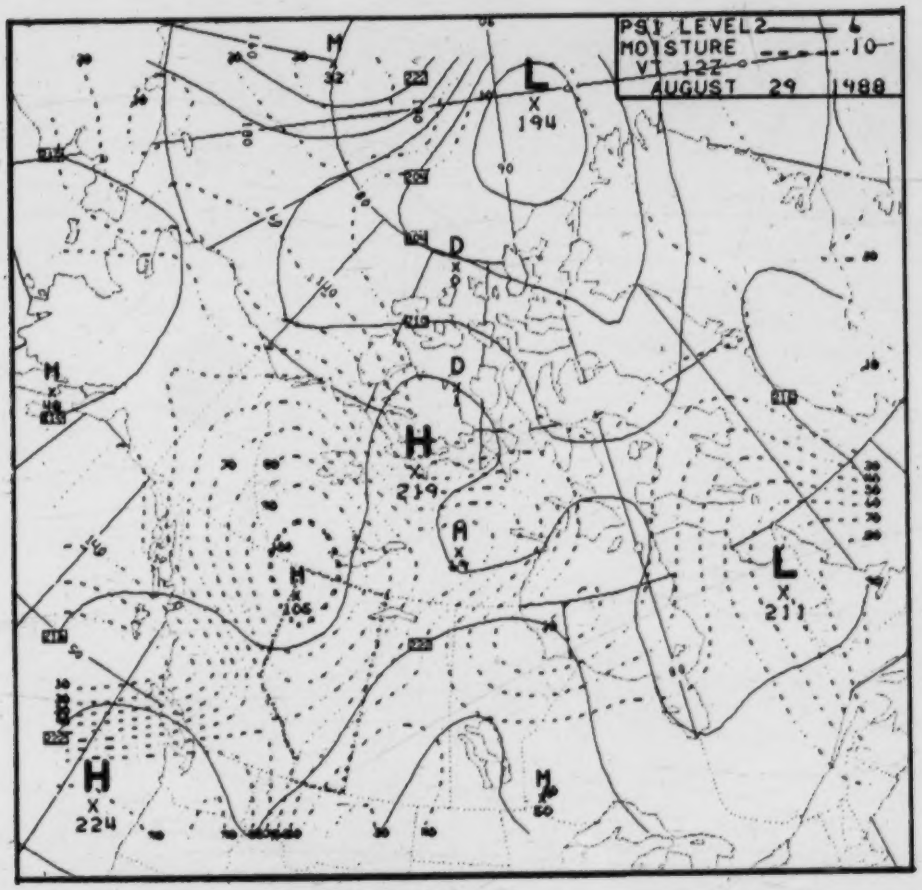

Figure 3.8: Moisture panel for the level 2 surface for 1200 UTC, 29 August, 1988. Montgomery contour (solid lines) notation as in Figure 3.5. Plotted moisture contours (dashed lines) in g/Kg*10 with 1g/Kg interval. M denotes local moisture maximum or Moist center, D denotes local moisture minimum or Dry center. Note the "center" of moisture in Northwestern Alberta.

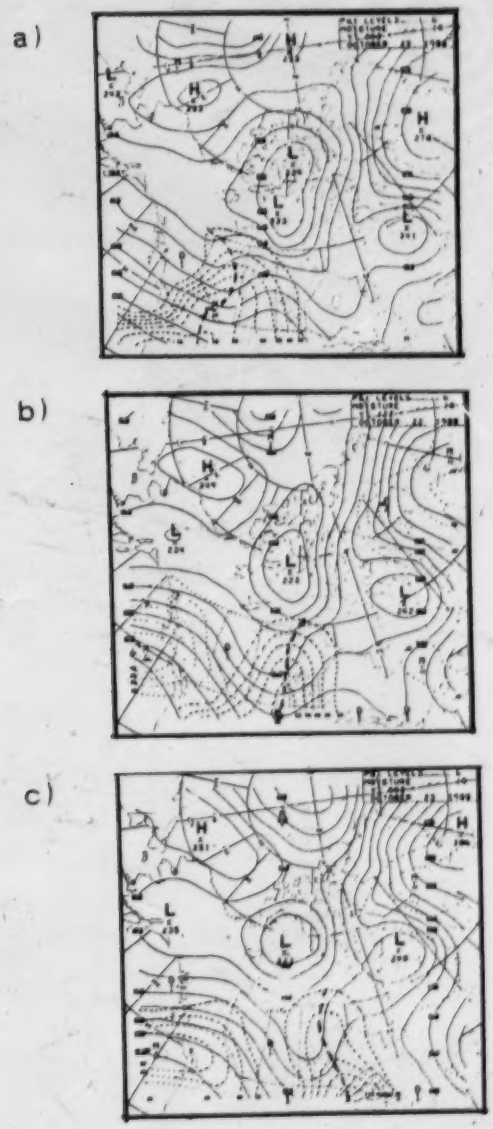

Figure 3.9: 24hr development of 298K surface moisture field. a) 0000 UTC, 22 October, 1988, b) 1200 UTC, 22 October, 1988, c) 0000 UTC, 23 October, 1988. Illustrates relationship between moisture-streamline solenoidal field and propagation of moisture axis.

surface. Clearly, the solenoidal field indicates the movement of moisture on the theta surface. The motivation for this technique is well documented by Moore et al. (1980) who have shown that moisture convergence or the advection of positive values of moisture will destablilize the environment by adding potential buoyant energy to the air column. If there is sufficient instability aloft, organized convection can be expected in these areas. Furthermore, the potential instability of an air column may be increased if moisture advection decreases with height. A three-level isentropic analysis can help reveal these conditions by displaying the advective rates of moisture at each level.

Another important diagnostic property of this chart is evident from the display of actual specific humidity values. No other operational chart reveals the "real" water content at any level except for the standard sea-level chart which has plotted dew-points. These surface dew-points, however, are not often representative of the moisture actually contained in the lower levels.

> *"Sources of moisture indicated within the layer adjacent to the surface may be found to be shallow and not representative of the conditions in a higher surface of constant potential temperature."*
>
> *Oliver and Oliver, (1951)*

The isentropic package used in this study displays several levels of moisture values. The specific humidity values provide the forecaster with two things;

1) A relative sense of convective potential. For example, an area with a local maximum of high specific humidity, will be able to support stronger storm complexes than an adjacent area of lower specific humidity. It is important then, to analyze moisture axes and especially moisture "centres", since they indicate a local maximum of buoyant energy. Figure 3.8 shows a moisture field containing a moisture centre surrounded by a strong gradient of moisture isopleths arranged in a circular pattern. These axes and centres are keys to delineating areas of strong convective potential.

2) An estimate of precipitable water. By knowing the actual water content in the lower troposphere, an estimate of the amount of precipitation to be expected should be more accurate than one using the surface dew-point and 700mb relative humidity only. By adding the isentropic moisture data contained on the three surfaces intersecting a column of air, an environment having the potential to produce heavy rainfall amounts (>25mm/hr) can be diagnosed.

To summarize, the upper right panel represents the moisture distribution on the isentropic surface. By contouring several isentropic surfaces, the moisture profile

within an air column can be better estimated. This panel contributes to the analysis of convective potential by displaying the following:

1) Moisture axes and centres.
2) The actual specific humidity values within these axes and centres. As the specific humidity increases, the buoyant energy (latent instability) and the potential for substantial rainfall increase as well.
3) Differential moisture advection. Potential instability is generated as moisture advection decreases with height.

The next two panels conveniently display derived fields that add to the operational utility of the charts. However, since these fields depend on the properties of layers bounded by two isentropic surfaces, the advection process is more complicated.

3.5 Lower Left Panel - Static Stability Field

The lower left panel contours the static stability field. It displays the thickness of an isentropic layer, bounded by the plotted base surface, and a second isentropic surface five degrees warmer and higher than the first (Refer to Figure 3.3). Figure 3.10 shows such a stability analysis, together with the stream lines appropriate to the

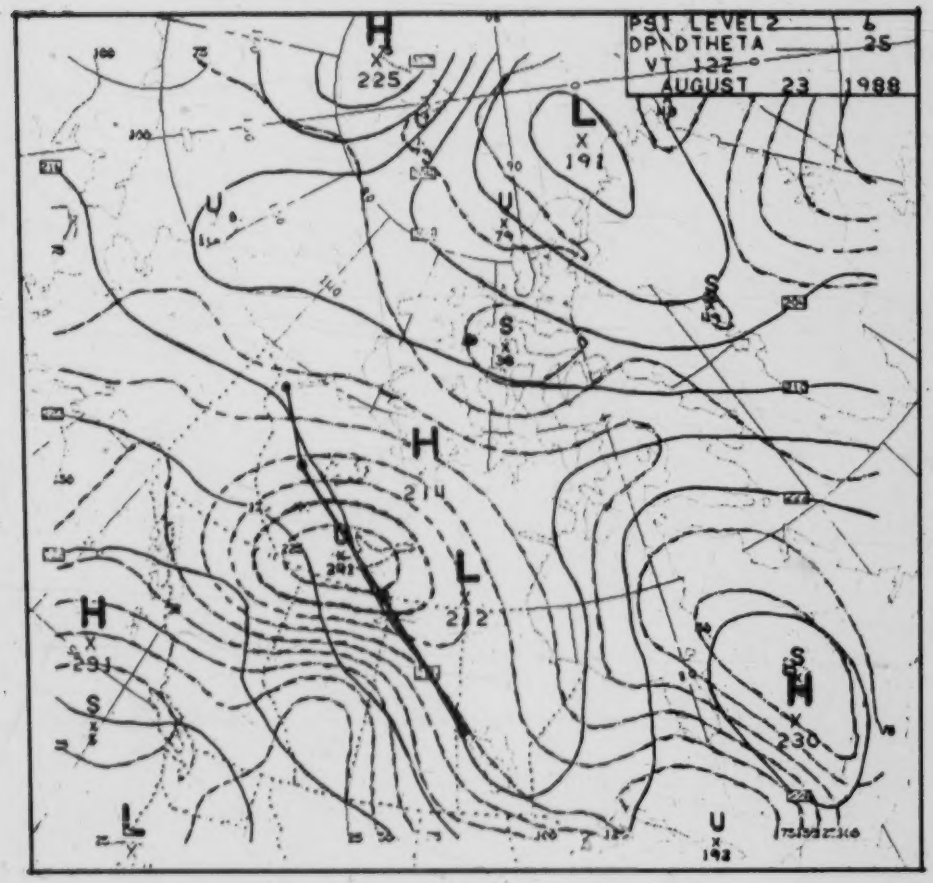

Figure 3.10: Static stability panel for level 2 surface for 1200 UTC, 23 August, 1988. Montgomery contour (solid lines) notation as in Figure 3.5. Plotted static stability values (dashed lines) in mb with 25mb contour interval. U denotes Unstable center, S denotes Stable center. Line shown is the cross-section depicted in Figure 3.11.

lower surface. To help show the physical meaning of this derived field, a cross-section in Figure 3.11 corresponding to Figure 3.10 is provided. Together, they provide a 3-dimensional "picture" of the distribution of the stability along the line from Inuvik, NWT (YEV) to The Pas, Manitoba (YQD). It will be seen that the 293K surface sags near Fort Smith (YSM) due to warm air confined to the low-levels in the region. This sagging increases the thickness between the 293K and 298K isentropes, which in turn produces a local maximum of static instability in the Fort Smith area. The higher plotted pressure values indicate more unstable lapse-rates. The axes and centers of high plotted values within this field provide a good overview of the regions likely to be subject to convective storm activity.

It should be noted that the stability or thickness field cannot be advected directly with the isentropic wind of the base surface. Unlike temperature and moisture, the thickness field is not a property of the base surface alone but rather a composite of the "five-degree" layer above it. The propagation of a layer is a function of the wind flowing through it at all levels. Therefore, it is inaccurate to advect the isopleths of thickness with the wind at the base of the layer. However, a thin layer, or a layer with little vertical shear, can be advected downstream with the mean flow for short time periods (<15 hrs).

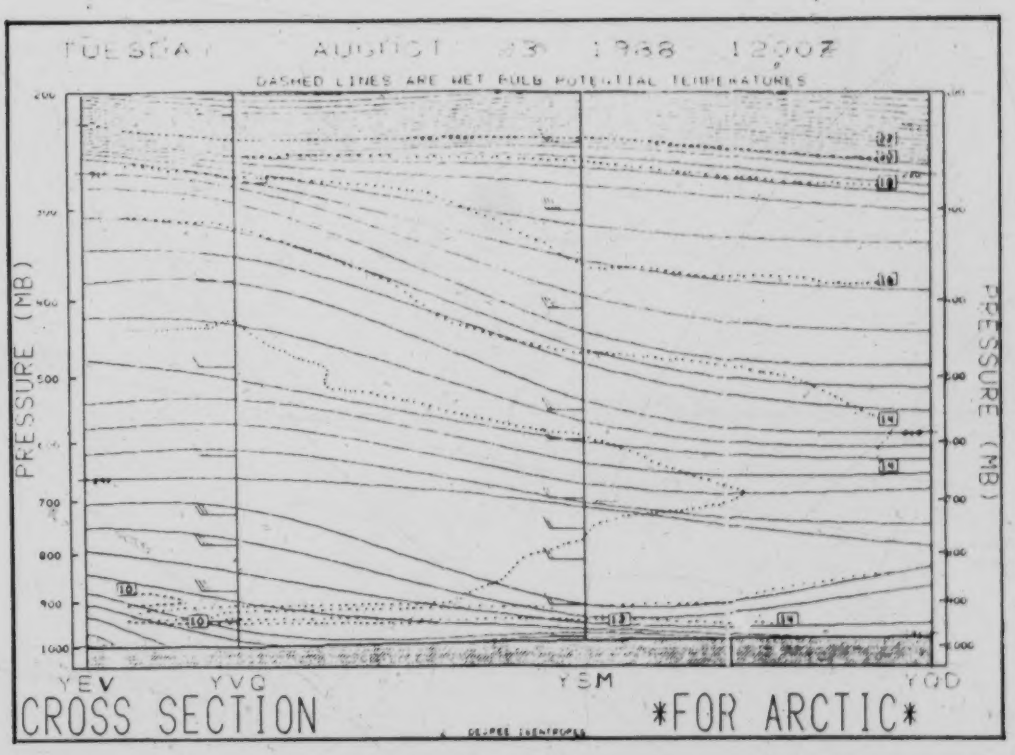

Figure 3.11: Isentropic cross-section for 1200 UTC, 23 August, 1988. Solid lines are isentropes with 2K spacing. Heavy dashed line denotes 293K isentrope corresponding to isentropic surface in Figure 3.10. Wind barbs denote wind speed tangential to plane.

Several researchers have used static stability analysis within an isentropic framework. Byers (1945) used an isentropic stability analysis for determining likely areas of cyclogenesis. Using the equation of continuity, he evaluated convergence and divergence within an isentropic layer. He suggested that, as air blows from a "thin" layer to a "thick" layer, the column of air bounded by the two surfaces will stretch vertically as the potential temperature surfaces spread apart. However, to conserve vorticity, this vertical stretching must be compensated by horizontal convergence within the layer. If this process takes place near the earth's surface, low level convergence and possibly associated cyclogenesis could ensue. Many years later, Petersen (1988) used short-term forecasts of mid-tropospheric isentropic static stability fields to trace several severe storm events. His model, which is similar to Bleck's (1973), used potential vorticity and mass continuity conservation to predict the propagation of instability over the Mid-Western U.S. He found that by simply advecting the isentropic layers over short time intervals (1-3hrs), he was able to follow the severe storm development.

This study will concentrate on delineating well-defined instability axes or centres. Instability below 700mb may produce environments less restrained by low level inversions. In such cases, the column's convective potential would be more easily realized (Moore, 1985). On

the other hand, low-level stability can indicate the existence of an inversion. It is well known that a "capping lid", that is a strong low-level inversion, is often associated with severe weather outbreaks.

To summarize, the lower left panel in this four-panelled scheme will contribute the following to the assessment of convective potential;

1) Delineate areas/levels of instability by analyzing axes, and more significantly, focus on centres of enhanced thickness.
2) The short-term advection of such relatively unstable areas by considering the flow through the isentropic layers.

It should be noted the information displayed in this panel can be inferred also from the height contours in the thermal panels, since the stability field reflects the height difference between the two adjacent five-degree isentropic surfaces.

The last panel to be discribed also displays a field that can be estimated from information contained in the first two panels.

3.6 Lower Right Panel - Relative Humidity Field

The fourth panel combines the content of the height and moisture panels. The temperature field is implicit in the upper left panel, and the moisture field in the upper right panel. Thus, if the temperature and moisture content of the parcels on the isentropic surface are known, the relative humidity of the surface can be plotted. In addition to the basic streamlines, this panel depicts what are essentially isopleths of relative humidity, such as are shown in Figure 3.12.

Note that the lines in the figure are not true isopleths of relative humidity, since they are plotted in units of millibars. The plotted values represent the vertical distance required to lift a parcel adiabatically to its condensational level (see Figure 3.3). Large values indicate large temperature-dewpoint spreads which in turn imply low relative humidity values. Conversely, low values represent small temperature-dewpoint spreads and high relative humidities. Mid-tropospheric values less than 20mb indicate relative humidity greater than 90%.

The relative humidity panel can aid the operational forecaster most directly by indicating areas of general cloudiness. By using a multi-level isentropic analysis package, volumes of atmosphere can be readily identified as

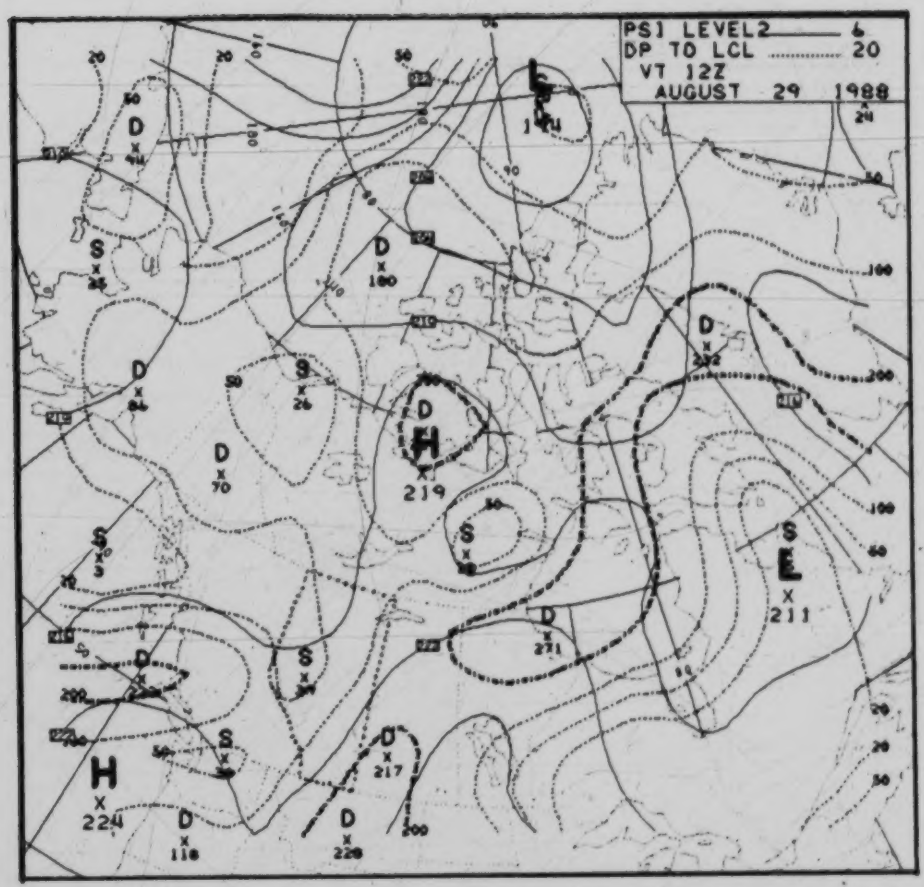

Figure 3.12: Relative humidity panel for level 2 surface at 1200 UTC, 29 August, 1988. Solid lines are Montgomery Streamline contours as notated in Figure 3.5. Plotted values indicate relative humidity contoured in millibars with a 20, 50, 100, 200 contour field. S denotes Saturated local center, and D denotes Dry local center.

having high values of relative humidity, if at each level the plotted values are small. From these near-saturated columns, condensation will often result and depending on the column's buoyant energy, will often produce wide-spread rain showers or local severe downpours.

In this thesis the significance of potential instability, as a requirement for the production of severe storm complexes, has been addressed. Mid-level "dry slots" or local minima of low relative humidity can be identified by delineating axes of high plotted values. Theoretically, as noted by Wilson et al. (1980), these axes may be advected with 100% of the normal wind component, since unsaturated parcels conserve their specific humidity and are confined to their isentropic surface. This technique may be useful to forecast dry-air intrusions into the mid-levels and thus indicate a possible increase of potential instability. On the other hand, these dry slots may also reflect very warm air at a particular level which may possibly indicate stability. Since the contribution of these dry slots to convective potential is difficult to assess, their use in practice is limited.

To summarize, this panel is most useful for detecting saturated environments. By analyzing axes and centres of minimal lift to saturation, areas requiring the least displacement to achieve condensation and possibly "free"

convection, can be readily diagnosed. However, the adiabatic assumption is not valid in these areas. The advection of these "wet" slots cannot be estimated, since the air parcels are forced off the isentropic surface, due to the release of latent heat from condensation. The dryness of an air column is important when evaluating severe weather types.

3.7 Summary - The Isentropic Package

This chapter contains an outline of the isentropic charts routinely produced at the Arctic Weather Centre. The focus of the next, Chapter 4, is to develop an isentropic procedure that will use these charts to assess the convective potential of the atmosphere. Before this procedure is discussed, however, it is worthwhile to review the key elements of this isentropic package.

1) Base chart - Displays station data and provides a means to delineate maximum isentropic wind.

2) Height panel - Displays temperature distribution within the atmosphere, indicating thermal axes and centres. Propagation of these "anomalies" is estimated in conjunction with the streamfunction field on the theta surface. This results in a qualitative assessment of the differential temperature advection

within the lower troposphere. The height panel also indicates the presence of strong temperature gradients, thus indicating frontal structures and associated zones of strong vertical wind shear.

3) Moisture panel - Displays moisture field on the isentropic surface, delineating axes and centres of high values of available moisture. The propagation of these local maxima is estimated from the moisture-streamline solenoidal field. This, in turn, facilitates the diagnosis of increasing potential instability.

4) Static stability panel - Depicts the static stability of a five degree layer above the isentropic surface. Indicates axes and centres of steep lapse-rates represented by local maxima in the plotted field. The propagation of these maxima can be estimated if the flow changes little through the layer.

5) Relative humidity panel - Shows a field of isopleths equivalent to the relative humidity distribution on the isentropic surface. It reveals environments that require little lift to condensation.

"Operational computer-produced constant pressure analyses are often smoothed and do not show detailed resolution of moisture and thermal gradients, and strong wind shear near jet streams. Analysis in isentropic coordinates could potentially fill a meteorologist's need for simple and convenient depiction of atmospheric structures on charts."

Wilson, Siok, and Marois (1980)

CHAPTER 4

THE ANALYSIS PROCEDURE

4.1 Choosing the Isentropic Levels

To facilitate an optimum diagnosis of the convective potential using an isentropic framework, the plotted surfaces should have heights below the 600mb level. However, since potential temperature surfaces are very sensitive to temperature and often have steep height gradients, care must be taken to choose them appropriately for a particular area of interest. To this end, isentropic cross-sections can help depict the best levels for analysis.

Figure 4.1 illustrates a vertical cross-section depicting the potential temperature profile of the atmosphere through Whitehorse (YXY), Fort Nelson (YYE), Edmonton (WSE), and Glasgow (GGW). Since the Alberta region is of interest in this study, particular attention to the height of the isentropes between YYE and GGW should be given. To assess the low-level environment, at least one surface should be chosen near the ground to intercept the boundary layer below the morning inversion. In these investigations, the 298K surface has been used to depict the low-level conditions. It is also important to assess the mid-level tropospheric conditions near the 600mb level. During June, July, and August, the 308K surface was used to this end. Of course, depending on local conditions, these particular levels will not always be at the optimal heights. However, it will be seen that the actual height of the potential temperature level is not of great significance. Additional levels may be chosen to provide further insight into the state of the atmosphere, but, since these investigations are, in a sense, exploratory, it was thought preferable to keep the analysis procedure as simple as possible. In this regard, only the 298K and 308K surfaces will be used to assess the convective potential. They will be denoted as the "low-level" and "upper-level" surfaces, respectively. Note that these terms provide no inherent information on the actual height of the surface but simply reflect their relative heights.

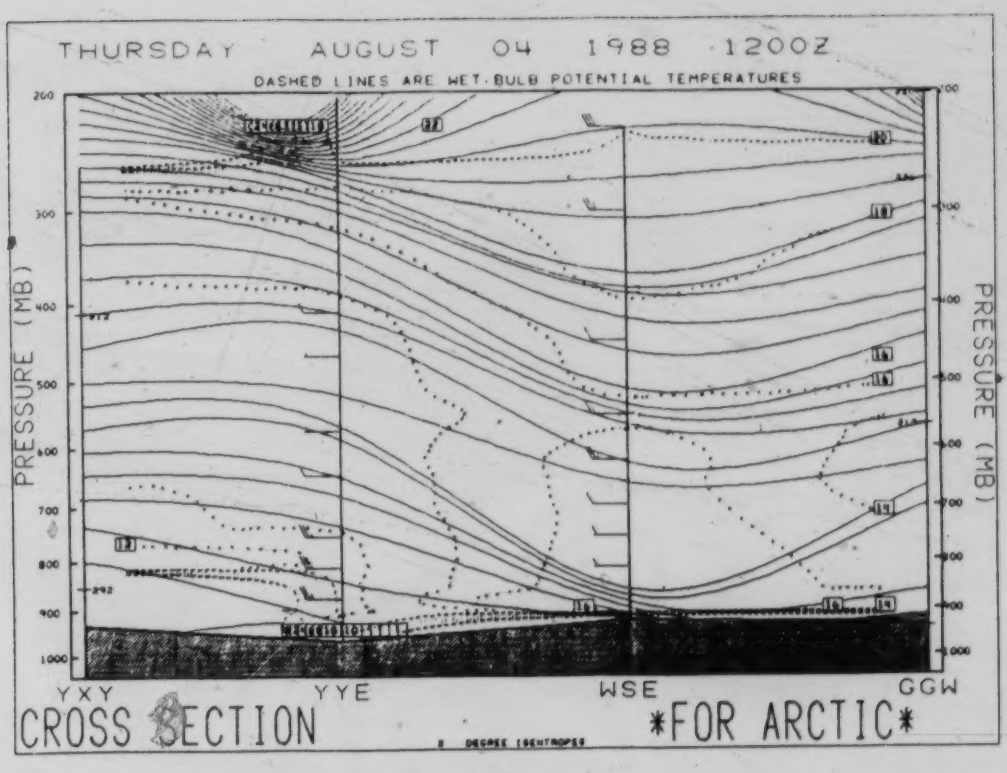

Figure 4.1: Potential temperature cross-section through Whitehorse (YXY), Fort Nelson (YYE), Edmonton (WSE), and Glasgow (GGW) at 1200 UTC, 04 August, 1988. Solid lines are potential temperatures spaced two degrees apart and the dotted lines are wet bulb potential temperatures.

These investigations only use the 1200 UTC (morning) isentropic data to forecast convective activity and the likelihood of severe weather. However, if the 0000 UTC is used operationally, allowances for radiational heating within the lower troposphere must be made. Higher isentropic levels must be chosen for evening analysis if data loss is to be minimized.

4.2 Checking the Data

Once the proper isentropic levels have been chosen and the morning charts have been produced, an inspection of each base chart for each level should be done to determine the validity of the corresponding contoured fields. Since the analysis of convective potential depends on the depiction of near-mesoscale environments, a complete station data base is necessary to obtain the best possible interpolation between station data. Any stations in or surrounding the Alberta region without data should be noted and, if a large portion of the region is without station data, the contoured plots for the level should not be considered in the analysis. In this study, both the 298K and 308K plots had very good data coverage throughout the forecast area.

4.3 Parameter Analysis

The procedure developed here requires the analysis of up to 11 parameters, all obtained by briefly inspecting the isentropic charts. The convective potential of the forecast area is then assessed by tracing selected parameters from the upper and lower isentropic analyses onto a "composite" chart. This helps to determine the organization of the parameter fields, and leads to the delineation of the main areas of convective activity. The parameters which are drawn on these composite charts will be represented by solid, dashed and hatched lines. The following table lists these parameters and their analysis decode.

TABLE 4.1 PARAMETER ANALYSIS DECODE

Parameter	Representation
1) low level Temperature axis	solid line, labelled T
2) low level Moisture axis	solid line, labelled M
3) low level Instability axis	solid line, labelled I
4) low level Saturated axis	solid line, labelled S
5) upper level Temperature axis	dashed line, labelled T
6) upper level Moisture axis	dashed line, labelled M
7) upper level Instability axis	dashed line, labelled I
8) upper level Saturated axis	dashed line, labelled S

9) Differential Temperature Advection..hatched, labelled DTA

10) Differential Moisture Advection....hatched, labelled DMA

11) upper level wind maximum.....arrow

It should be noted that for highly organized environments, the upper level and lower level temperature and moisture axes along with the differential temperature advection (DTA) and differential moisture advection (DMA) will be the only parameters that will be drawn on the composite analysis. This helps to minimize confusion and highlights the most important isentropic parameters associated with strong convective outbreaks.

4.4 Verification

In order to evaluate the effectiveness of this procedure, a verification scheme is required to test it. Lightning data and severe weather reports are used to this end.

4.4.1 Lightning Data

Since these investigations involve the evaluation of numerous case studies, a simple but reliable verification technique is highly desirable. While reflectivities from radar and cloud-top temperatures observed on satellite images offer very good resolution of individual storm complexes, they only provide a "snap-shot" of the convection taking place. Vast numbers of radar plots and satellite pictures would be needed to trace storm evolution, and a lengthy analysis would be required to compare various storm intensities. Lightning plots, however, provide a quantitative assessment of convective history on a single plot.

With the advent of lightning detection systems, meteorologists have been provided with a new way of tracing the path and intensity of convective storms. Thirteen direction finders placed strategically throughout Alberta detect, in real-time, the position of lightning strikes within the province. In this way, a storm's movement and (to some extent) its intensity can be constantly monitored.

In the examples presented here, each lightning plot displays 24 hours of data between 00:00 and 23:59 local time. To distinguish between strike times, each 4-hour interval is coded with a different strike color. Table 4.2 lists this color-code/strike time relationship:

TABLE 4.2 LIGHTNING PLOT COLOR CODE

Time of strike (MDT)	Corresponding strike color
00:00 - 03:59	Pink
04:00 - 07:59	Yellow
08:00 - 11:59	Green
12:00 - 15:59	Black
16:00 - 19:59	Red
20:00 - 23:59	Blue

The forecast procedure developed here is mainly concerned with forecasting the black, red, and blue strikes, as the pink and yellow strikes are produced by pre-analysis convection.

Consider the lightning plot shown in Figure 4.2. This plot displays all of the positive (+) and negative (x) lightning strikes recorded in the Alberta region on 27 June, 1988. By inspection, the main line of convection originated along the foothills in the early afternoon (black) and propagated towards the northeast before losing intensity in the central regions near midnight. The majority of the 9086 strikes were recorded between 4:00pm and midnight in West-Central Alberta. This information delineates the main area of convective activity and provides an estimate of convective strength. The isentropic procedure in this study aims to forecast the position and strength of these "main" convective events six to eighteen hours prior to development.

4.4.2 Severe Weather Reports

Very strong convection may support severe weather. In these cases, additional verification initiatives are required to supplement the lightning plots.

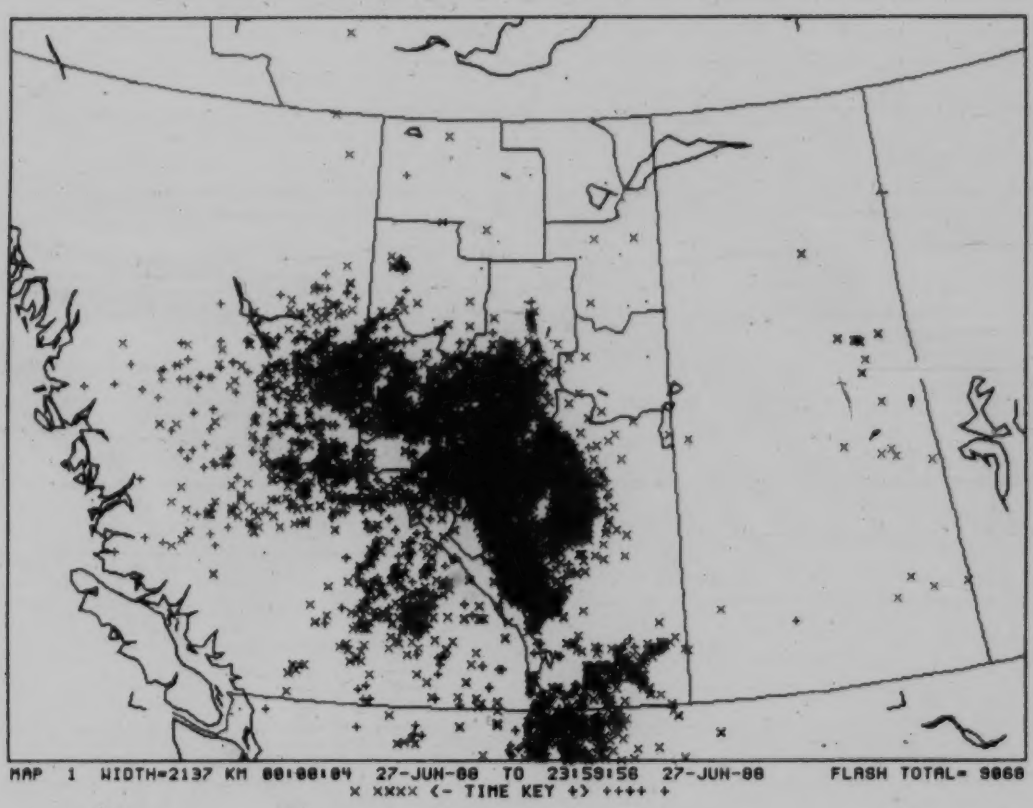

Figure 4.2: Lightning plot for 27 June, 1988.

A "severe weather log" detailing the time, place and strength of all reported severe weather occurrences in 1988 was used to this end. Produced by the Alberta Weather Centre, this log provides "reliable" reports of events meeting the following criteria;

a) Tornadoes
b) Hail with diameter > 20mm
c) Rain with rainfall rate > 25mm/hour
d) Wind > 90Km/hr
e) Funnel Clouds

4.5 Summary

To summarize this analysis methodology, the following procedures are applied;

1) Chose appropriate potential temperature levels.

2) Assess the validity of the isentropic data by consulting the base charts.

3) Inspect the various isentropic fields for distinct parameter axes or centres.

4) Carefully trace these axes onto a composite chart.

5) Delineate the areas of highest convective threat by considering the relationship of the parameter axes with one another.

6) Shade the regions having the highest convective potential.

7) Verify the convective forecast using lightning data and severe weather reports.

Note that steps 1 and 2 will not be discussed further, as they are pre-analysis considerations which have been previously addressed.

To illustrate these procedures explicitly, several case studies from the summer of 1988 will follow in Chapter 5.

"Diagnostic studies are an essential means of forging the link of mutual understanding and respect between the theoretician generating the fundamentals of the science based on idealized models, and the weather analyst or forecaster attempting to apply his theories."

R.P. Pearce (1974)

CHAPTER 5

CASE STUDIES

5.1 Introduction

Ten case studies have been chosen to illustrate the isentropic forecast procedure. Using only 1200 UTC isentropic data, a convective forecast delineating the area of highest convective threat is produced for each case. To represent a wide range of atmospheric forcing, three cases with relatively weak convective potential, two cases with moderate convective potential, and five cases having strong (severe) storm potential have been selected. Though the study is restricted to June, July, and August, 1988, there was no shortage of suitable cases, in fact, too many to be discussed here.

Each case includes a brief discussion of the key isentropic parameters which help to outline the area of convective "threat". To supplement these discussions, the following charts are included with each case and should be referred to correspondingly;

1) The four-panel 1200 UTC upper level (308K) isentropic chart
2) The four-panel 1200 UTC lower level (298K) isentropic chart
3) The composite chart
4) The lightning plot

To provide additional background, the isobaric charts (CMC, 00hr) corresponding to each case study are given in Appendix B. These provide an inexperienced isentropic user with familiar isobaric analysis fields and the opportunity to compare the two analysis schemes. Also, selected isentropic cross-sections are given in Appendix C. They help to visualize the vertical stratification of the troposphere.

5.2 Case Studies

5.2.1 July 07 1988

Figure 5.1 shows the upper-level (308K) isentropic surface for 1200 UTC 07 July, 1988. The Montgomery low centered near Lake Athabasca provided a northwesterly wind maximum (isentropic jet) through Alberta. Weak, negative temperature advection (cooling) within this jet is indicated by the crossing of streamlines and isobars from northeastern British Columbia to Southeastern Alberta. Weak negative moisture advection (drying) is also evident in the St.Paul, Edmonton, and Coronation regions (see Appendix D for map of Alberta and forecast regions). A weak axis of instability lies near the Alberta-Saskatchewan border.

Figure 5.2 illustrates the lower-level (298) isentropic surface. A weak moisture axis through Eastern Alberta curving towards Northwestern Alberta is depicted on the moisture panel. An axis of instability and high relative humidity are indicated in the Alberta region as well.

The composite chart in Figure 5.3 depicts an unorganized environment with the various parameters scattered throughout the forecast region. The highest threat of convective activity is likely to be in a northwest

- southeast band through Alberta, corresponding to the juxtaposition of the upper and lower instability axes with the wind axis. The convective potential, however, should be weak due to the unorganized parameter fields depicted by the morning analysis. Also, small low-level moisture values throughout Alberta indicate weak low-level support.

Figure 5.4 displays the lightning recorded on July 07, 1988. By inspection, the main line of activity is confined to a band through Alberta. The strikes are scattered within this band and dissipate in the early evening (i.e. few blue strikes). Radiational heating clearly fuelled this convection, suggesting that the cells had weak upper level support.

To summarize, the main convective band was well correlated with the isentropic jet and the axis of cold air observed on the upper isentropic surface. Weak cooling and drying aloft, along with radiational heating at the surface, provided the instability for the afternoon convection. The weak cells then were driven downstream by the strong northwesterly flow.

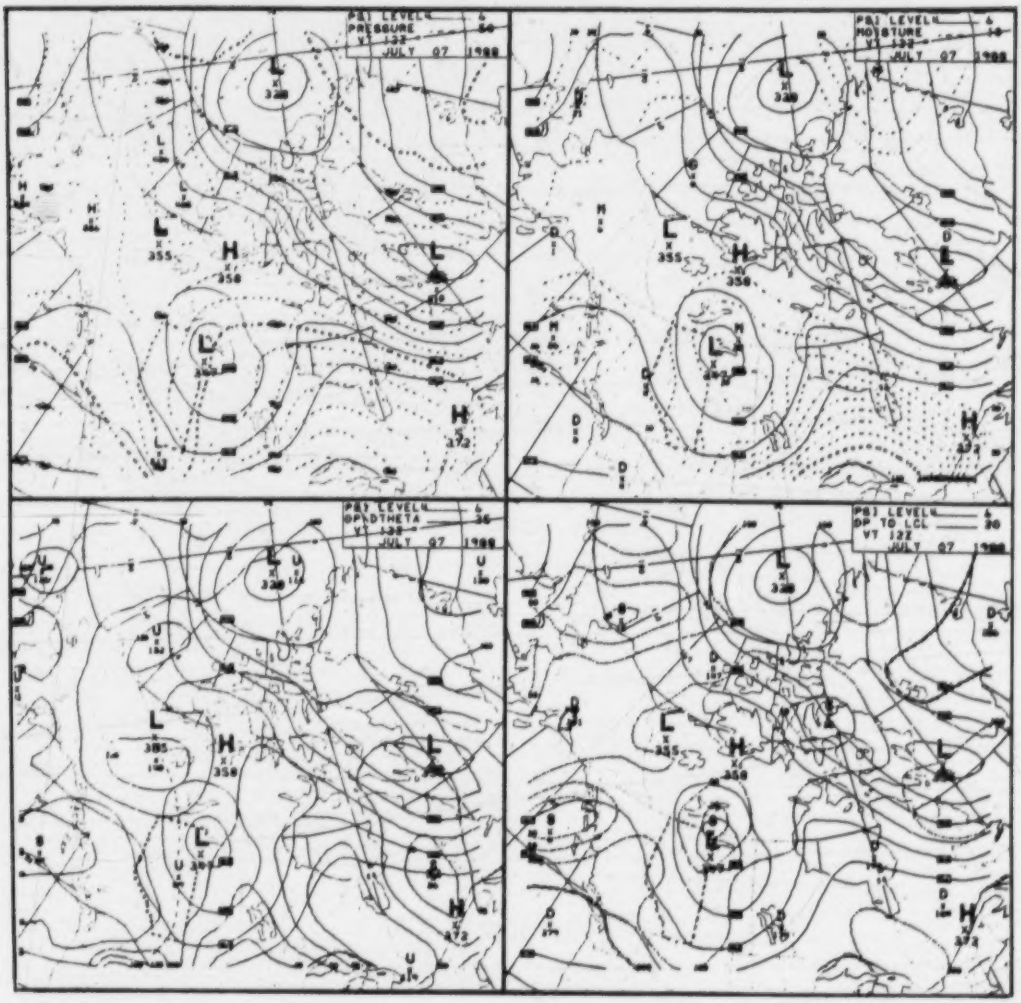

Figure 5.1: Upper level (308K) potential temperature analysis for 1200 UTC, 07 July, 1988.

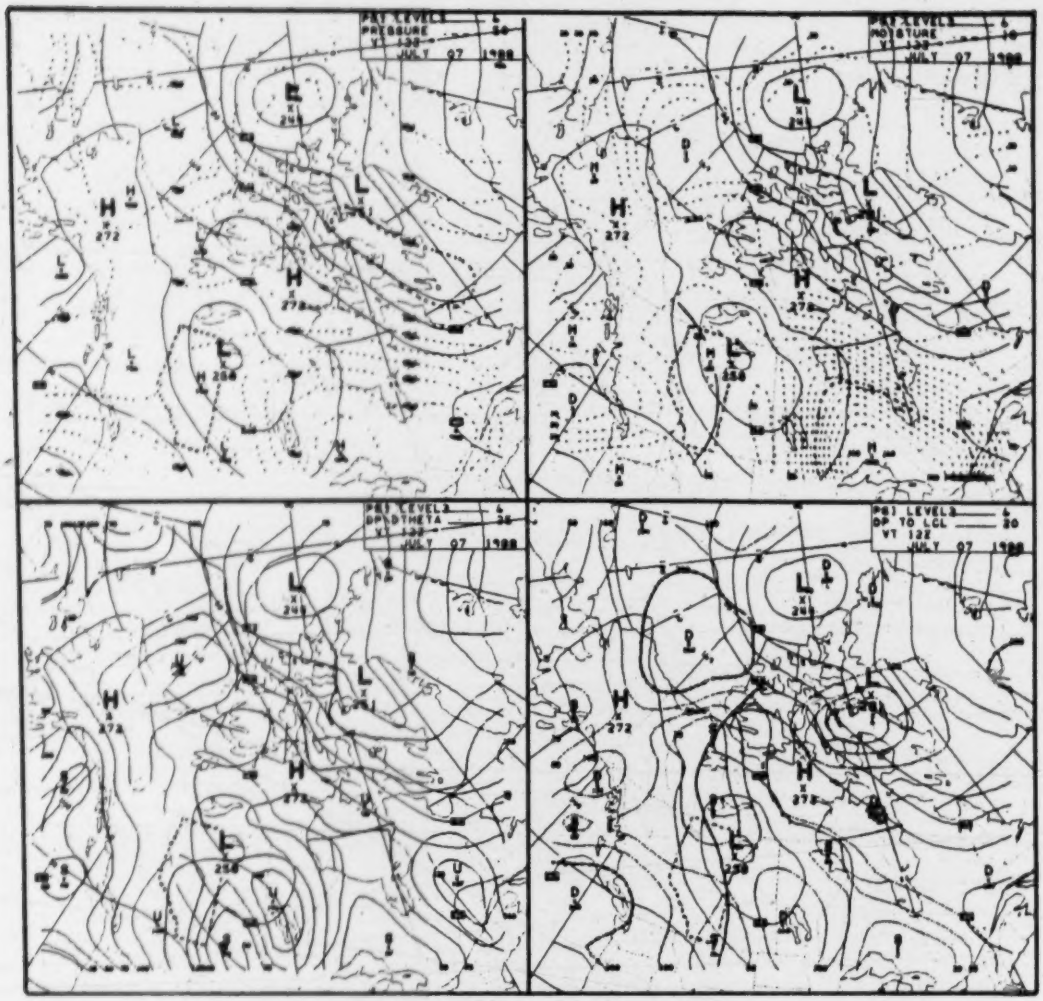

Figure 5.2: Lower level (298K) potential temperature analysis for 1200 UTC, 07 July, 1988.

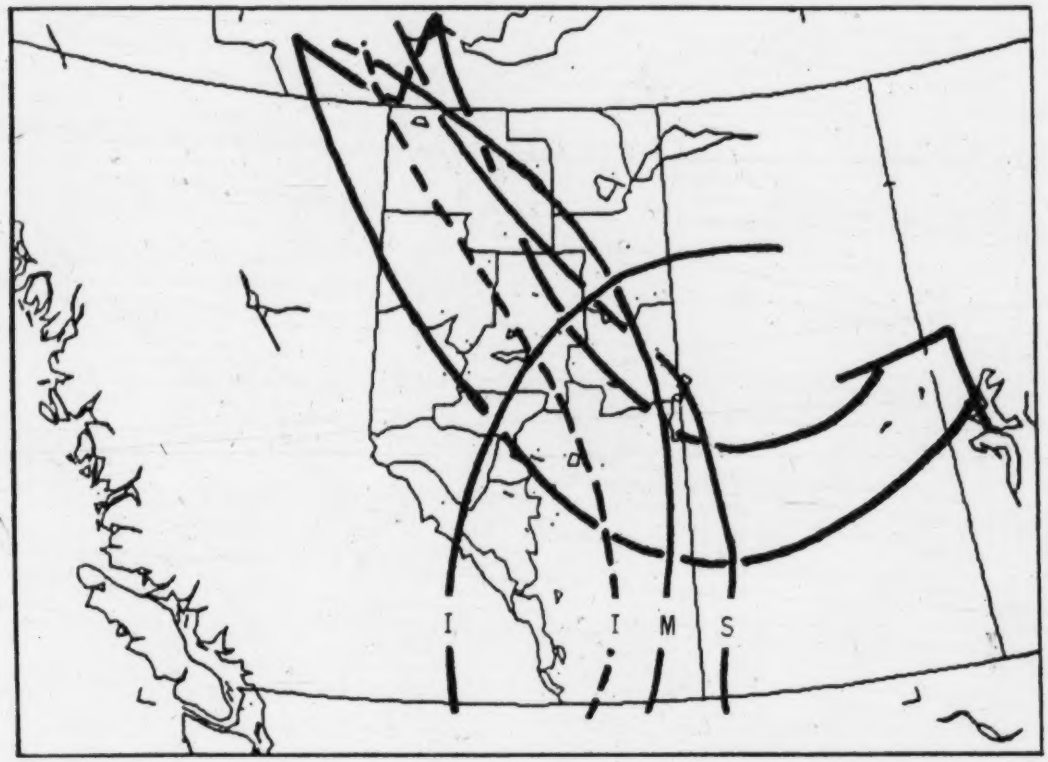

Figure 5.3: Composite chart for 1200 UTC, 07 July, 1988.

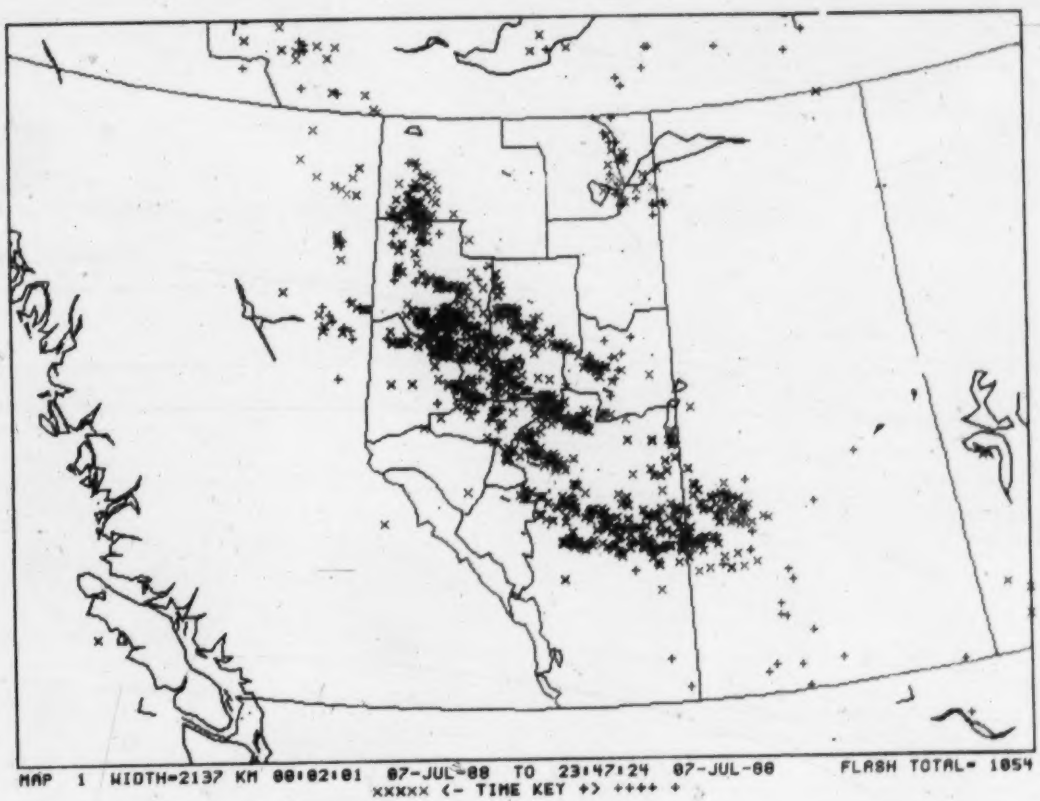

Figure 5.4: Lightning plot for 07 July, 1988.

5.2.2 09 August 1988

The upper and lower isentropic plots are given in Figure 5.5 and 5.6 respectively. Particular attention should be paid to the low-level instability axis in Figure 5.6. It is no coincidence that this instability "maximum" is found near the thermal axis, depicted in the height panel. The thermal maximum implies an axis of warm air at the low levels, effectively creating low-level instability. The moisture field on this lower surface is also maximized through Alberta, with a central maximum in Northeastern and Southwestern Alberta.

The upper-level panel, in Figure 5.5, displays less distinct parameter axes. A relatively strong westerly jet through Central and Southern Alberta and a moisture maximum in Southeastern B.C, are discernible. It should be noted that, as the upper level moisture centre advects into Southern Alberta, the potential instability will decrease there, due to the increase of moisture aloft. Significant convection, then, is not likely in the southern regions as the troposphere is becoming thermodynamically stabilized there. A weak axis of upper level instability penetrating into Central Alberta, along with a broad area of high relative humidity throughout Northern and Central Alberta are also indicated.

The composite chart in Figure 5.7 delineates the intersection of several isentropic parameters in Central Alberta. The wind maxima through central and southern regions intersect the low-level moisture and instability maxima in the Red Deer and Edmonton regions. This is where the main convective activity should be expected. As the convection develops, the strong westerly flow will drive the cells eastward into Eastern Alberta and Western Saskatchewan. Note that the composite chart denotes the low-level instability as only an axis. In reality, the instability is present along a band approximately 300Km wide. With this in mind, the convective threat may be extended to northern regions as well. It is important to realize that the axes traced on to the composite chart are only drawn for convenience and simplicity. A more accurate representation of the parameter maxima would be to trace the entire maxima "bands" or centres on the composite chart. However, if this were carried out, the composite analysis would soon become too cluttered to be useful as an operational tool.

Figure 5.8 shows the main convective activity confined to two areas. The convection through Central Alberta is well correlated with the area depicted by the intersection of the upper-level wind axis and the low-level instability centre. It appears as though these cells propagate rapidly eastward until the low-level radiational heat supply is cut

off. The convection to the north seems to be weaker, more scattered, possibly due to the absence of the wind axis through the area. Again, these cells have little upper level support, dissipating soon after sundown. No severe weather was reported on this day.

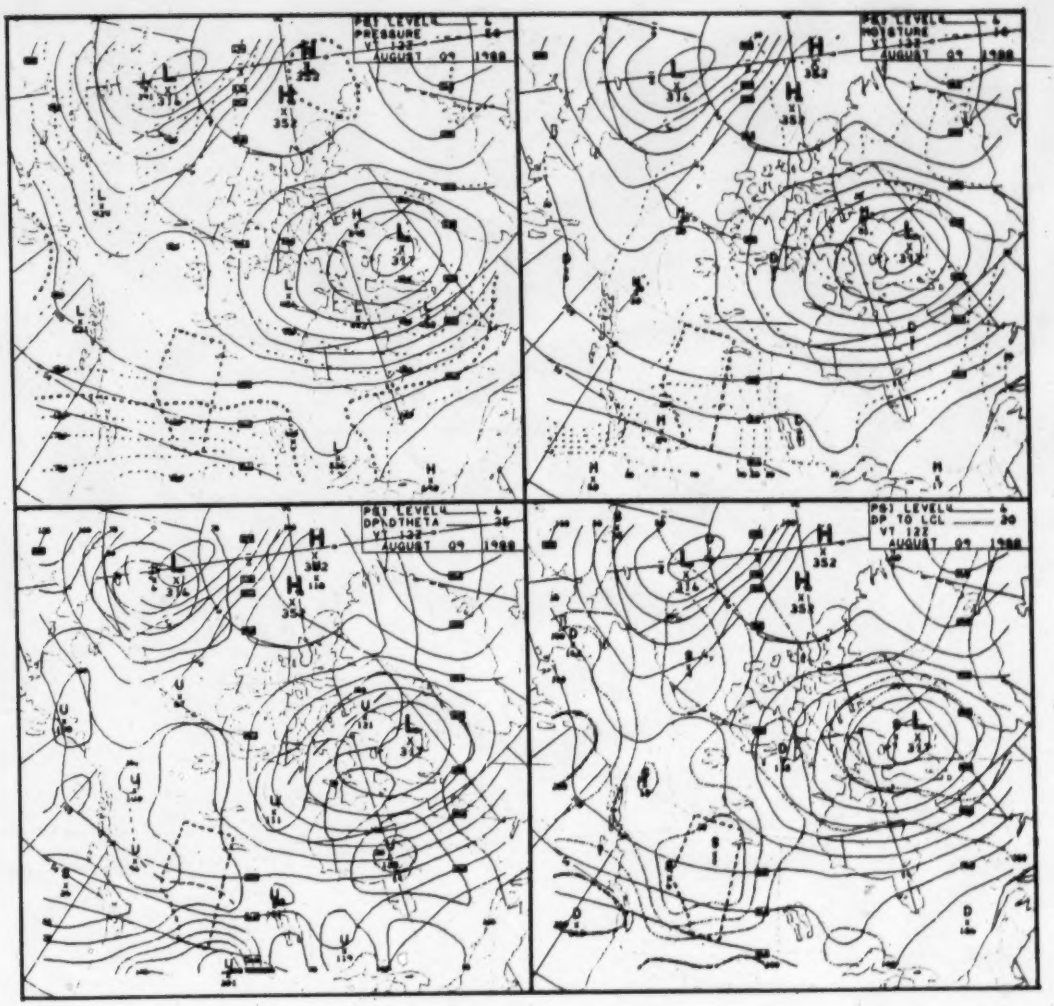

Figure 5.5: Upper level (308K) potential temperature analysis for 1200 UTC, 09 August, 1988.

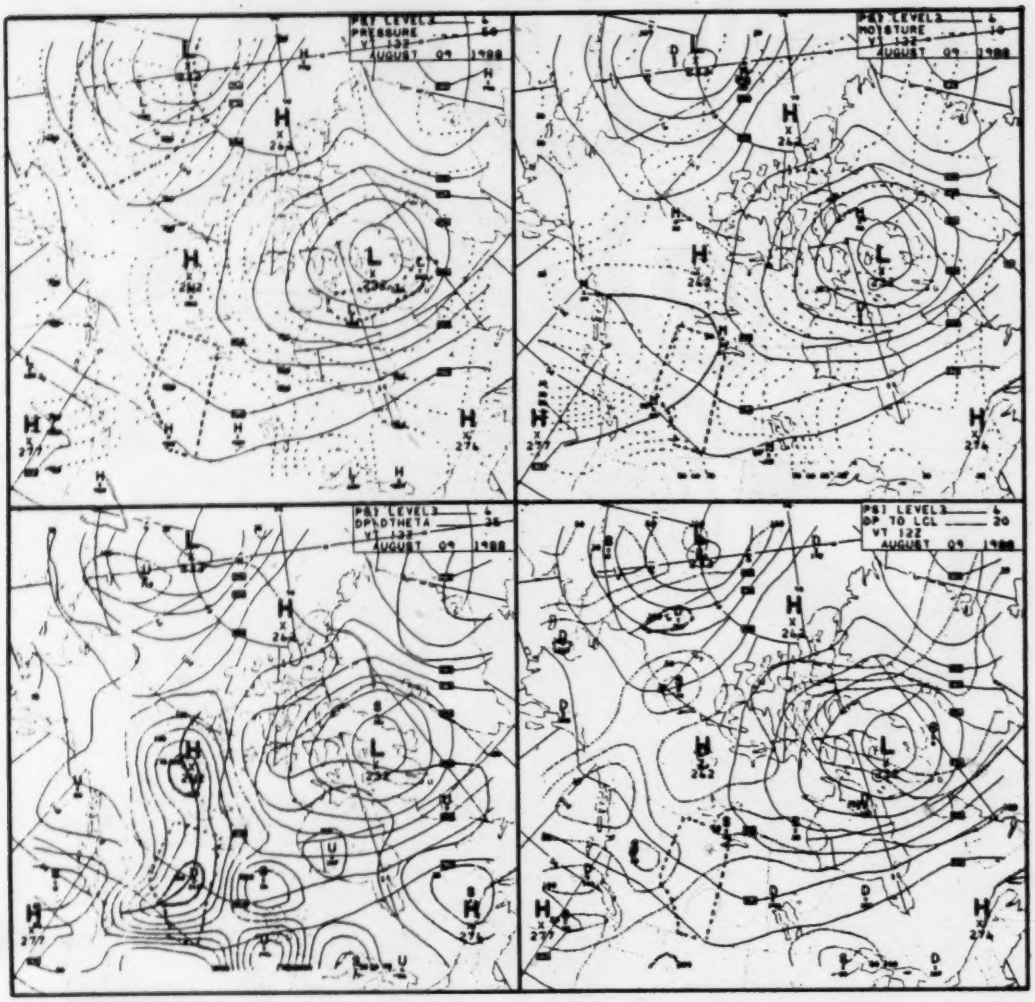

Figure 5.6: Lower level (298K) potential temperature analysis for 1200 UTC, 09 August, 1988.

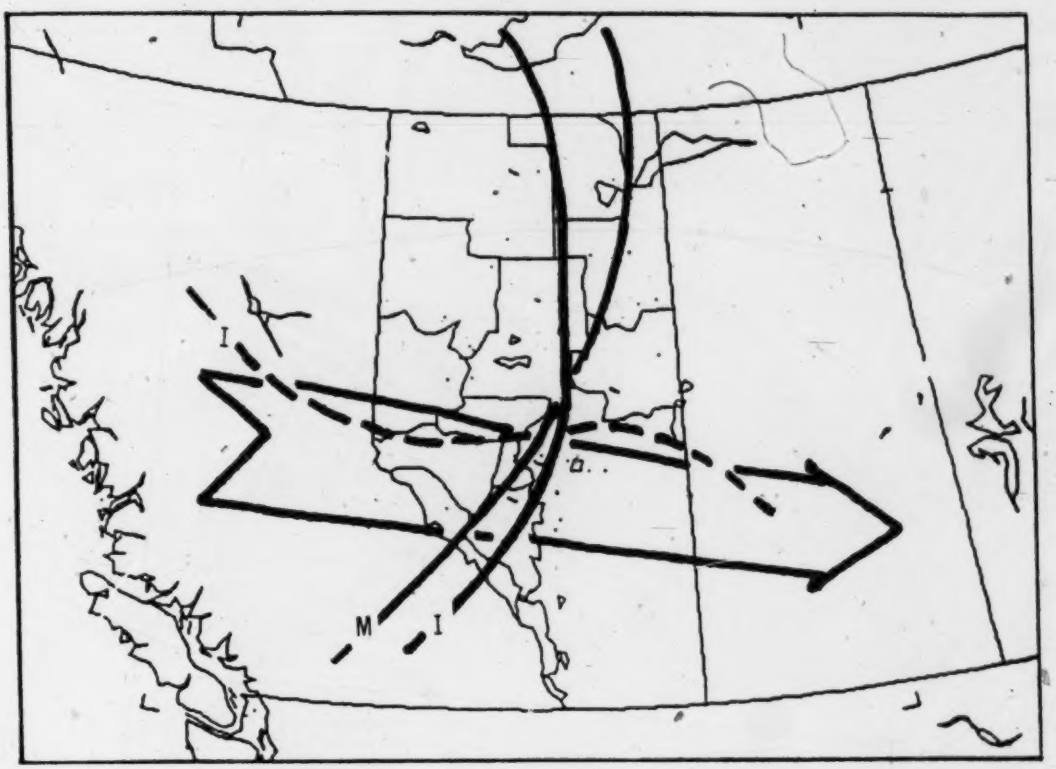

Figure 5.7: Composite chart for 1200 UTC, 09 August, 1988.

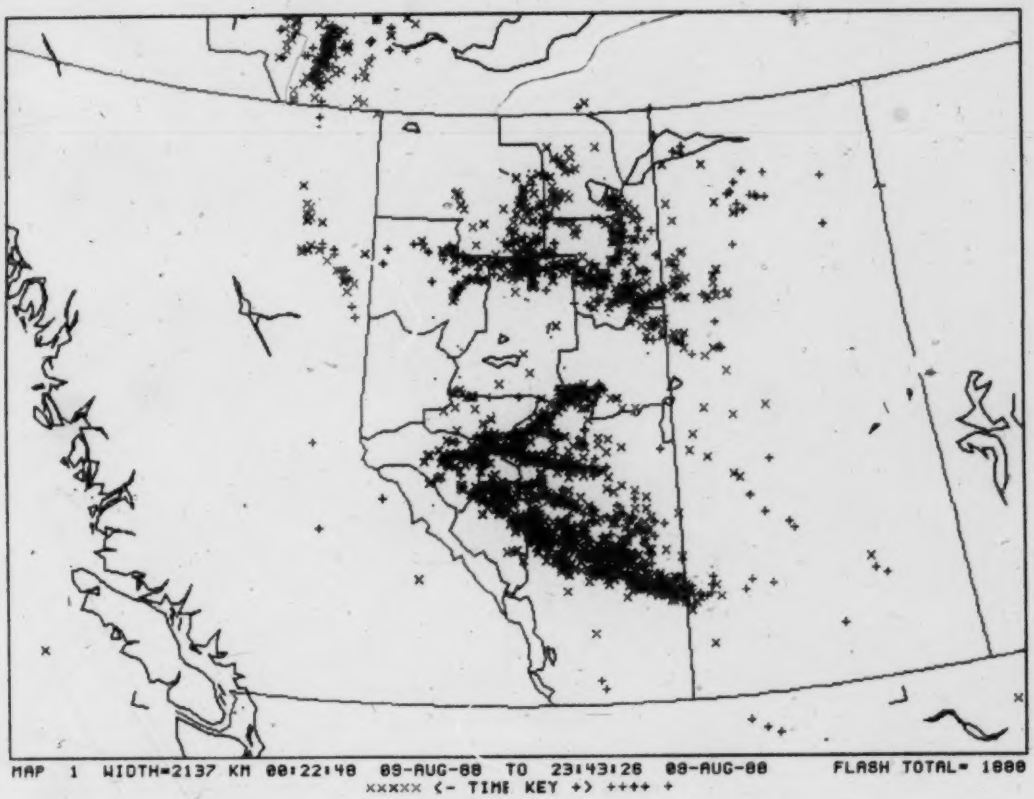

Figure 5.8: Lightning plot for 09 August, 1988.

5.2.3 11 August 1988

By quick inspection of the lower-level isentropic surface, Figure 5.10, a centre of instability is present in East-Central Alberta. It is associated with the low-level axis of warm air through Eastern Alberta underlying a local temperature minimum located in East-Central Alberta on the upper surface given in Figure 5.9. The vertical potential temperature gradient is smallest in this area, implying a static instability maximum. Because the flow at both levels is rather weak, this maximum can be expected to remain near East-Central Alberta during the day. An axis of low-level moisture is also indicated crossing the area, but it is considered weak, with values less than 6.0g/Kg. A weak axis of upper-level instability is also seen to run from the Central to Northeastern regions.

The composite analysis in Figure 5.11 tends to indicate that East-Central Alberta has the highest organization of isentropic parameters. The instability centre depicted on the lower analysis in this area indicates a preferred location for convection. However, the weak low-level moisture values, the lack of upper-level support, and the weak isentropic flow, suggest that the convective cells will be of little vertical extent and will dissipate rapidly.

The lightning plot (Figure 5.12) shows that the main convective activity occurred between noon and 8:00 pm local time in the East-Central Alberta and West-Central Saskatchewan regions. The storms were slow moving, as shown by the conglomerate of strikes in one area. The cells appear to be arranged in west-east lines, an orientation similar to the upper-level isotherms. The strikes in Southern Alberta and Southern Saskatchewan represent pre-analysis activity and are not of interest here. As found from the previous case, the lightning activity seemed to be well correlated near the intersection between the instability centre and the wind axis depicted on the 1200 UTC lower level analysis.

These three cases have shown that when thermodynamic and dynamic atmospheric forcing are weak, the static instability field in correlation with the wind maxima help to delineate the area of convective threat.

The following seven case studies consider more organized environments which tend to support stronger storm complexes.

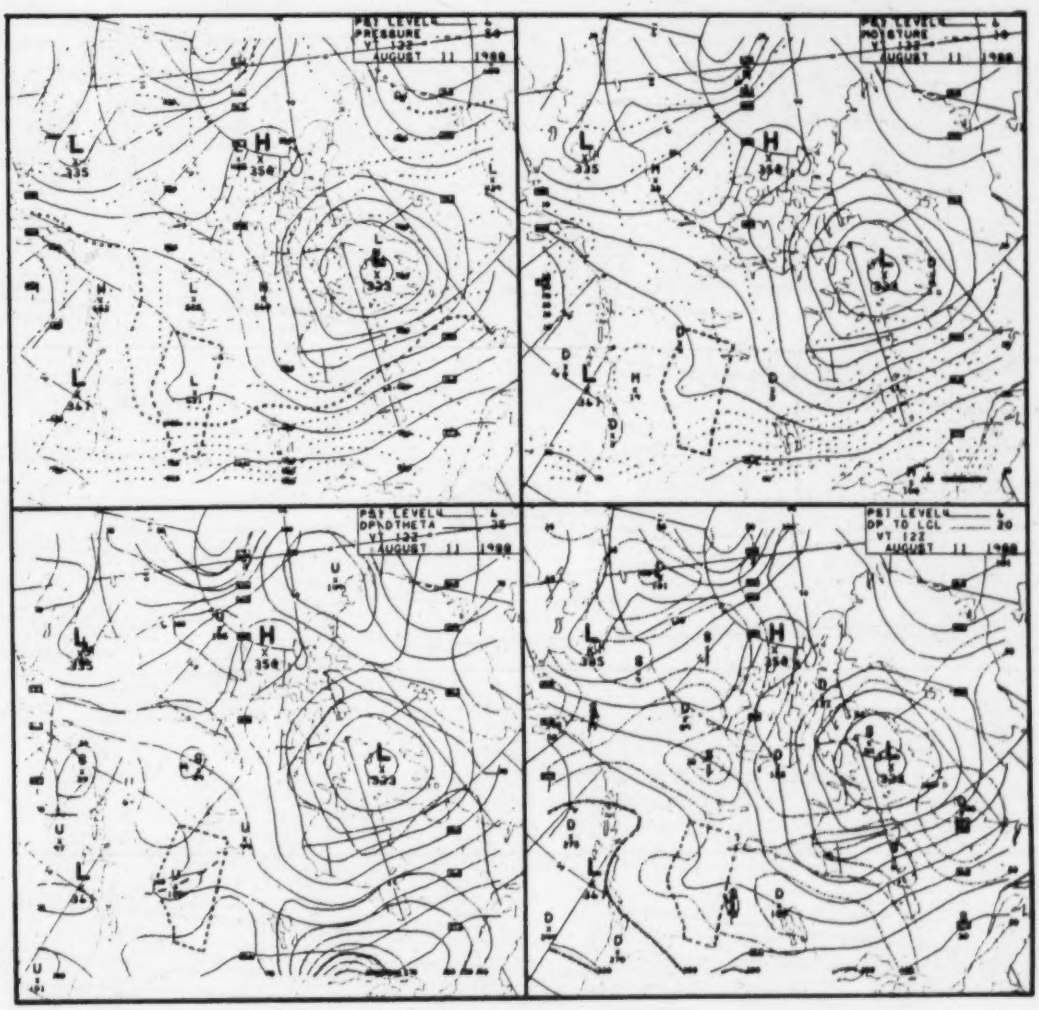

Figure 5.9: Upper level (308K) potential temperature analysis for 1200 UTC, 11 August, 1988.

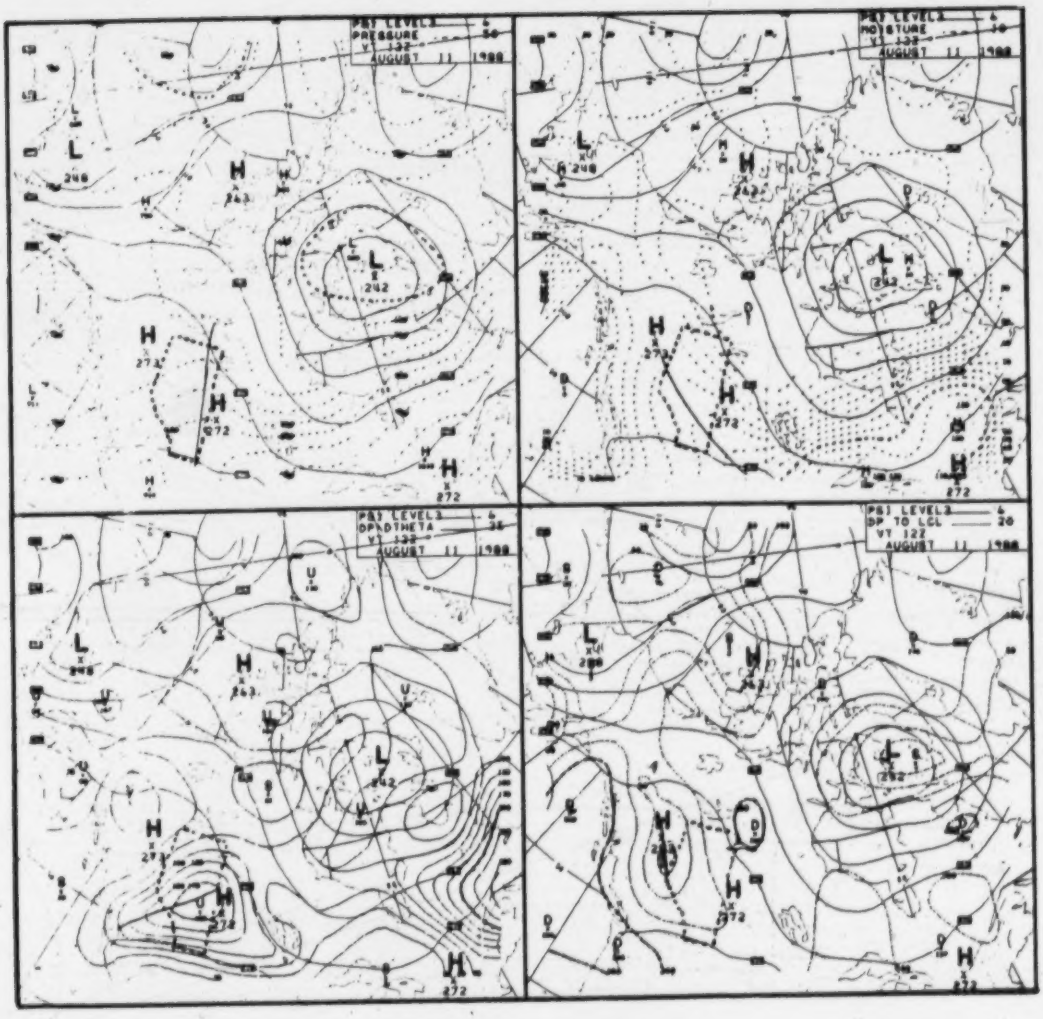

Figure 5.10: Lower level (298K) potential temperature analysis for 1200 UTC, 11 August, 1988.

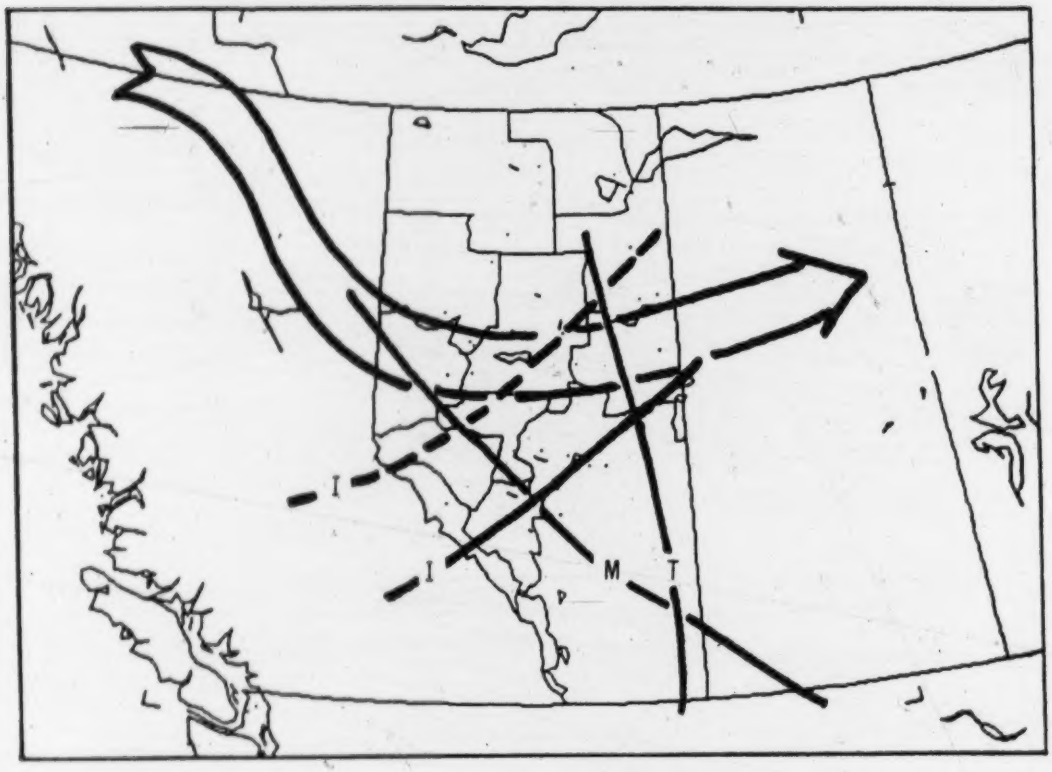

Figure 5.11: Composite chart for 1200 UTC, 11 August, 1988.

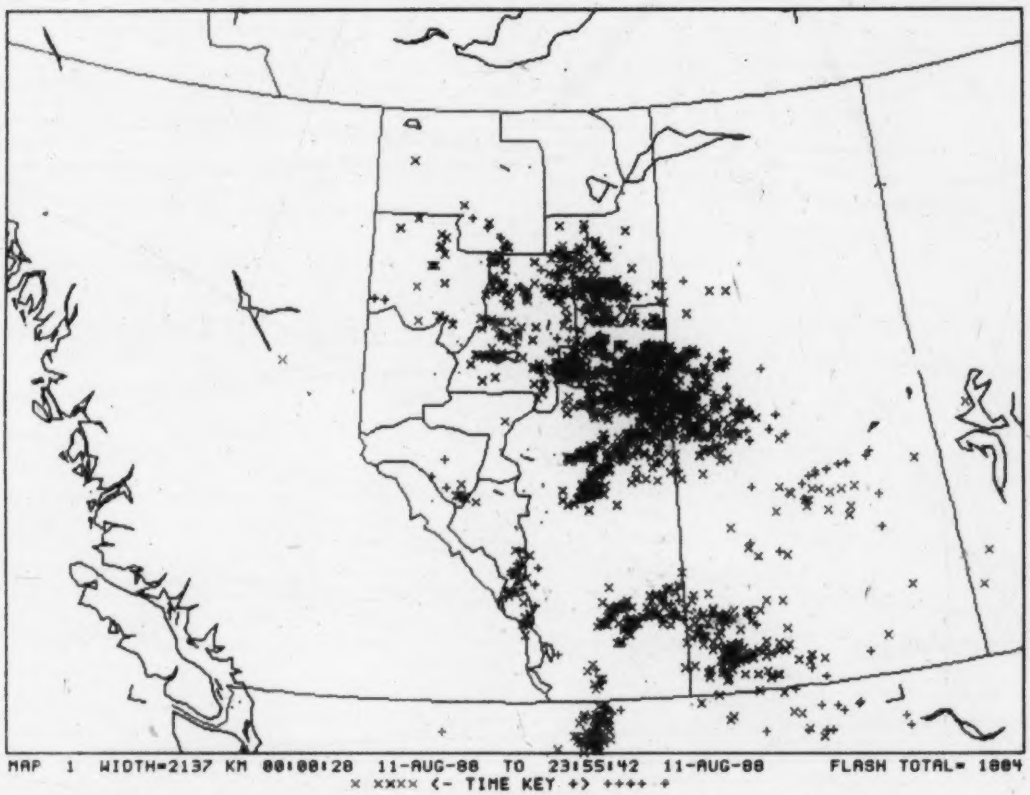

Figure 5.12: Lightning plot for 11 August, 1988.

5.2.4 22 June 1988

The upper-level analysis in Figure 5.13 depicts a high amplitude temperature axis along with a distinct axis of moisture through Northwestern Alberta and Northeastern B.C. A strong southwesterly flow is also present in this area, perpendicular to the temperature/moisture axes. This orientation suggests that these axes will be subjected to strong advection towards the northeast, implying strong advection of relatively cooler, dryer air into the region behind these maxima. The stability and relative humidity panels show the unstable, dry air associated with the temperature and moisture minima.

The lower panel in Figure 5.14 depicts well-defined thermal and moisture axes as well. However, their positions lag behind the corresponding upper-level maxima. This "out-of-phase" relationship indicates the existence of potential and latent instability, maximized in-between the positions of the upper and lower parameter axes. As the upper and lower isentropic fields propagate eastward, the cooler, dryer air aloft can be expected to overtake the low-level warm, moist air, since the upper-level flow is stronger. This differential advection increases the potential and latent instability within the air column, effectively destabilizing the atmosphere along an axis in-between the upper and lower temperature and moisture

maxima. The generation of instability through the air column should provide the upper level support needed to sustain convective activity past sunset and well into the night. The strength of this activity will depend largely on the amount of moisture in the low levels. The analysis depicts high moisture values in Southeastern B.C., but shows the moisture field decreasing rapidly towards northern regions. Axes of low-level instability and relative humidity reflect the low-level thermal and moisture maxima.

The composite analysis in Figure 5.15 only uses the upper and lower thermal and moisture axes, as well as the wind axis to delineate the zone of main convective threat. The greatest cooling and drying is indicated by the shaded area in the Fort St. John, Grande Prairie, Edson and Edmonton regions. Since the flow is quite strong, this well-organized instability will propagate northeastwards during the day. The main area of convection can be expected along an axis through Central and Northern Alberta, with an orientation similar to the shaded area marked on the composite analysis. Since the low-level moisture values are considered only moderate, and the upper-level isotherm gradient is not particularly strong, severe convective potential is not evident.

The main lightning activity shown in Figure 5.16 is confined to an axis from Central Alberta to Northeastern B.C. It began in the late afternoon in the Grande Prairie region but became extensive in the early and late evening hours. By inspection, the axis is well correlated with the upper-level moisture axis present and detectable up to 18 hours earlier. However, by the time convective development began, this axis had moved downstream, leaving dryer air in its wake. Upper-level cooling then followed to destabilize the atmosphere further, providing support for the night-time convection. Since the activity had a similar orientation to the shaded area on the composite chart, the dominant processes producing the convection, differential temperature and moisture advection, can be inferred. No severe weather was reported with any of these storms.

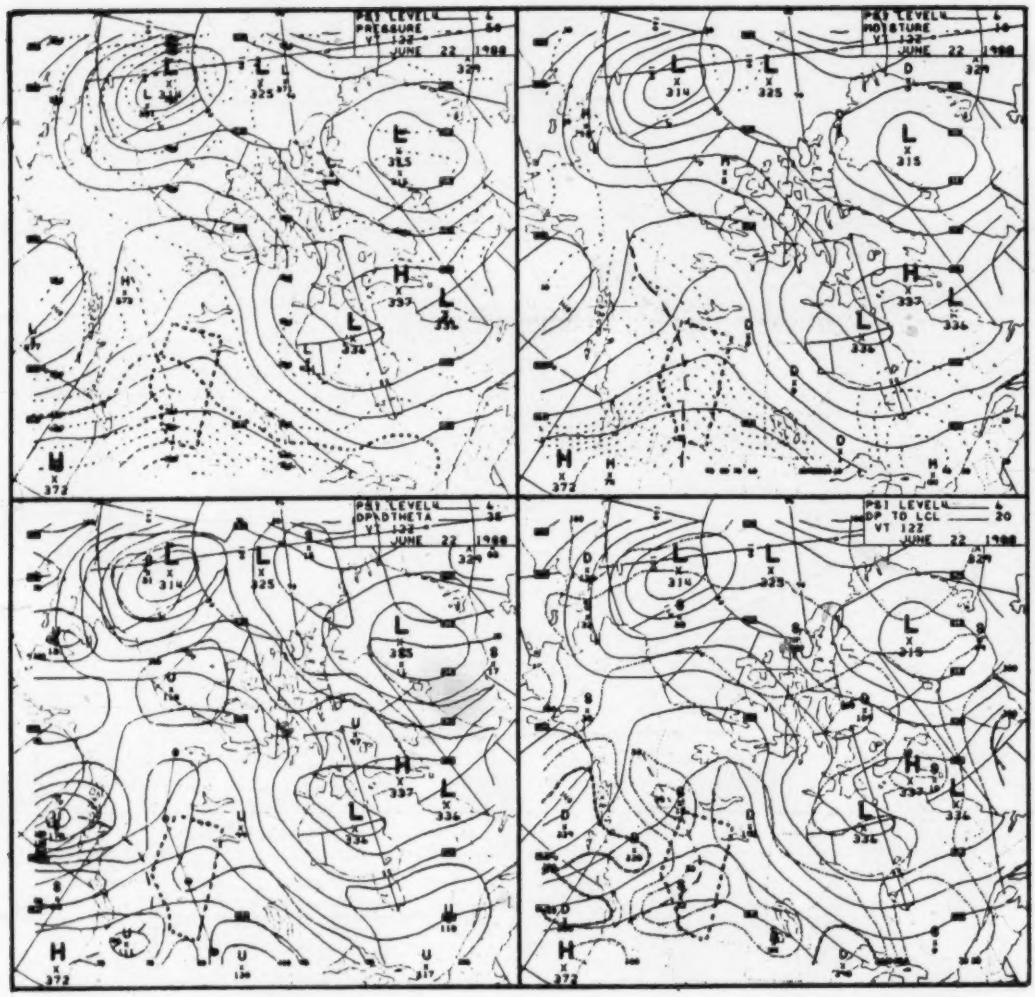

Figure 5.13: Upper level (308K) potential temperature analysis for 1200 UTC, 22 June, 1988. Line drawn on stability panel represents cross-section plane given in Appendix C, Figure C1.

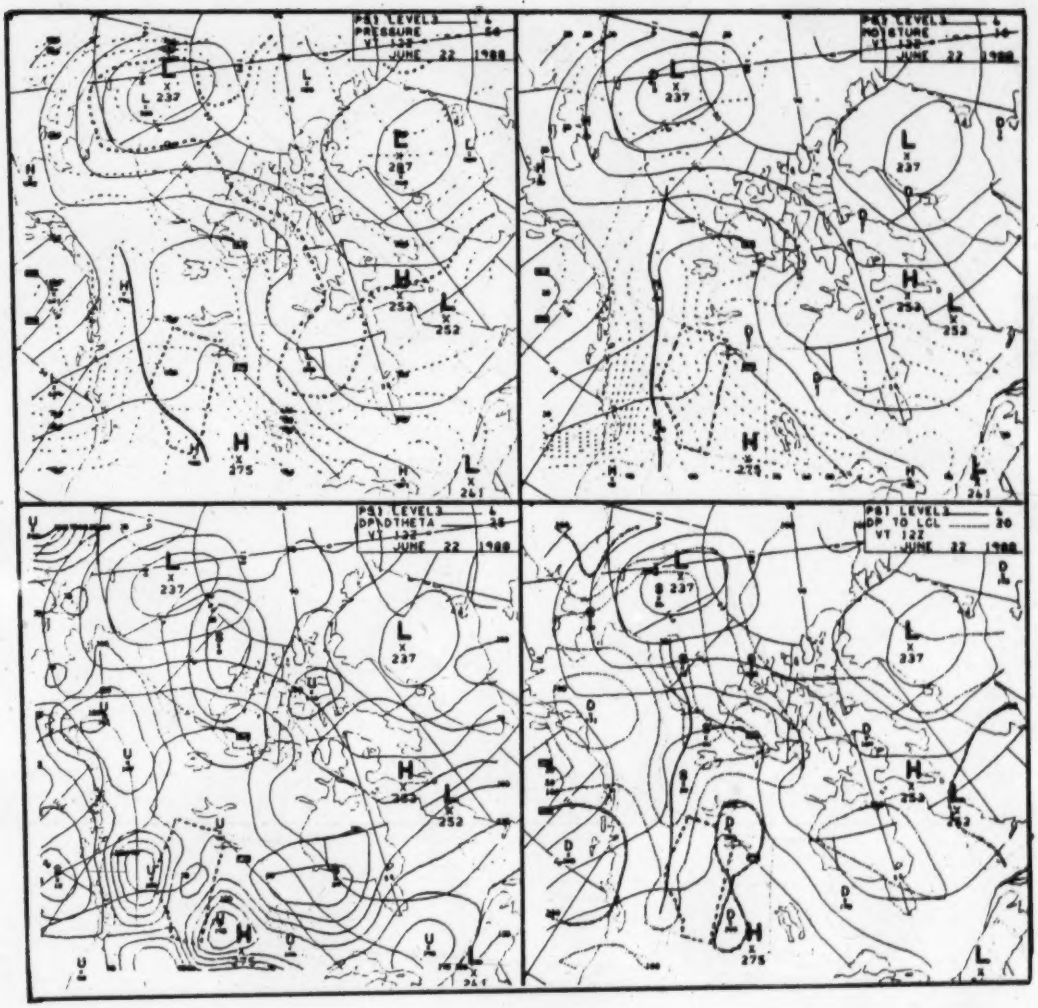

Figure 5.14: Lower level (298K) potential temperature analysis for 1200 UTC, 22 June, 1988.

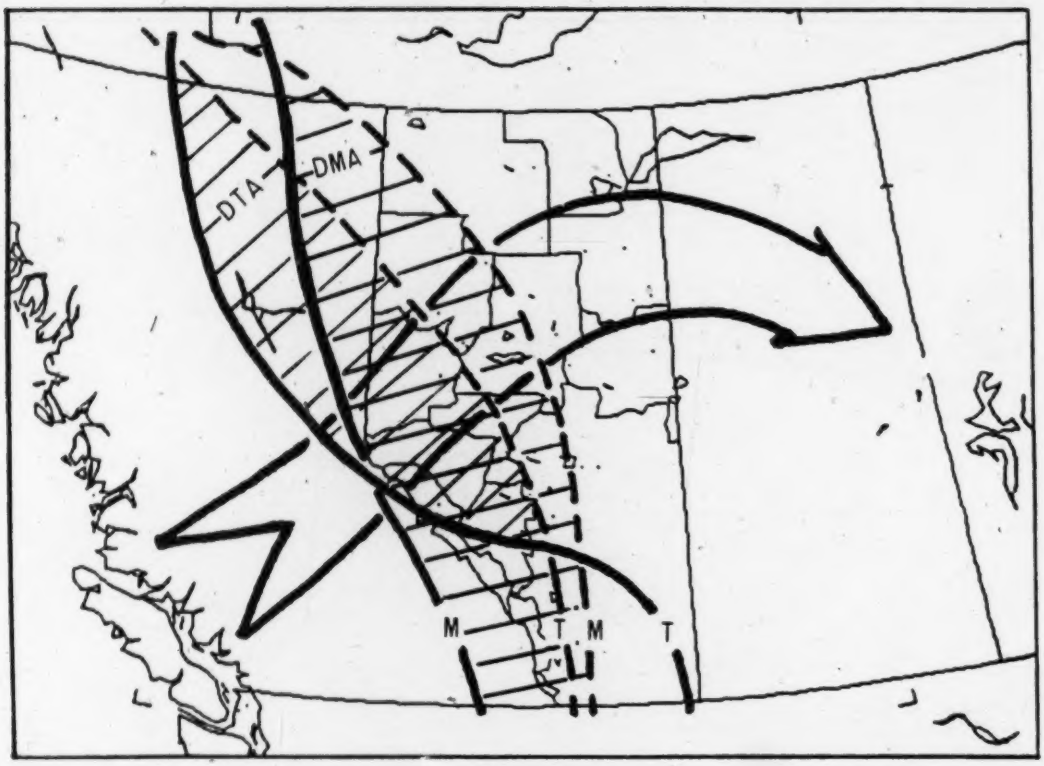

Figure 5.15: Composite chart for 1200 UTC, 22 June, 1988.

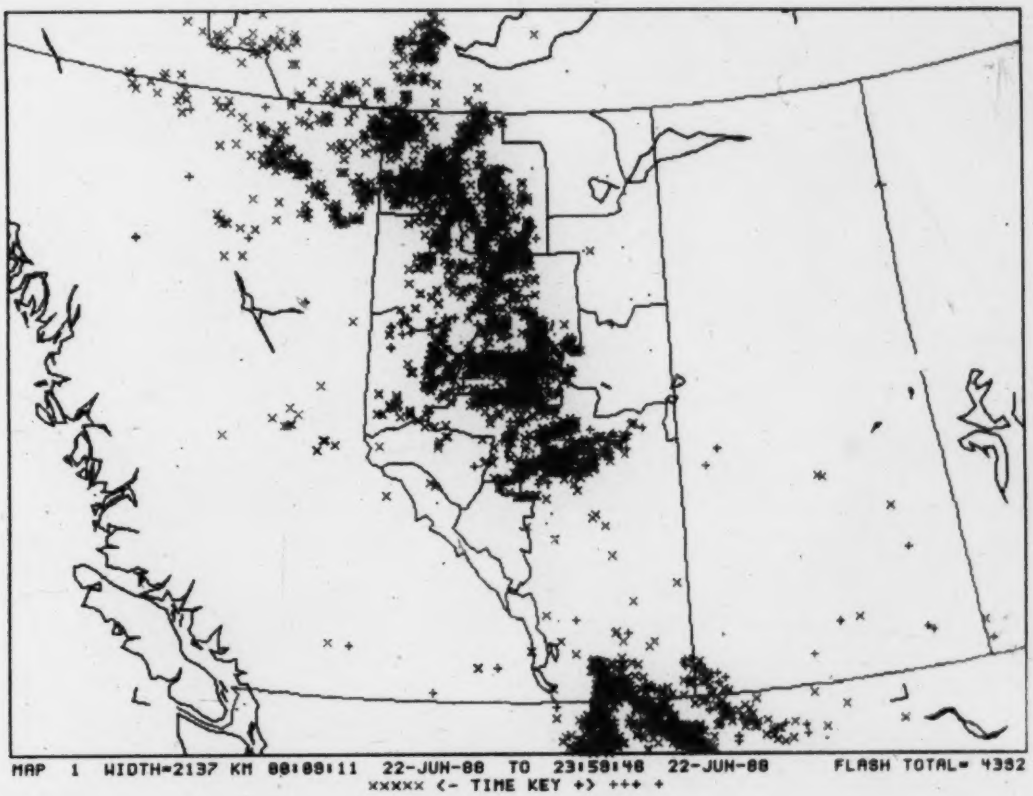

Figure 5.16: Lightning plot for 22 June, 1988.

5.2.5 20 July 1988

The upper-level isentropic analysis (Figure 5.17) displays temperature and moisture axes similar to those in the previous example. They extend into Northern B.C., where the streamline gradient tightens, indicating strong flow normal to temperature/moisture maxima. These axes can be expected to propagate eastward into Northern Alberta, leaving relatively colder, drier air behind. It should be noted that the bottom panels again reflect the instability and dry conditions along the temperature and moisture axes, respectively.

The lower-level analysis (Figure 5.18) depicts strong thermal and moisture axes in Northern B.C. as well. The local temperature maximum (Hx938) and the local moisture maximum (Mx83) in the Fort Nelson and Southern Mackenzie regions, indicate a maximum of low-level potential energy. Since the flow on this lower level is very weak, this maximum can be estimated to remain in this area during the day. The static-stability panel reveals relatively stable conditions throughout much of Alberta, suggesting the possibility of a broad low-level inversion acting to suppress low-level vertical perturbations throughout much of the province.

By comparing the two levels, the following diagnosis of the convective potential leading to a convective forecast can be made. As the upper-level thermal and moisture axes propagate eastward, the troposphere in Northeastern B.C. and Northern Alberta will actually be stabilized with the increase of mid-level temperature and moisture. However, as the cooler, dryer air replaces the warm, moist air behind the axes, the destabilization process begins. The greatest increase in buoyant energy will occur near low-level temperature and moisture maxima.

The composite chart in Figure 5.19 depicts strong upper-level advection of the thermal and moisture axes northeastward. By early evening, these axes can be estimated to be through Northeastern B.C. and the Southern Mackenzie region. Since the low-level moisture and thermal centres in the Fort Nelson and Southern Mackenzie regions can be expected to remain "quasi-stationary", a well-organized synoptic environment, able to support strong, possibly severe storms is evolving in the Northeastern B.C., Northern Alberta, and the Southern Mackenzie region.

The lightning plot in Figure 5.20 shows an area of intense activity along the 60th parallel. The convection appeared to become highly organized in the late evening, as the plot is dominated by an area of blue strikes. This possibly suggests that the strong convection was not so

dependent on radiational heating, but rather on the timing of the passage of upper-level temperature and moisture minima over low-level parameter maxima. Also, the lightning activity was confined to the northern regions, possibly due to the low-level stability and the slower propagation of the thermal axis into Central and Southern Alberta, effectively stabilizing the atmosphere in these areas.

Often, convective storms with high lightning intensities, similar to the storm in the Southern Mackenzie Valley, indicate severe storm strength. However, no severe weather was reported on this day, but accurate verification of severe events is difficult in these northern regions, because of the poor observing network.

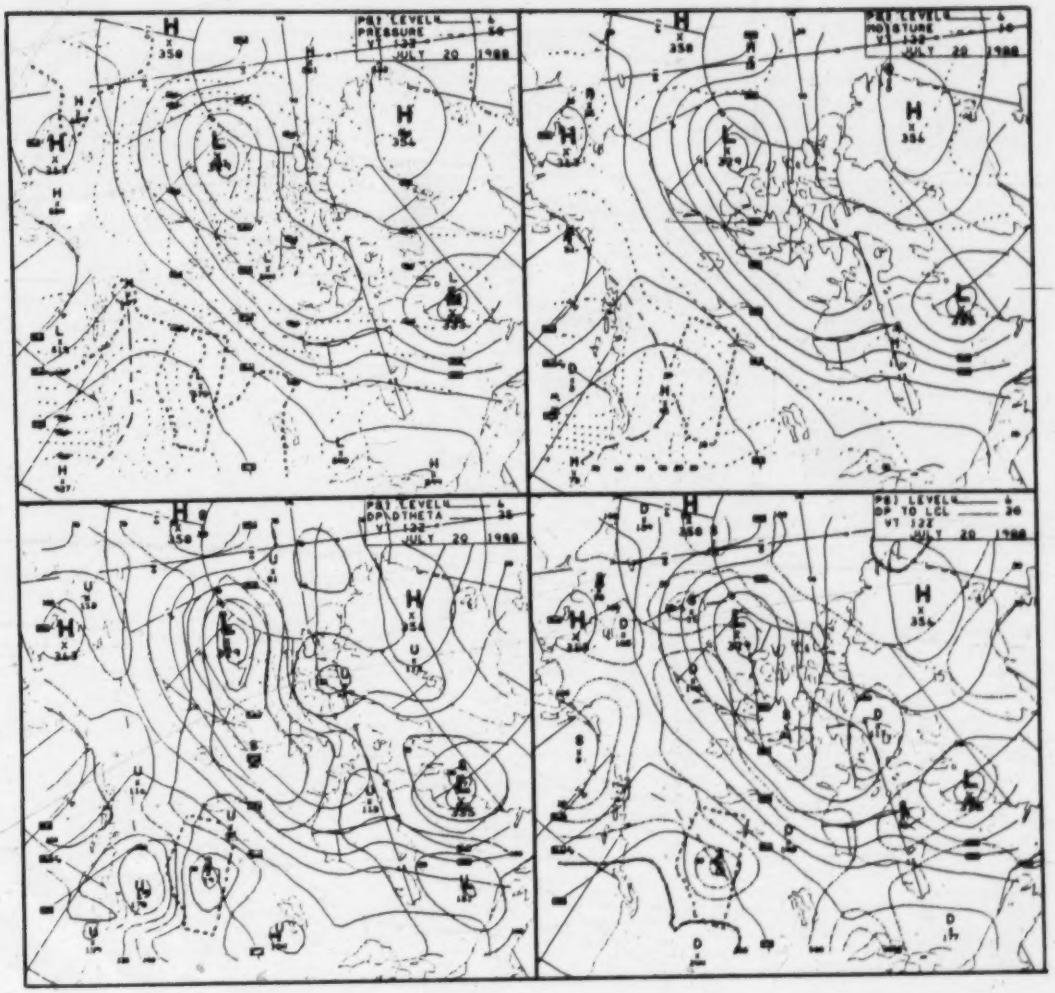

Figure 5.17: Upper level (308K) potential temperature analysis for 1200 UTC, 20 July, 1988.

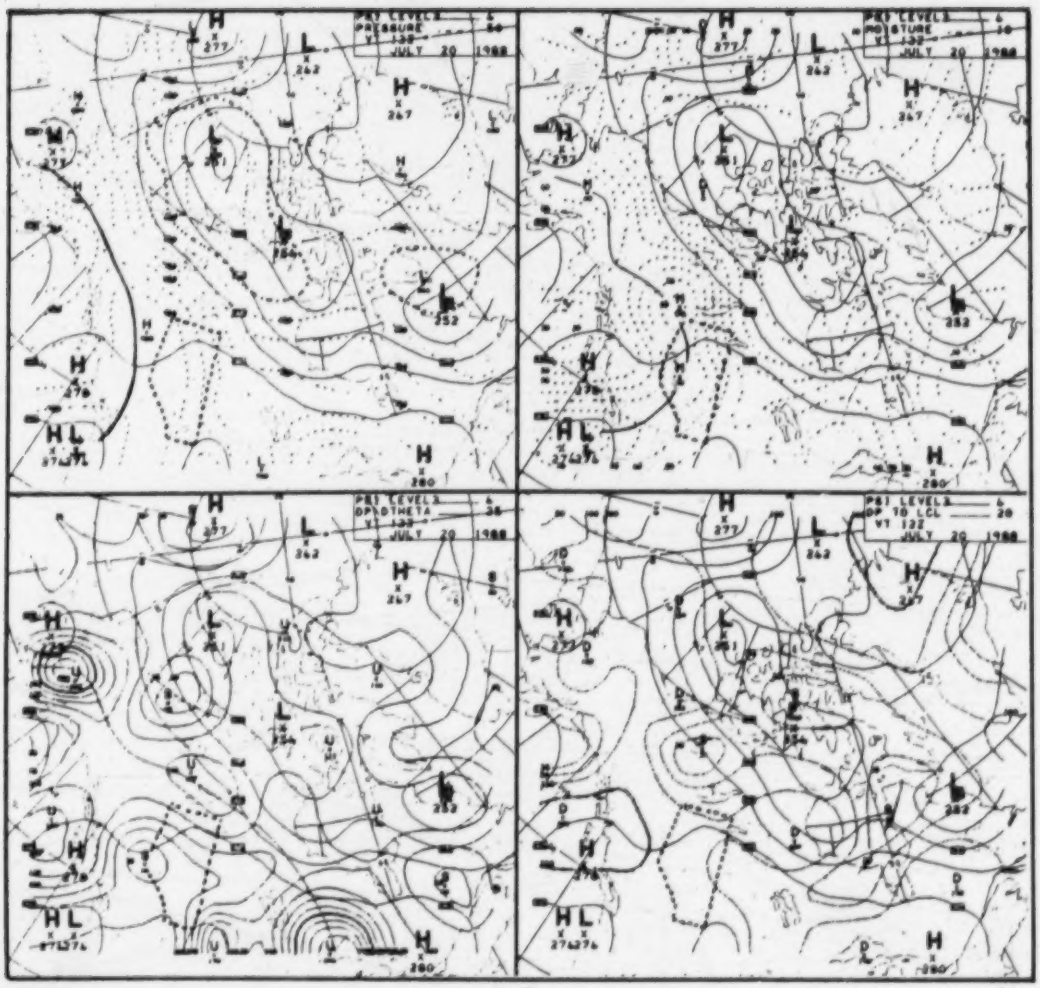

Figure 5.18: Lower level (298K) potential temperature analysis for 1200 UTC, 20 July, 1988.

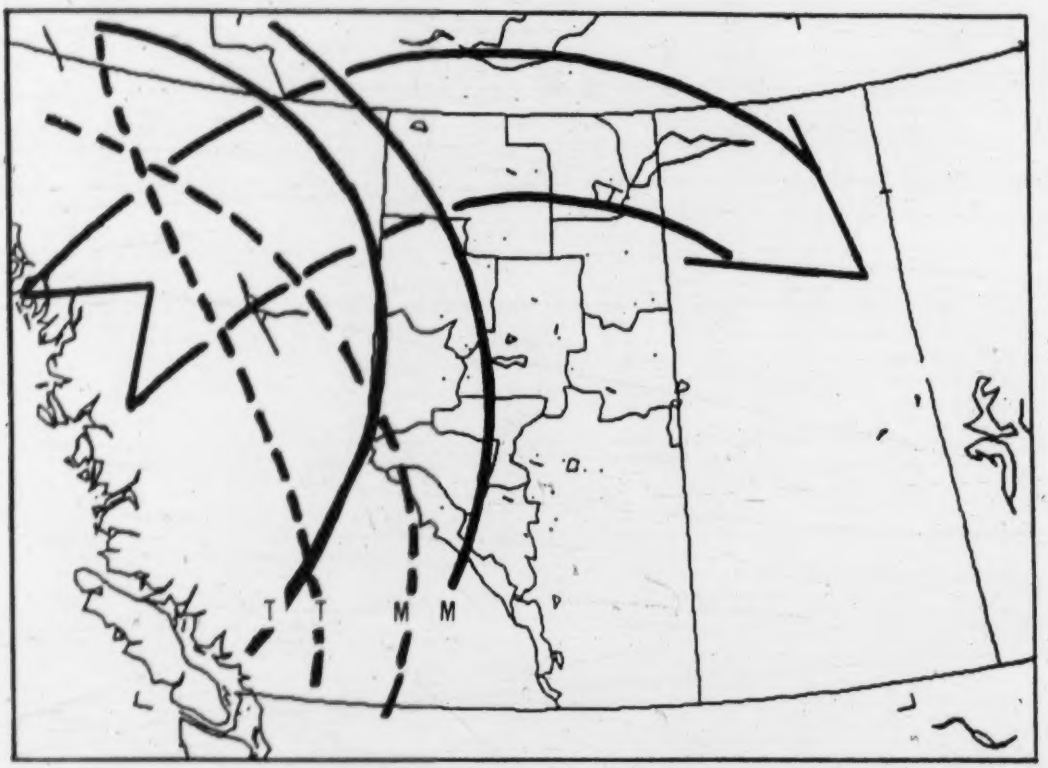

Figure 5.19: Composite chart for 1200 UTC, 20 July, 1988.

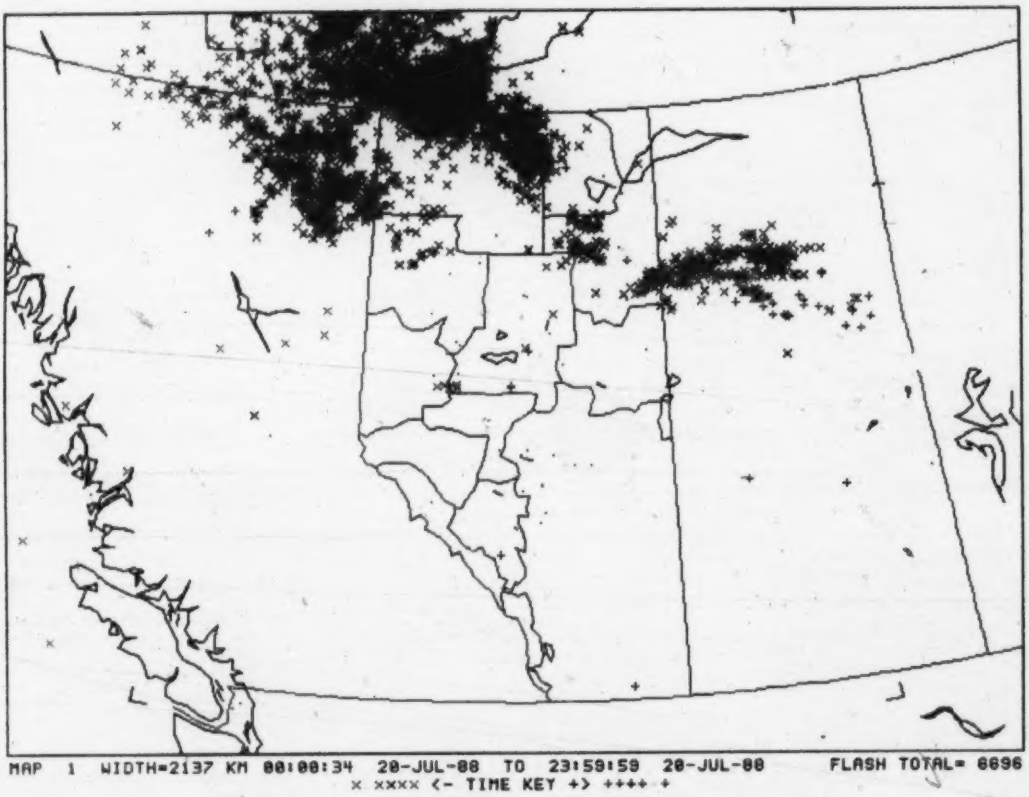

Figure 5.20: Lightning plot for 20 July, 1988.

5.2.6 11 July 1988

Figure 5.21 the upper-level chart depicts very well-defined, high-amplitude temperature and moisture axes from Southern Alberta to the Northern Mackenzie. A southerly flow through Western Alberta appears to be responsible for these axes, as positive temperature and moisture advection is evident throughout this region.

Similarly, the temperature and moisture maxima on the lower surface in Figure 5.22 are of high amplitude and have strong gradients on either side. However, these lower axes are seen to lie west of the upper level maxima. This indicates that the axis of warm, moist low-level air lies below the leading edge of the colder, drier conditions aloft (See Appendix C, Figure C2, for representative cross-section).

The composite analysis in Figure 5.23 depicts a well defined axis of high convective threat along the B.C-Alberta border, associated with the positions of the upper and lower parameter maxima. Since the upper flow parallels these axes, this area of potential risk should remain quasi-stationary along the Continental Divide throughout the day. The strength of this convective threat again depends largely on the low-level moisture near the convective area. The highest values of low-level moisture, near 8g/Kg in

Southern Alberta are not considered particularly high. However, the southerly flow is advecting higher values of moisture into the province, increasing the potential instability throughout the forecast region.

The lightning plot in Figure 5.24 displays over 23000 strikes, the highest strike total recorded in one day in 1988. The main activity began after 4:00 pm local time along the foothills. The activity became well organized along a line from Southern Alberta to Northeastern B.C. While the convection along the mountains was anticipated, the intense, well organized activity in Southeastern Alberta was not. A change in the flow pattern in Southern Alberta from southerly to westerly during the day was responsible for the strong convection there. Figure 5.25 displays the upper level analysis for 1200 UTC, 12 July, 1988, the next morning. Strong upper-level cooling and drying in southern regions, associated with the wind shift, is clearly evident from this later analysis. Of course, these changes were not anticipated, since neither the instability nor the advection of instability was properly diagnosed in southeastern regions. However, the isobaric progs could have been used to indicate a shift in the upper-level winds. Strong, differential advection, acting to destabilize the environment, could then have been anticipated throughout Southern Alberta, resulting in a forecast of strong convective threat for Southeastern Alberta as well. The

strong convective activity along the mountains propagated eastward and was supported well into the night and the next day, as seen from the next lightning plot (not shown). This suggests again that the convection was rooted with upper-level processes that propagated from west to east.

The only severe weather event reported on July 11 occurred in Grande Prairie where 30mm hail was reported. This event corresponds to the location where the upper-level wind maximum intersects the shaded area on the composite chart. In this area, good thermodynamics and dynamics are indicated, depicting the environment with the highest convective potential. The next morning, a storm near Wetaskiwin (Edmonton region) dumped 72mm of rain in less than two hours. This area is downstream of the previous severe environment, possibly suggesting that the intense convective potential may have remained organized throughout the night while propagating eastward, leading to redevelopment in the Edmonton region at the onset of radiational heating.

To summarize, the main convective threat area along the lee of the Rocky Mountains was well diagnosed as being present between the positions of the upper level thermal and moisture axes and the lower level thermal and moisture axes. The highly organized thermodynamic and dynamic

atmospheric structure provided support for the intense convective development which continued well into the next day.

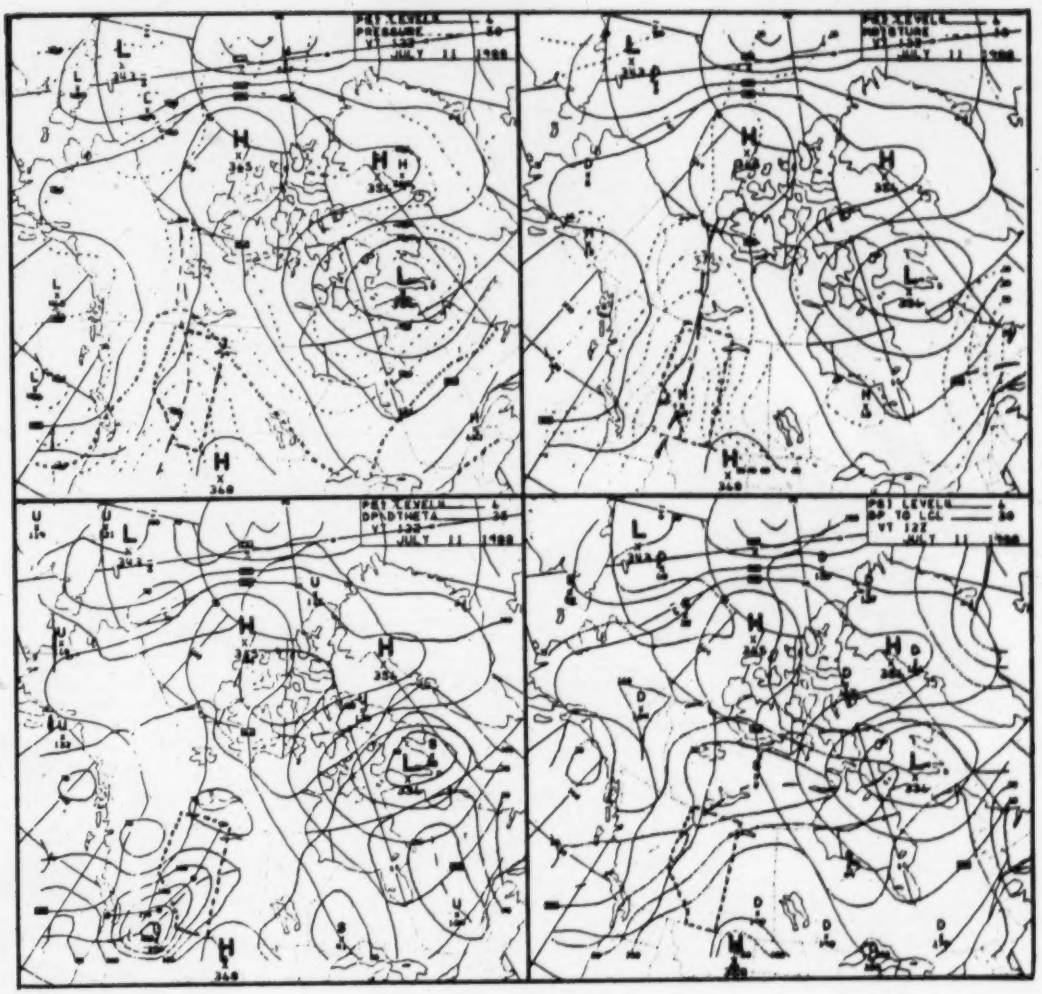

Figure 5.21: Upper level (308K) potential temperature analysis for 1200 UTC, 11 July, 1988. Line drawn on stability panel represents cross-section plane given in Appendix C, Figure C2.

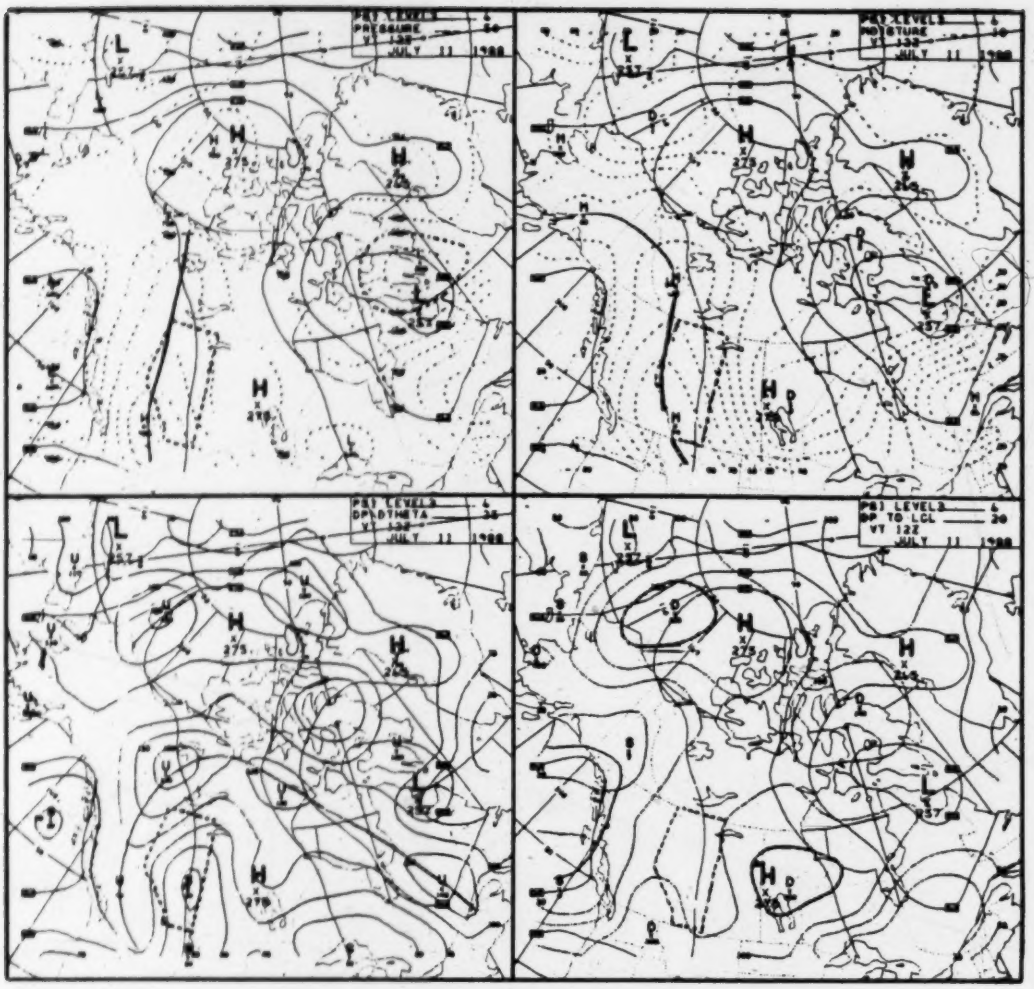

Figure 5.22: Lower level (298K) potential temperature analysis for 1200 UTC, 11 July, 1988.

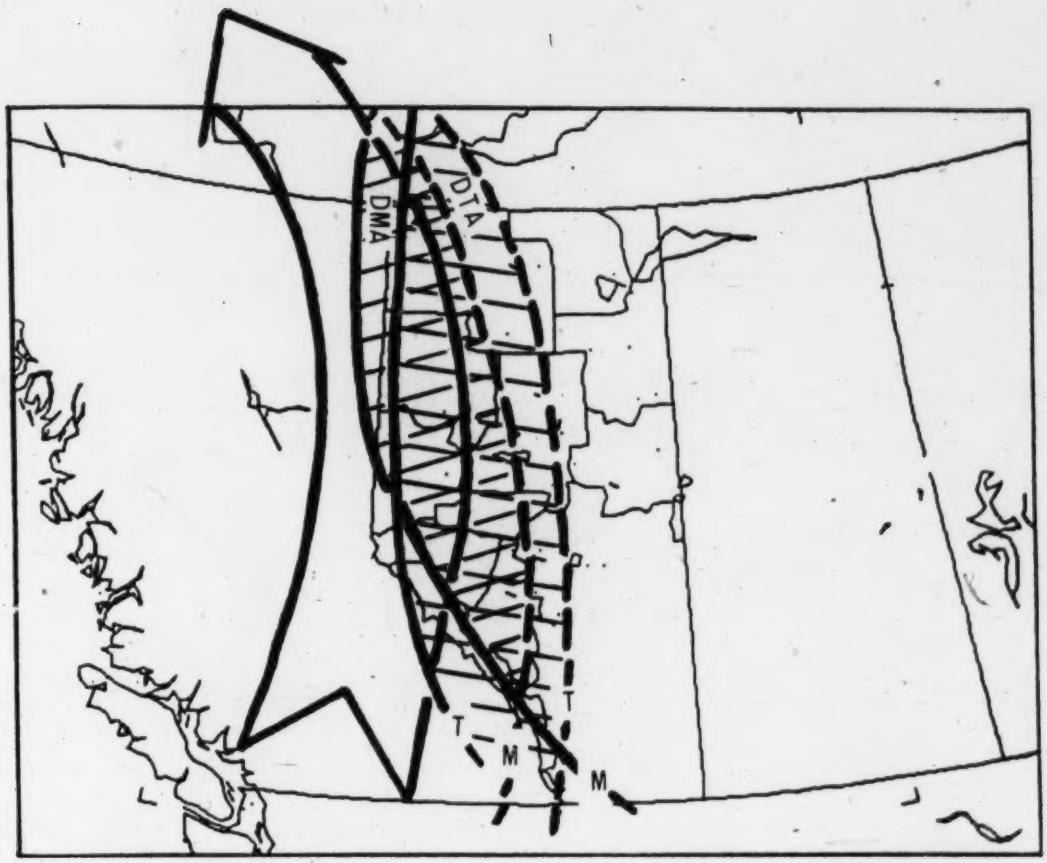

Figure 5.23: Composite chart for 1200 UTC, 11 July, 1988.

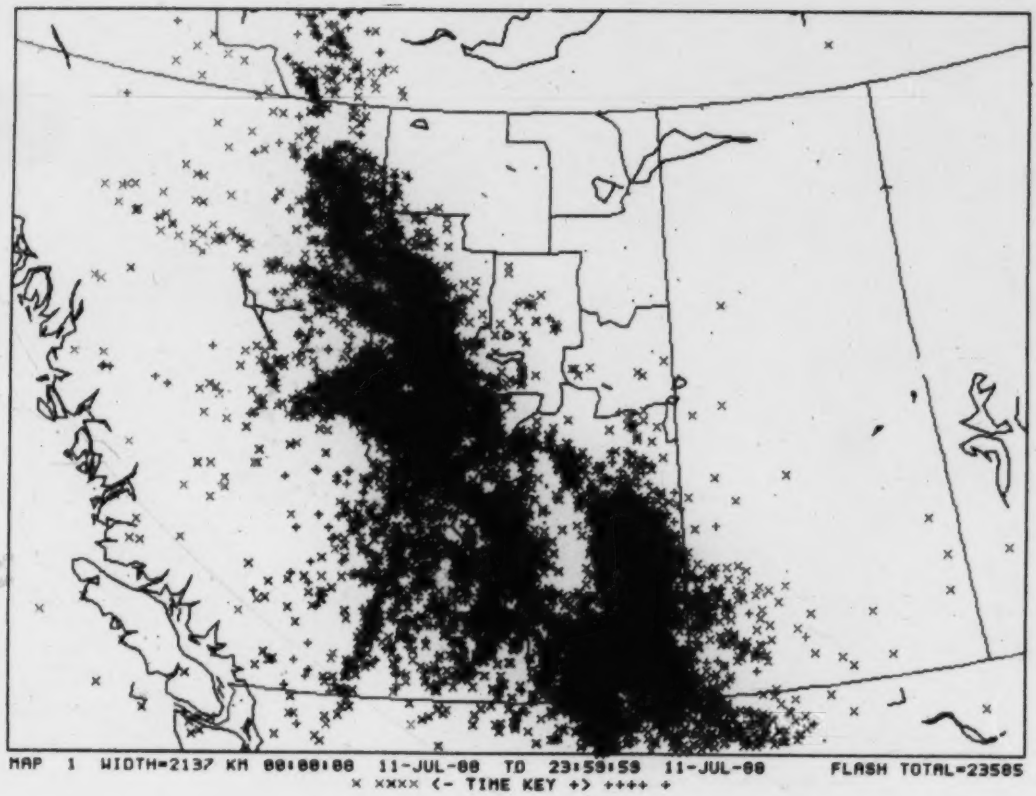

Figure 5.24: Lightning plot for 11 July, 1986.

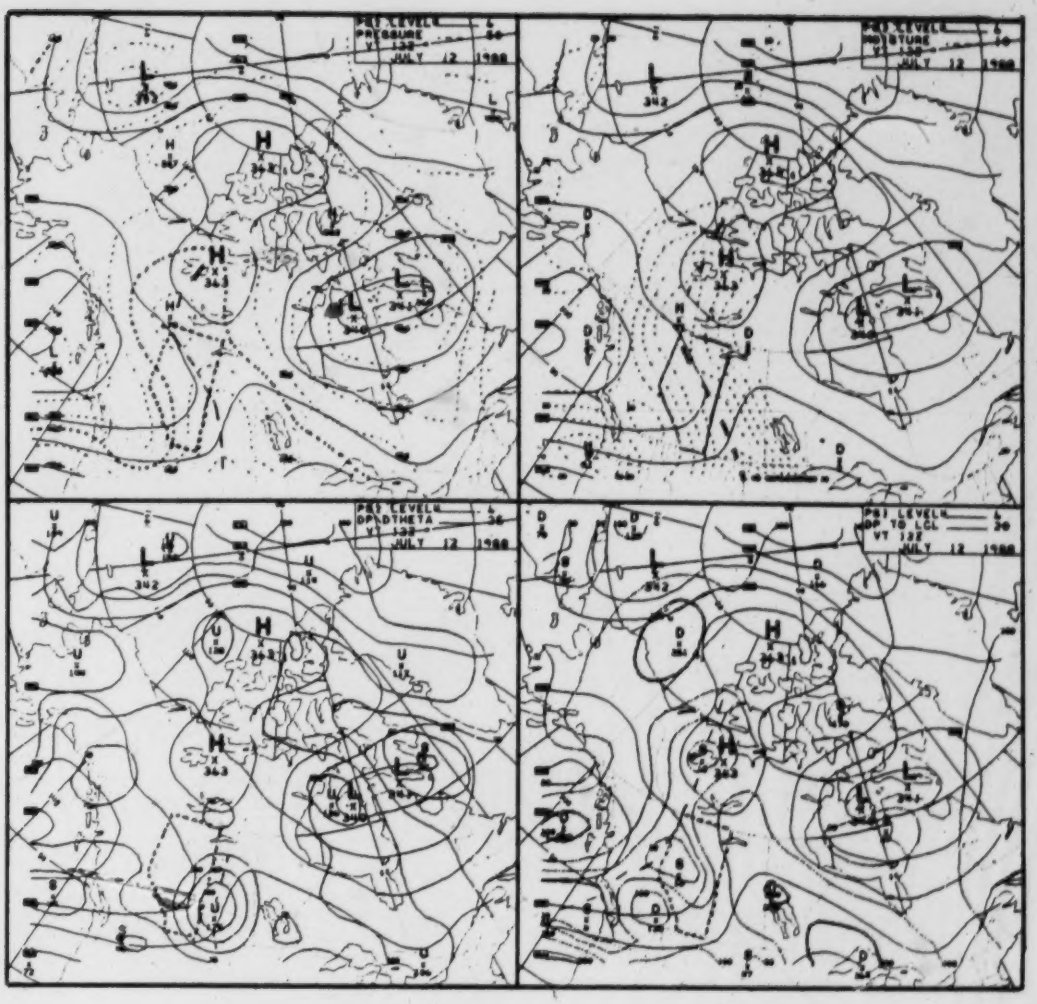

Figure 5.25: Upper level (308K) potential temperature analysis for 1200 UTC, 12 July, 1988 (24 hours after the analysis in Figure 5.21).

5.2.7 21 July 1988

The upper-level thermal and moisture axes through Alberta are very prominent features in Figure 5.26. The streamlines indicate a strong west-southwesterly flow through Central and Northern Alberta perpendicular to these maxima. By inspection, the strongest negative advection of temperature and moisture is seen to occur in the central and northwestern regions of the province. An instability axis is also present through Alberta, with a very strong centre in Central Alberta.

A prominent temperature axis extending well into the Mackenzie Valley with a centre in Northwestern Alberta, along with a moisture centre through Northern Alberta and Southern Mackenzie, are present on the low-level chart in Figure 5.27. A very weak westerly flow at this level, as seen from the base chart (not shown), indicates weak advection of these maxima to the east.

The area of strongest convective threat is again outlined by the differential temperature and moisture advection between the upper and lower parameter maxima. The composite chart, Figure 5.28, shows the Northwestern Alberta-Southern Mackenzie regions to have the highest convective potential, based on the positions of the low-level temperature and moisture maxima. Note that the

local moisture maximum (Mx88) in Northern Alberta is in excess of 8.0g/Kg, indicating high buoyant energies in these areas. The upper-level instability centre in Central Alberta also signals strong convective threat. However, since the west-southwesterly flow through the local instability maxima is strong, the threat area would be more accurately placed to the northeast of the instability "bullet". As mentioned earlier, it is difficult to estimate the changes in the static stability field. However, this particular maximum clearly reveals very significant mid-level instability (800mb, see cross-section in Appendix C, Figure C3) that can be estimated to propagate northeastward, considering the winds on the upper and lower surfaces. As this instability propagates downstream, it encounters higher low-level moisture values, eventually overtaking the moisture axis. Increasing convective potential develops as this instability propagates downstream.

The lightning plot in Figure 5.29 depicts two distinct, well-organized storms. The lightning confined to Northwestern Alberta began early and seems to be well correlated with the shaded area depicted on the composite analysis. The activity in Eastern Alberta and Western Saskatchewan can be correlated with the propagation of the upper-level instability centre. This particular storm intensified as it moved closer to the low-level moisture

axis. Because the lightning strike colors of both storms appear to be aligned along an orientation similar to the upper level temperature and moisture axes (southeast to northeast), the energy needed to sustain these convective complexes is found to be highly correlated with the passing of these upper-level maxima. The cooler, drier air behind these maxima destabilize the atmosphere, providing convective instability, greatest where the low-level parameters are maximized.

As further supporting evidence, the upper-level plot from the evening analysis (0000 UTC, July 22, 1988) is provided in Figure 5.30. It shows how the upper-level parameters became highly organized in Northwestern Saskatchewan only 12 hours after the morning analysis. The satellite picture in Figure 5.31 shows an intense storm well correlated with the location of these centres. A forecast of these isentropic fields would be extremely useful to help estimate their development. However, a correct diagnosis of the "morning" environment, estimating the propagation of the key parameters, delineates the high-risk area quite well.

Lightning with this intensity most often indicates severe convection. While there was no severe weather reported on this day, the accuracy of the verification is, however, suspect, since these areas are inhabited by few people.

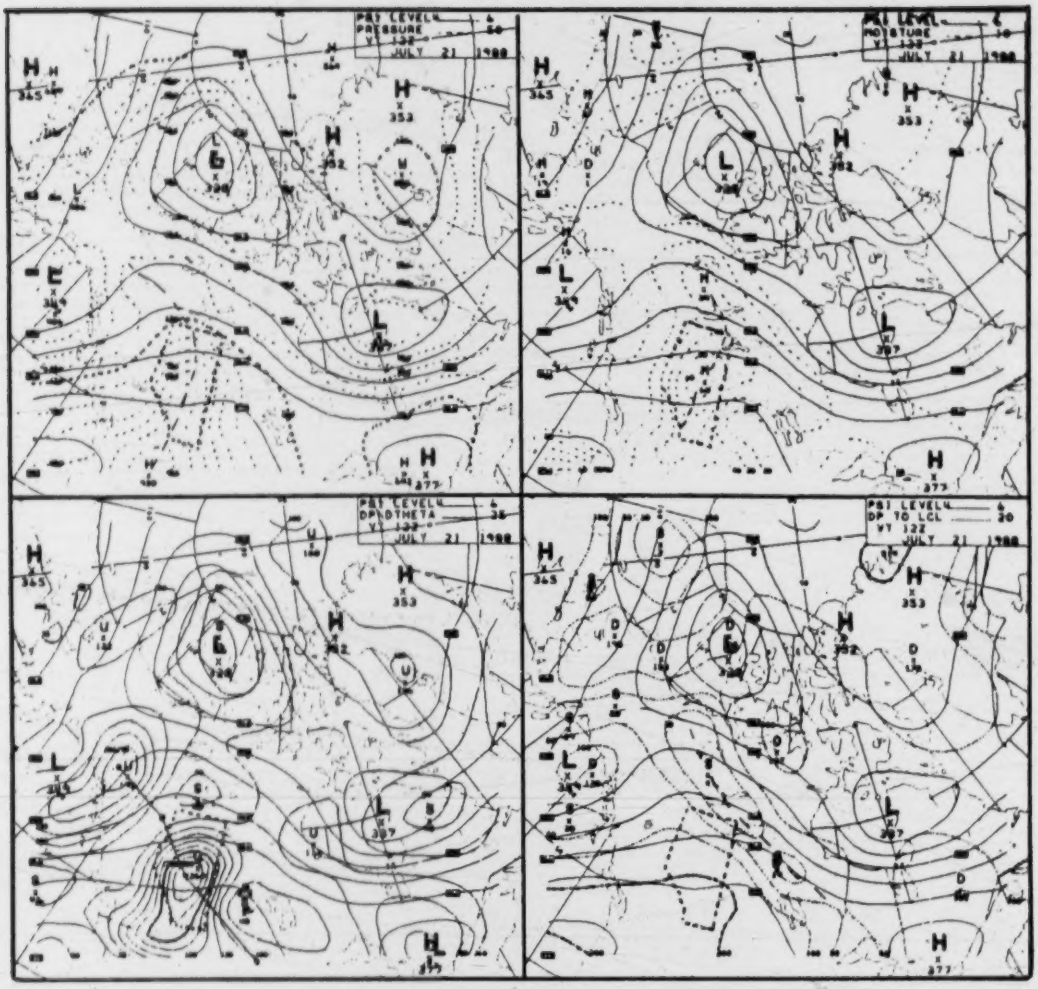

Figure 5.26: Upper level (308K) potential temperature analysis for 1200 UTC, 21 July, 1988. Line drawn on stability panel represents cross-section plane given in Appendix C, Figure C3.

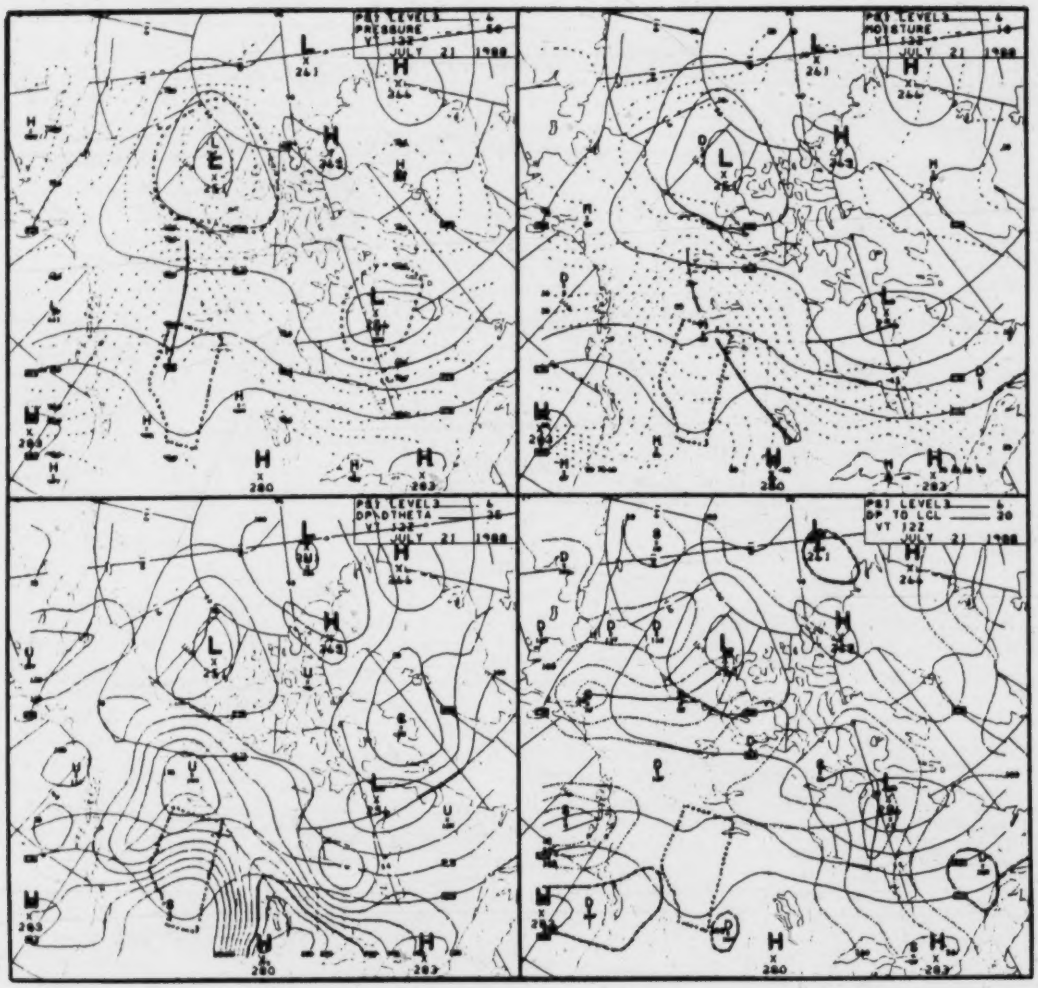

Figure 5.27: Lower level (298K) potential temperature analysis for 1200 UTC, 21 July, 1988.

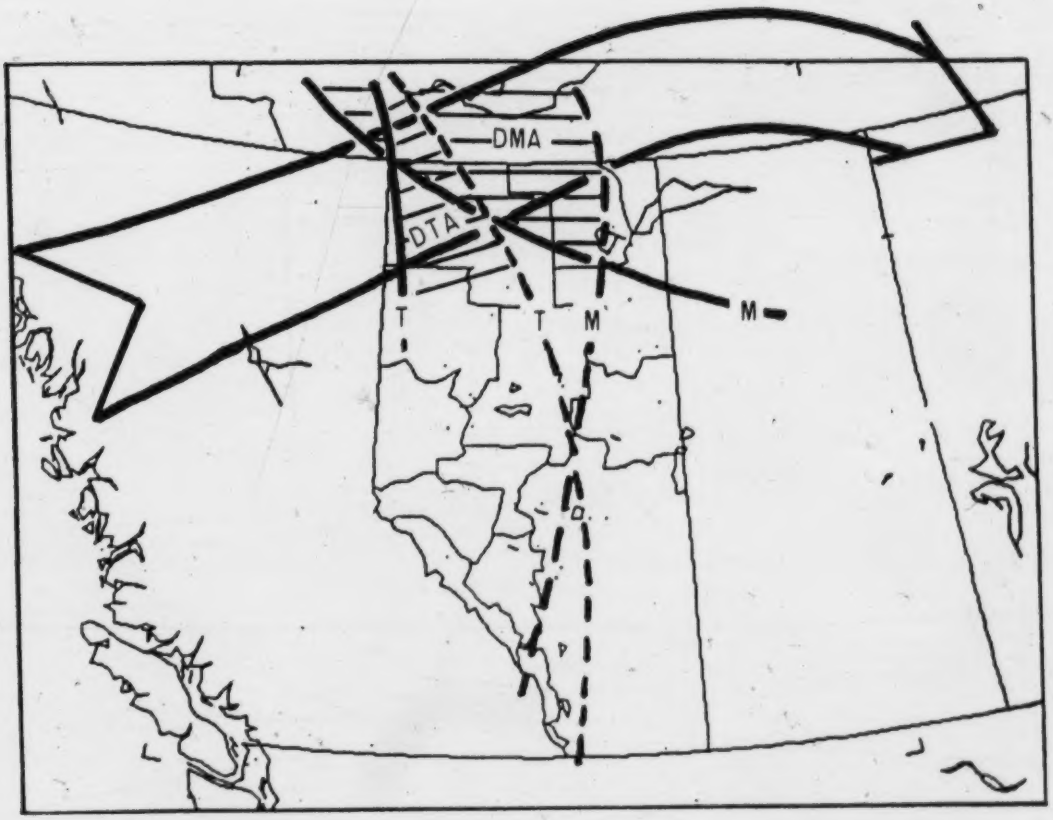

Figure 5.28: Composite chart for 1200 UTC, 21 July, 1988.

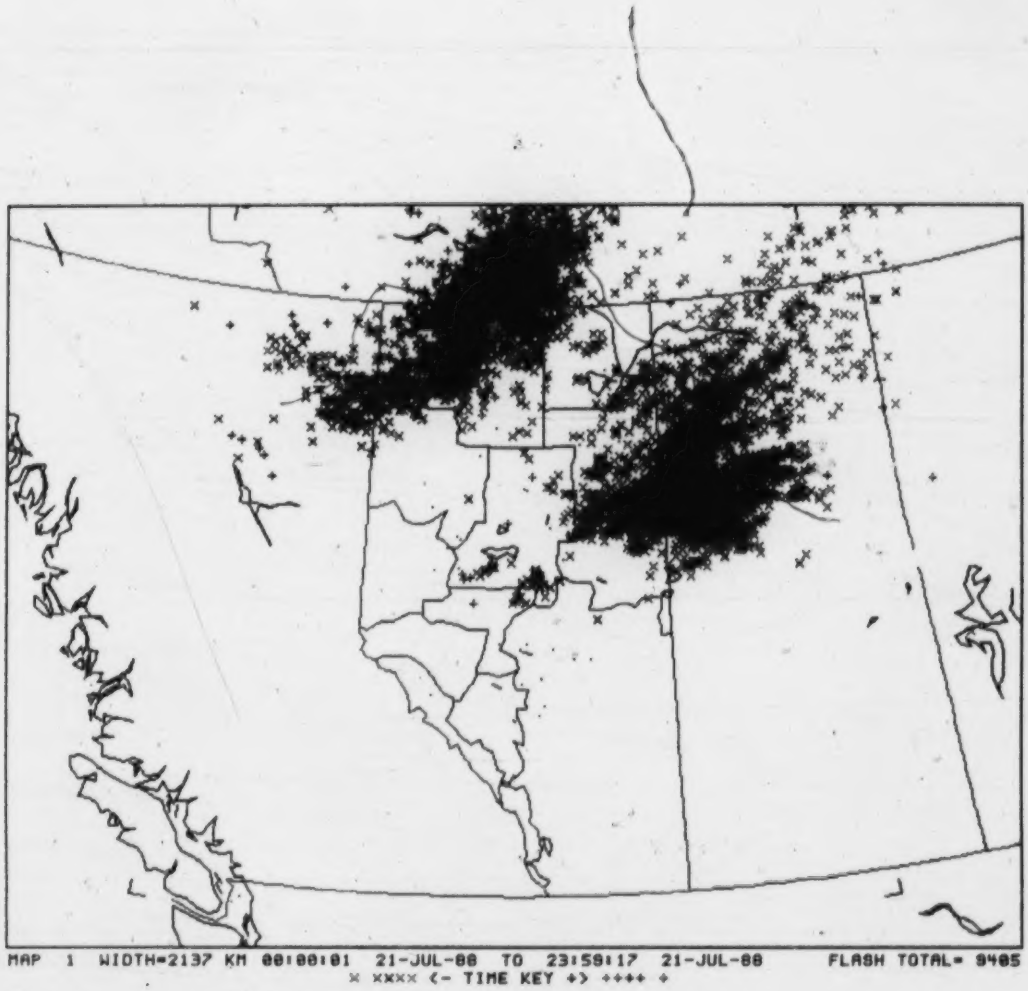

Figure 5.29: Lightning plot for 21 July, 1988.

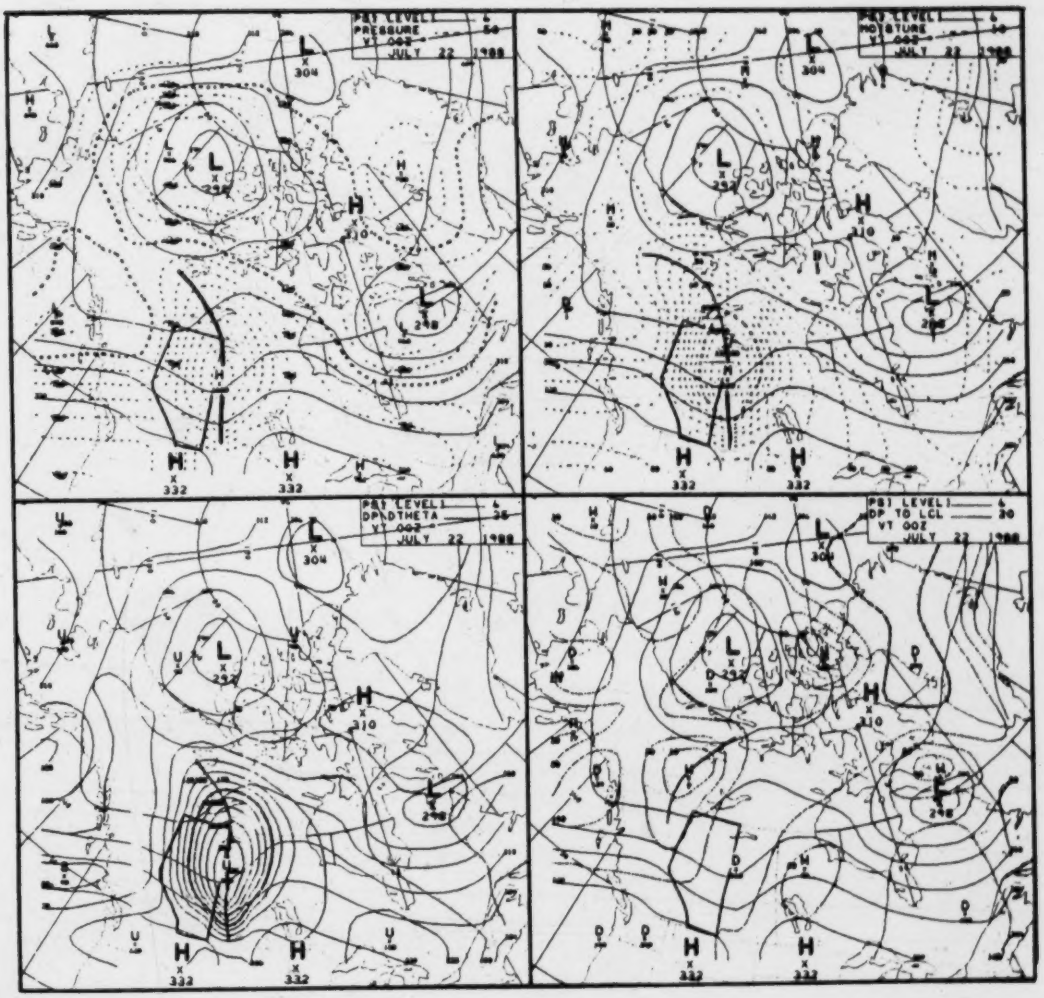

Figure 5.30: Upper level (303K) potential temperature analysis for 0000 UTC, 22 July, 1988 (12 hours after the analysis in Figure 5.26).

Figure 5.31: Infared (band 04) satellite image from NOAA-10 at 02:58 UTC, 22 July, 1988. Arrow indicates storm complex corresponding to parameter maxima centres shown in Figure 5.30.

5.2.8 04 August 1988

The upper-level maxima are clearly depicted in Figure 5.32. The height, moisture and instability fields all have local maxima centred in Central Alberta. A strong westerly flow through Central and Northern Alberta is evident by the tight streamline gradient in these areas. Intense negative temperature and moisture advection is present in West-Central Alberta as the streamlines intersect the tight temperature and moisture gradient. The instability centre has very high values, indicating strong low to mid-level instability localized in the Edmonton region. It is no coincidence that the instability maximum is positioned near the thermal maximum, as the instability is simply a reflection of the thermal variation on the isentropic surface (see the cross-section in Appendix C, Figure C4, corresponding to the line drawn on the instability panel in Figure 5.32).

A low-level moisture centre, also near Central Alberta, is shown in the lower-level chart in Figure 5.33. With a central maximum of 8.4g/Kg (Mx84), Central Alberta can be expected to support strong convection. However, the sharp axis of low-level stability through southern and central regions may trap the low-level potential energy below a strong inversion, suppressing wide-spread convection. A tight, low-level thermal gradient through Central B.C and

Northwestern Alberta is also present, indicative of a frontal zone with a cold front near its leading edge. The northwesterly flow through the region produces low to mid-level cooling behind the front, thereby effectively stabilizing the environment.

The composite chart in Figure 5.34 reveals Central Alberta as the area able to support the most intense storms. The strong, upper-level cooling and drying associated with the tight gradients above a low-level moisture centre, tend to indicate the potential for strong convection in central regions. This potential will only be realized if the low-level inversion is penetrated. Any convective cells that develop will be driven quickly eastwards by the strong westerly flow.

A lightning plot and severe weather reports are used to verify the accuracy of this diagnosis. Figure 5.35 is a plot of the lightning activity produced by the convective storms during the day. Only 1700 strikes were recorded, with many of them occurring before analysis time (strikes along 60th parallel). This early morning activity dissipated as low-level, negative temperature advection stabilized Northern Alberta behind the front. The main area of lightning is along the axis of black, red, and blue strikes in Central Alberta, extending into Eastern Saskatchewan. The convective strength appears rather weak,

as the lightning intensity shows little organization. However, 50mm hail (close to baseball size) and a funnel cloud were observed near Barrhead, northeast of Edmonton, at 5:15 pm local time. Again, the location of these severe weather reports corresponds quite well to the area shaded on the composite chart. This is an area of severe storm threat in which both strong dynamic and thermodynamic atmospheric conditions are present.

The isentropic data tend to support an area of maximum instability and destabilization northwest of Edmonton. It is in this region that the strongest storms were expected. However, wide-spread convection was not observed, since the low-level inversion apparently suppressed the weak vertical velocities, providing an environment in which only the most vigorous storms could survive. The lightning data show that only a few intense, isolated cells developed which then moved rapidly eastward.

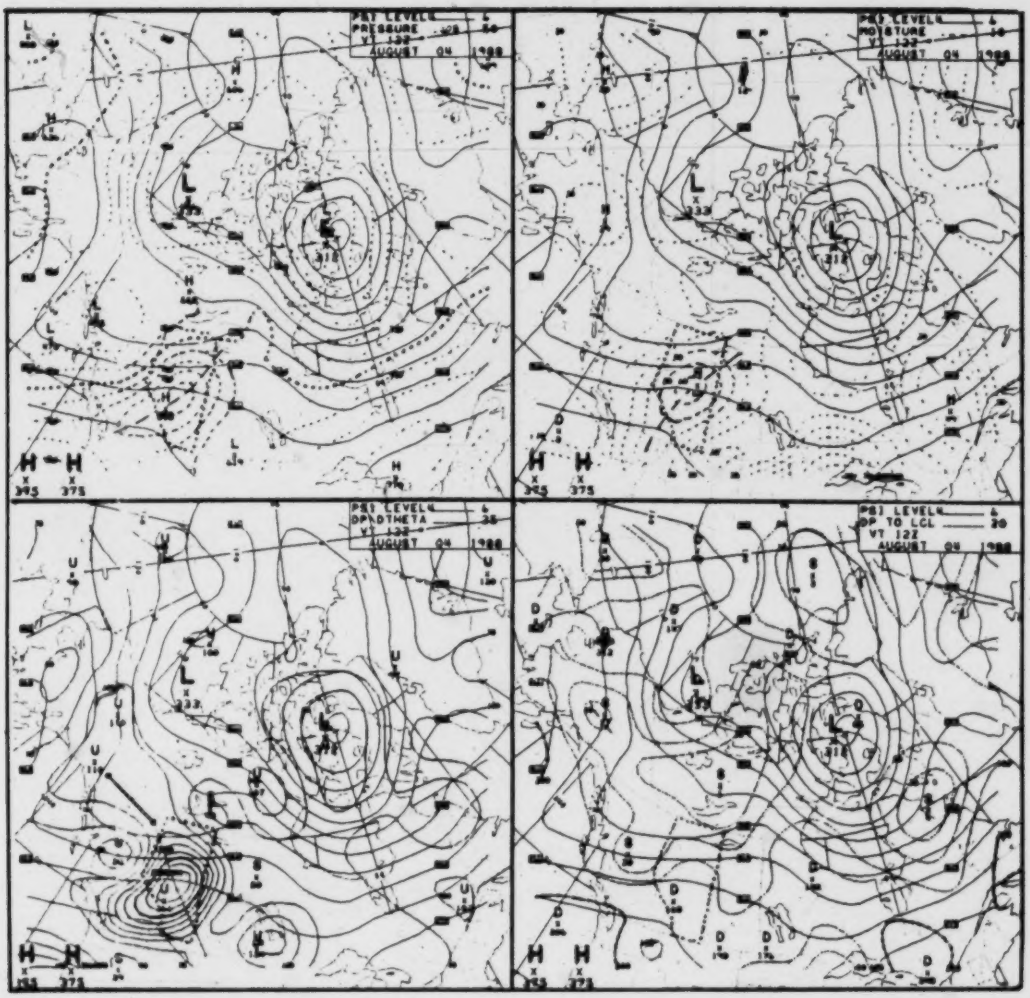

Figure 5.32: Upper level (308K) potential temperature analysis for 1200 UTC, 04 August, 1988. Line drawn on stability panel represents cross-section plane given in Appendix C, Figure C4.

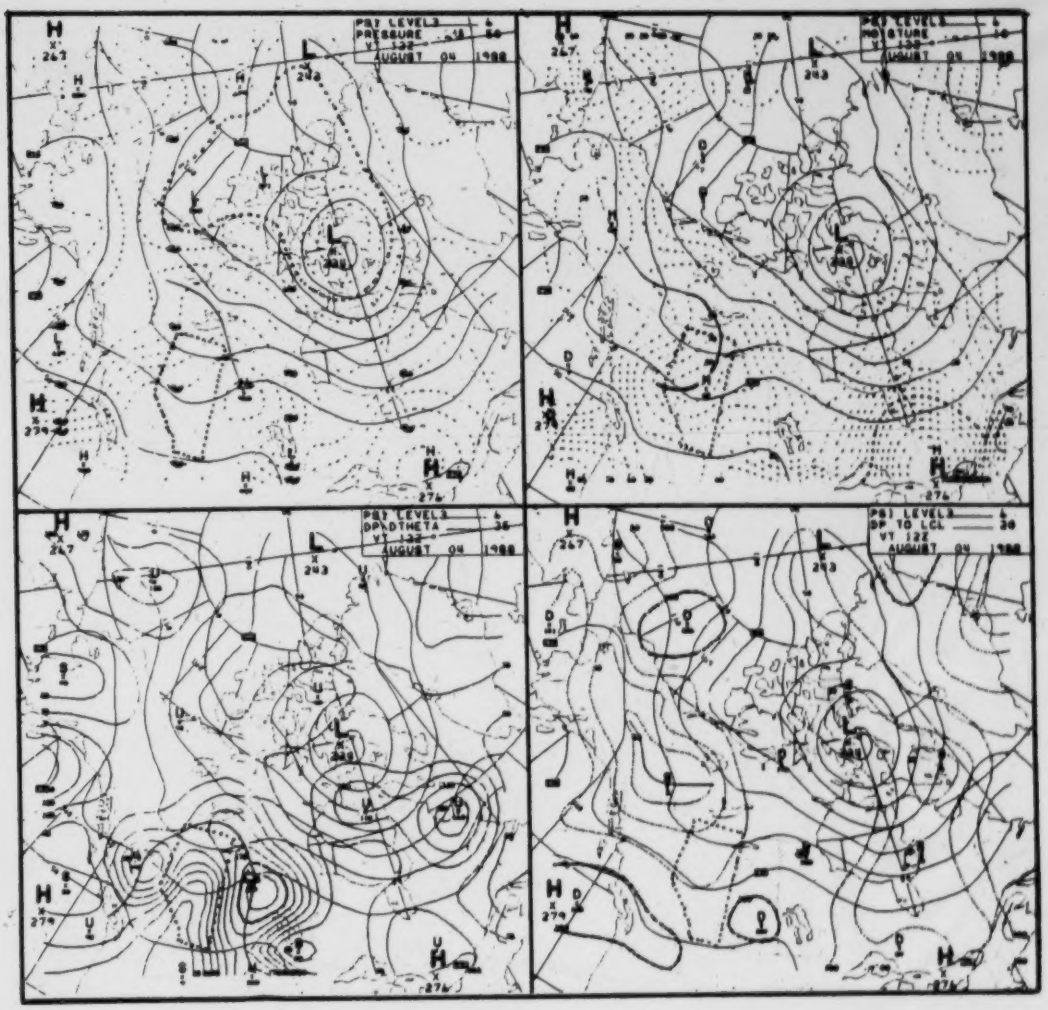

Figure 5.33: Lower level (298K) potential temperature analysis for 1200 UTC, 04 August, 1988.

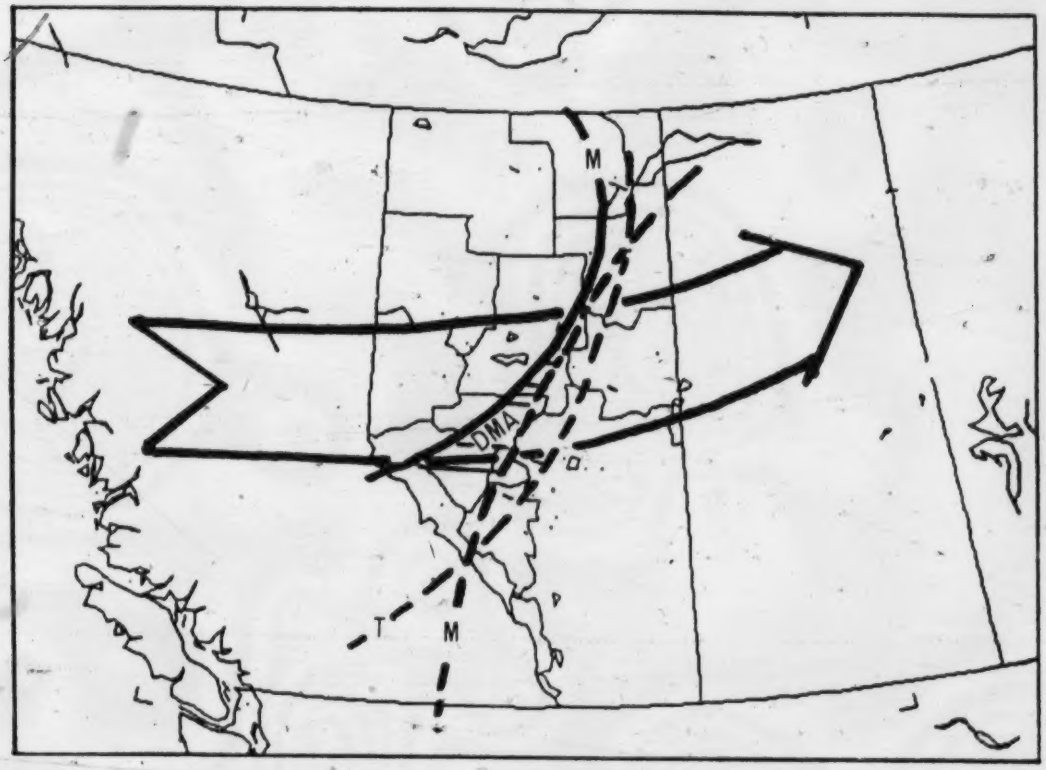

Figure 5.34: Composite chart for 1200 UTC, 04 August, 1988.

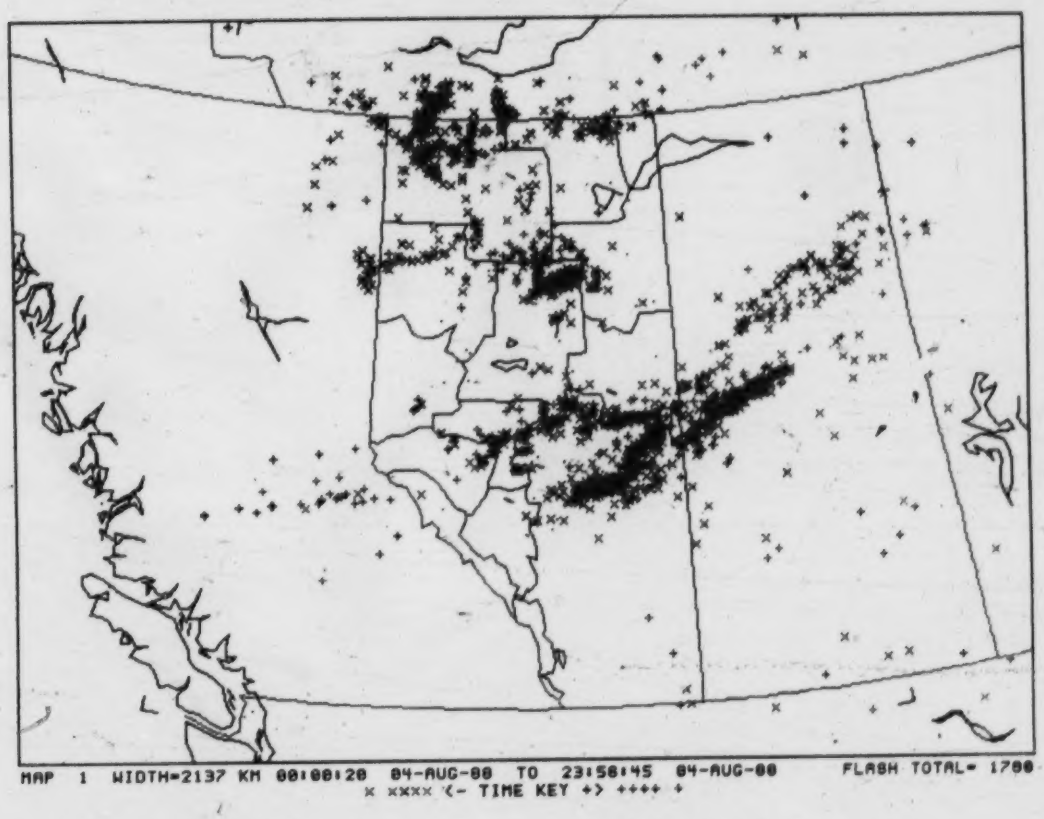

Figure 5.35: Lightning plot for 04 August, 1988.

5.2.9 16 August 1988

On this day, the upper-level surface, Figure 5.36, shows a weak thermal axis through Southern and Central Alberta, with an east-west moisture axis through the central part of the province. An axis of instability in the south along with an area of high relative humidity in central regions are also indicated. The axis of maximum wind, obtained from the base chart (not shown), curves up from Washington towards Central Alberta then turns back toward the Pacific ocean. Negative temperature and moisture advection induced by this flow is relatively weak. Nevertheless, this panel suggests that cooler, drier, and more unstable air is moving into Southern Alberta.

The lower-level chart, Figure 5.37, displays a weak thermal axis in South-eastern B.C., along with a prominent axis of moisture through Southern Alberta. A weak axis of instability is also present in the south and a local relative humidity maximum is evident in Central Alberta. The southeasterly flow on this surface is raising the temperature and moisture values in Southern Alberta, resulting in an increase in low-level potential energy.

The composite analysis in Figure 5.38 outlines the Southwestern Alberta and Southeastern B.C. regions with the highest convective potential (shaded area). The Calgary and

Red Deer regions show particularly strong storm potential since this is where the wind maximum intersects the threat "box". Here, both dynamic and thermodynamic support provides strong evidence, indicating the potential for well-organized storm potential.

The lightning plot in Figure 5.39 displays two areas of significant convective activity. The strikes in Southeastern Alberta and Southern Saskatchewan are a result of nocturnal thunderstorms, originating before 1200 UTC. The strikes of interest here are those recorded in the Calgary and Red Deer regions. They appear to be well correlated with the shaded threat region shown on the composite chart. The convective cells, however, appear largely unorganized and dissipated rapidly, indicating the absence of wide-spread convective support. A cell near Calgary, however, developed and moved through the city in the early evening. The storm dumped 31mm of rain in an hour, flooding many parts of the city. This "severe" storm was not accompanied by intense lightning, but formed within the strongest threat area, where the wind axis intercepted the threat region.

The 1200 UTC isentropic data helped to diagnose the atmospheric conditions leading to the heavy rainfall. Both of the levels displayed high relative humidity over the convective threat region, indicating that much of the lower

troposphere was near saturation. Also, the advection of low-level moisture not only increased the potential instability, but also the amount of precipital water in the air column. The relatively weak streamline gradient implies that any cells within the area would propagate slowly. These three conditions suggest that the convective cells developing within the threat area could give heavy rainfall amounts. A much more organized environment with strong vertical wind shear is needed to support tornadic events, and drier, more unstable conditions are most often associated with the production of large hail. Further analysis of this kind is statistically evaluated and presented in Chapter 6.

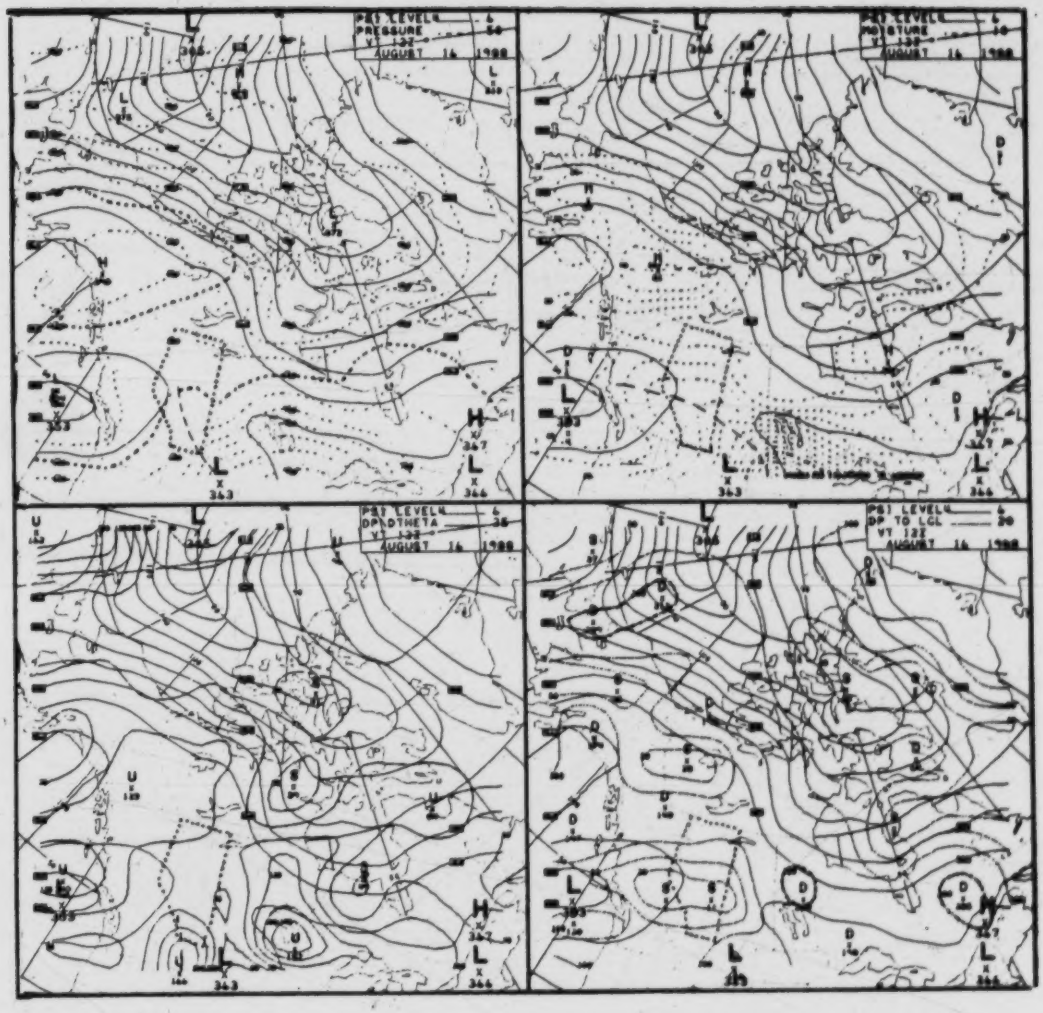

Figure 5.36: Upper level (308K) potential temperature analysis for 1200 UTC, 16 August, 1988.

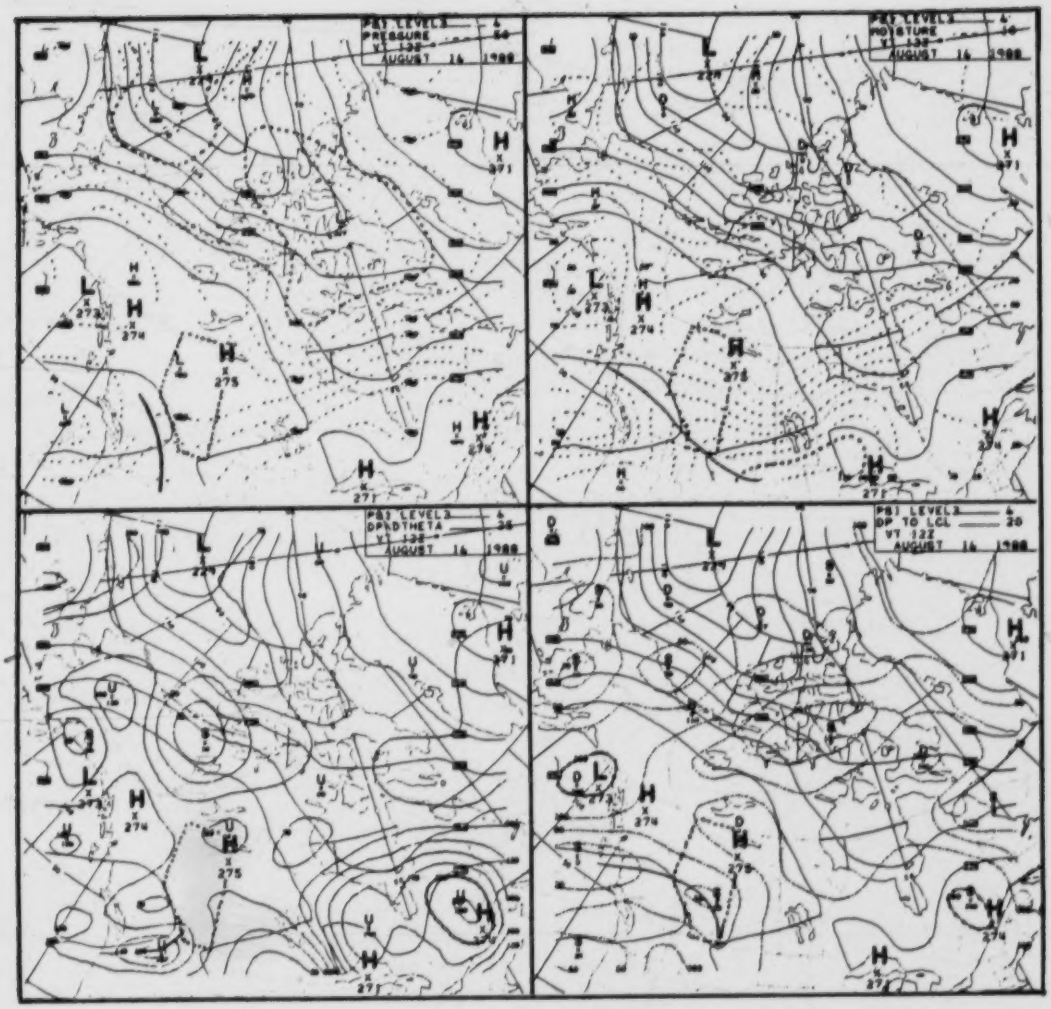

Figure 5.37: Lower level (298K) potential temperature analysis for 1200 UTC, 16 August, 1988.

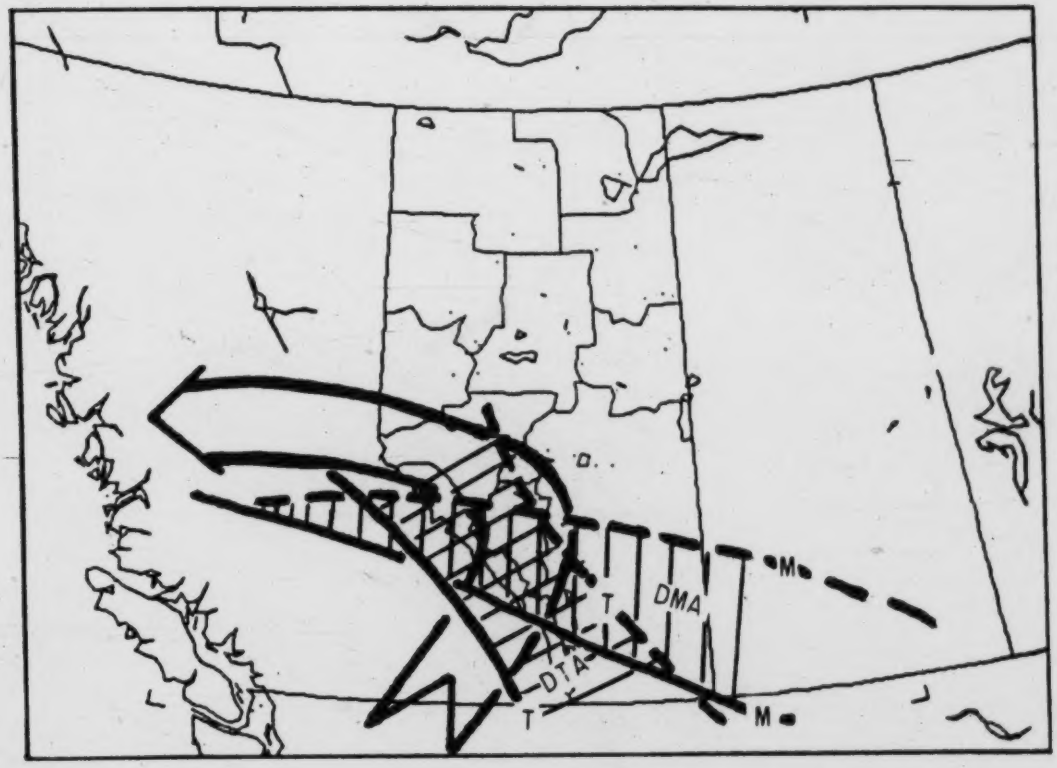

Figure 5.38: Composite chart for 1200 UTC, 16 August, 1988.

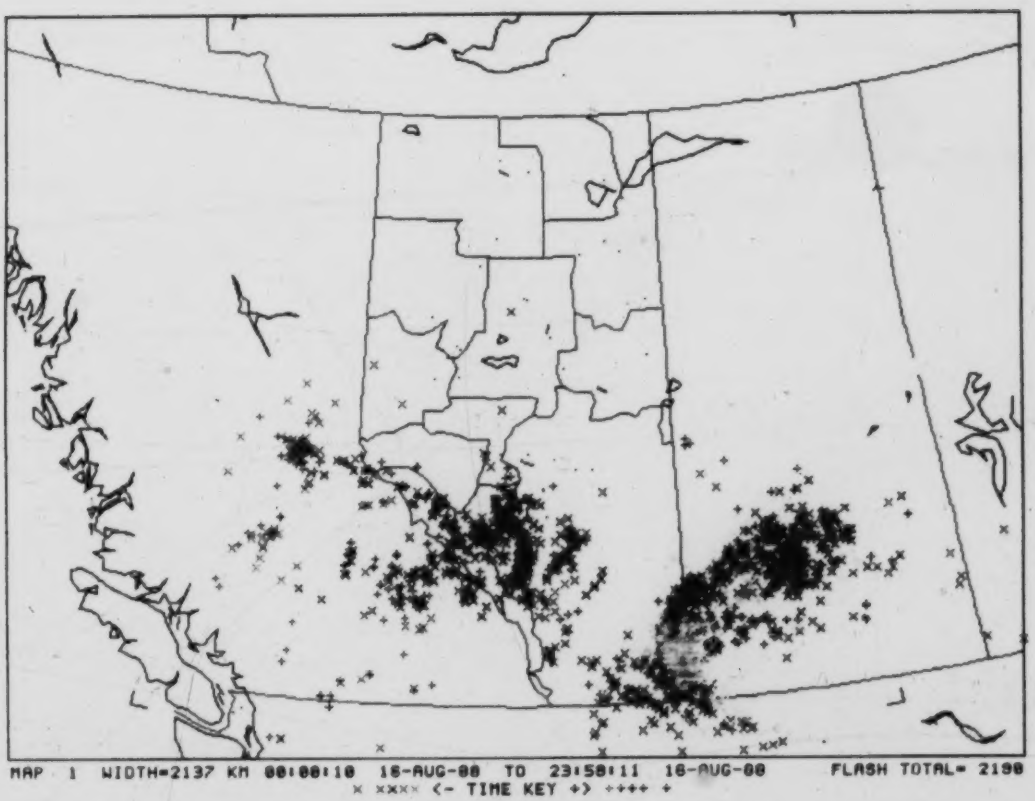

Figure 5.39: Lightning plot for 16 August, 1988.

5.2.10 29 August 1988

This final case study uses three isentropic levels to diagnose convective potential. The 293K potential temperature surface is added to the analysis, replacing the 298K surface as the "low level". As before, the upper-level surface is 308K, but the 298K surface will now be denoted as the "mid-level" surface, since it lies between the 293K and 308K isentropic surfaces.

On the upper-level isentropic chart of Figure 5.40, a broad thermal wave is shown, with its axis through Alberta. A moisture axis with its centre in Central Alberta is positioned near the temperature maximum. Also, an instability axis with a local maximum containing high values is located over Southeastern and Central Alberta. A strong southwesterly flow through the central and northern regions intersects the temperature and moisture gradient, indicating maximum cooling and drying just behind these axes. Particularly strong drying through Central B.C. and Central Alberta is evident, along with strong cooling in Central Alberta.

The mid-level surface (low-level in previous cases), given in Figure 5.41, tends to indicate the thermal maximum centred in Northwestern Alberta and the Southern MacKenzie. A well-defined moisture centre is depicted in the

Northwestern Alberta, Northeastern B.C, and Southern Mackenzie regions as well, with local maximum values greater than 11.0g/Kg (Mx111). These values are considered extremely high, indicating large low-level potential energies, capable of supporting severe convection. An identifiable low-level stability axis is evident through much of South and Central Alberta, possibly indicative of a low-level inversion. The flow on this surface is very weak, tending to reveal little advection of these lower-level fields.

Figure 5.42 shows the lower surface (293K) with similar temperature and moisture maxima in Northeastern Alberta - Southern Mackenzie regions. The moisture values greater than 10.0g/kg (Mx105) near the mid-level maximum indicate the existence of a deep layer of low-level potential energy in these areas. The stability panel depicts a sharp axis of stability lying through Alberta and well into the Mackenzie Valley.

The composite chart in Figure 5.43 clearly indicates strong convective potential along an axis from East-Central Alberta northward to the Southern Mackenzie Valley (shaded area). The upper-level cooling and drying is well organized over the low-level moisture and temperature maxima. The most severe storms can be expected to occur where the wind

axis intersects the shaded area. The Southern High Level and Northern Grande Prairie regions have strong dynamic and thermodynamic support.

The lightning plot given in Figure 5.44 displays a very well organized band of convective activity extending from Central to Northern Alberta. Lightning with weaker intensity was also recorded in the Southern Mackenzie, Central and Southeastern B.C regions. The black strikes scattered over Central B.C are well correlated with the area of strongest cooling and drying indicated on the upper-level analysis. But because of the rough mountainous terrain, and the fact that the low-level moisture maximum was not near the area, the convection was not well organized. As the upper-level minimum crossed into Alberta, intense, well-organized, convective cells developed. By this time (early evening), the low-level moisture axis had propagated into the province as well, providing strong low-level support to the upper-level destabilization. Very strong convection resulted within the north-south band, producing the majority of strikes recorded (9231) in less than eight hours. As mentioned above, the highest convective potential was diagnosed in the Southern High Level region. A tornado (F1) was observed near Fort Vermillion (High Level region) at 10:00 pm local time.

This analysis tends to show the atmospheric processes responsible for these convective events. Strong differential temperature and moisture advection along with the isentropic wind maximum are the key parameters driving these severe storms. The 1200 UTC isentropic charts indicated the potential for severe weather development, particularly in the Southern High Level region where the key parameters are juxtaposed.

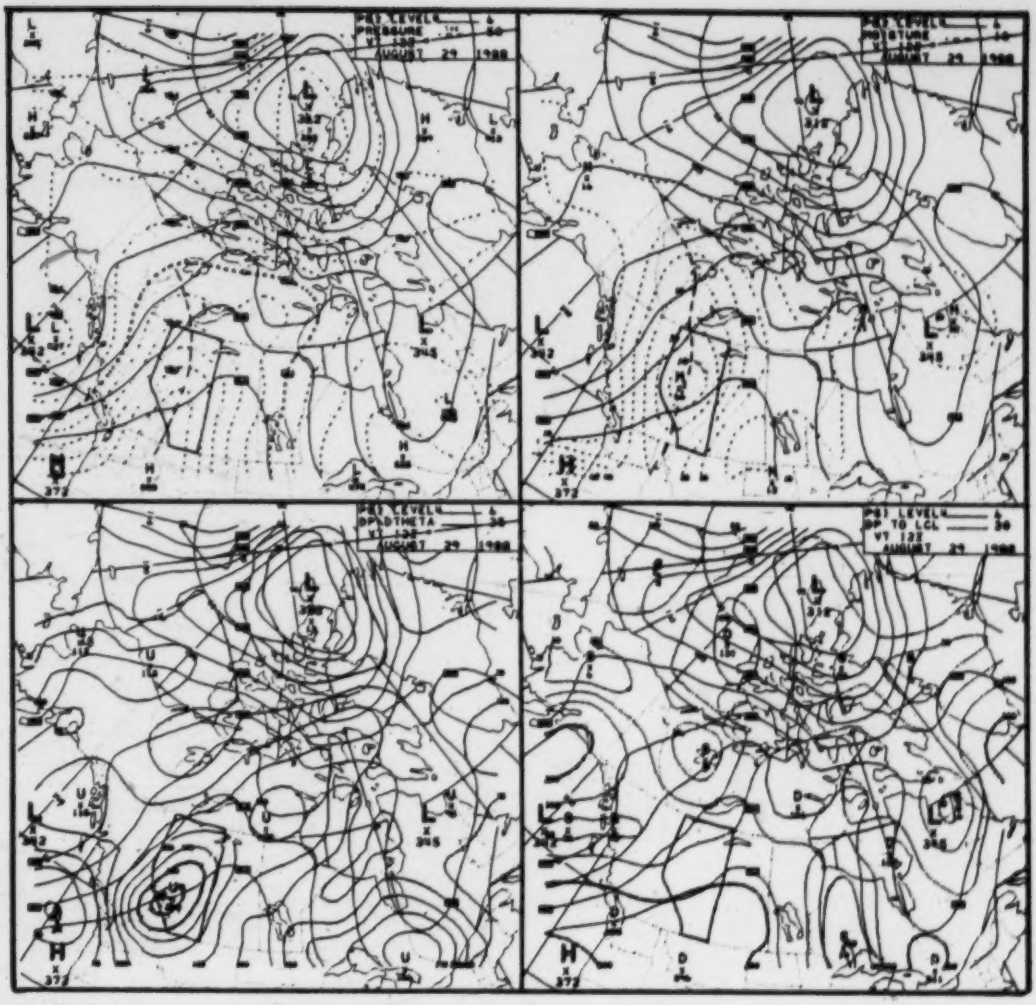

Figure 5.40: Upper level (308K) potential temperature analysis for 1200 UTC, 29 August, 1988.

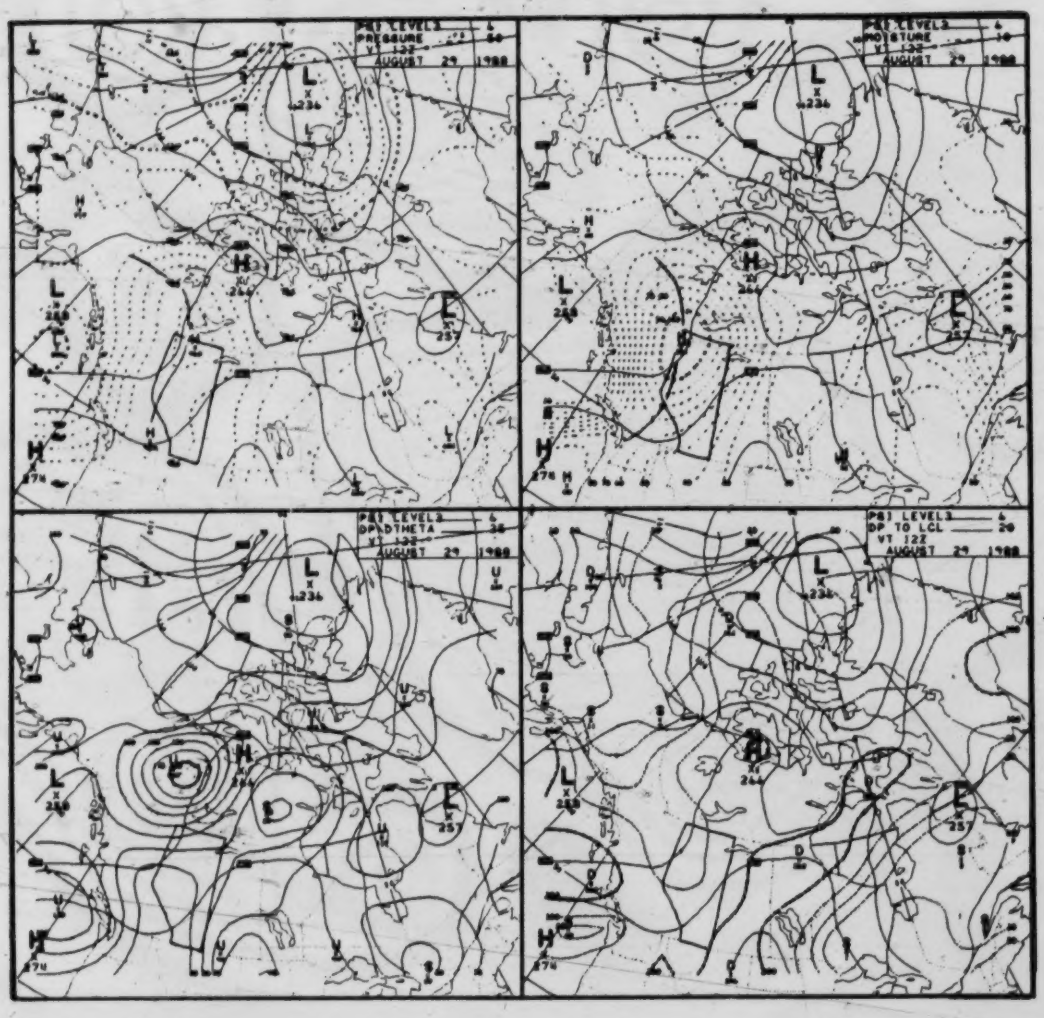

Figure 5.41: Mid level (298K) potential temperature analysis for 1200 UTC, 29 August, 1988.

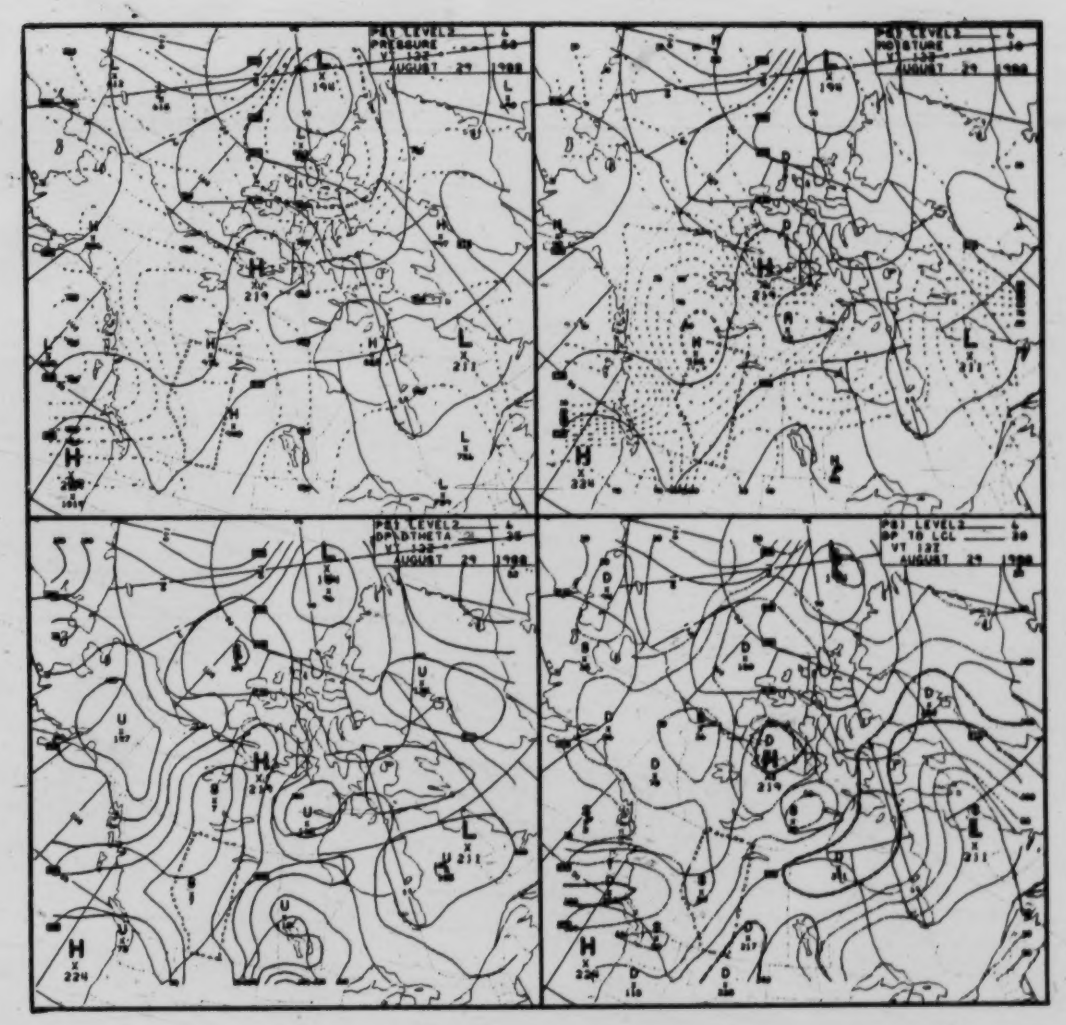

Figure 5.42: Lower level (293K) potential temperature analysis for 1200 UTC, 29 August, 1988.

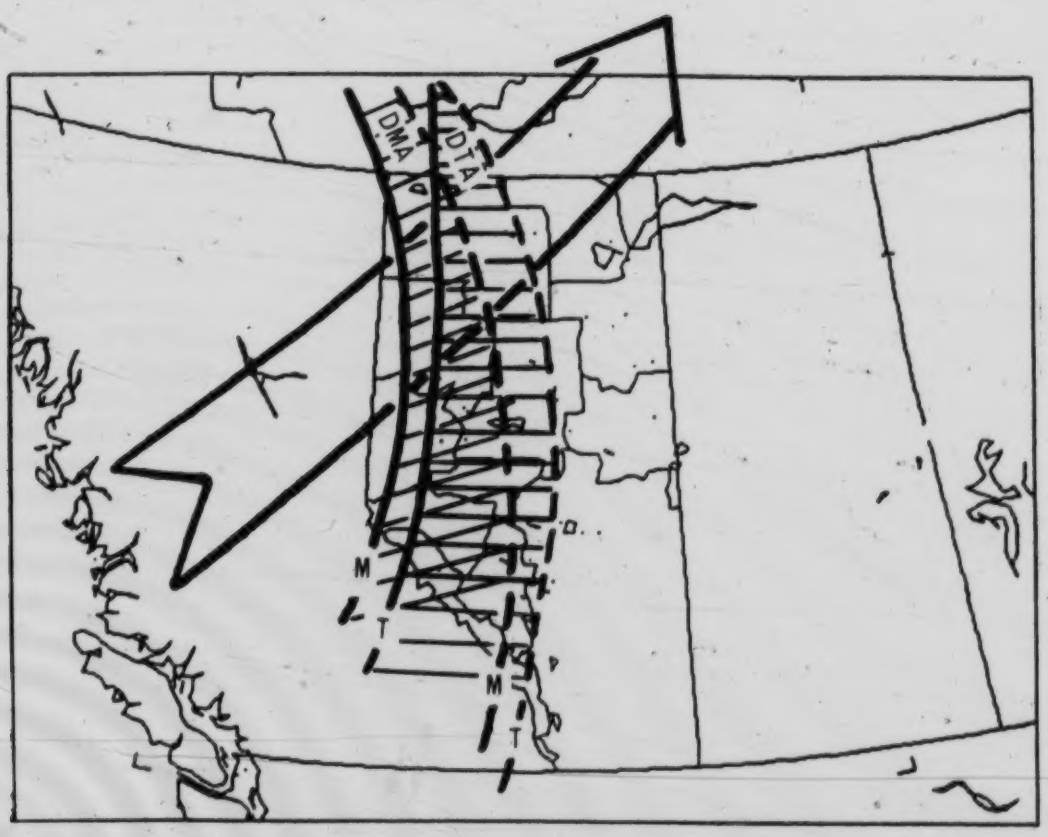

Figure 5.43: Composite chart for 1200 UTC, 29 August, 1988.

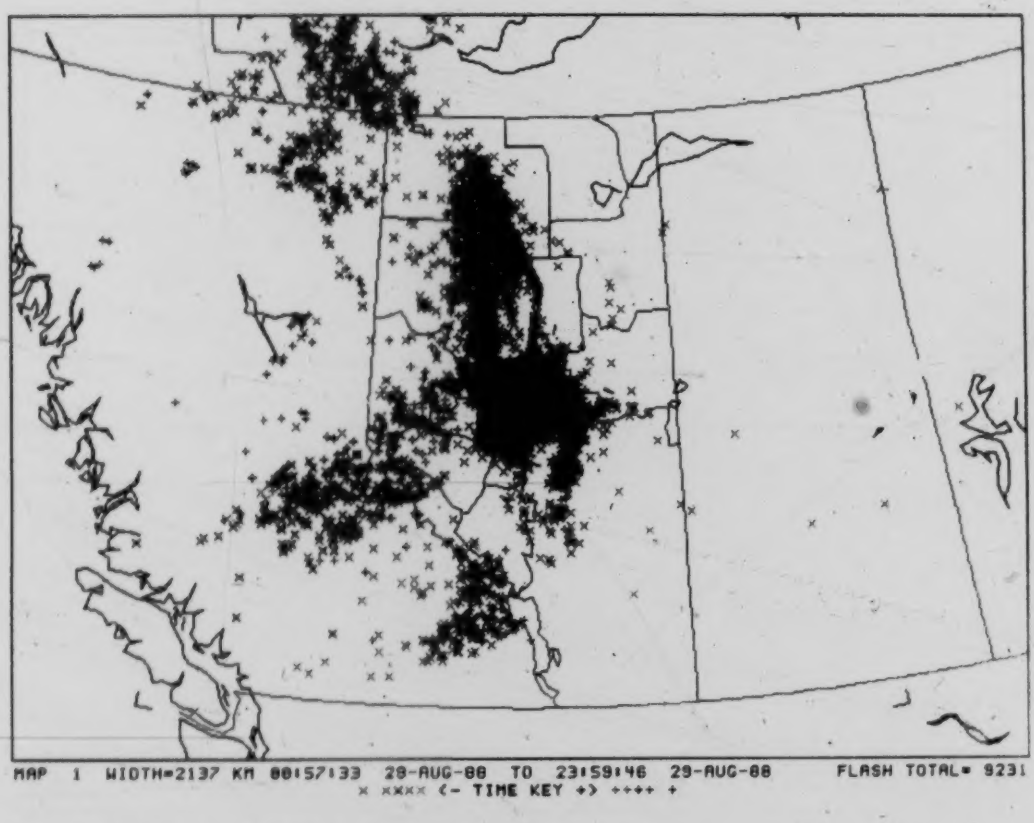

Figure 5.44: Lightning plot for 29 August, 1988.

5.3 Discussion

Some general observations can be made based on these ten case studies.

Isentropic data can often help to diagnose convective potential by assessing the organization of the various isentropic parameter fields. Weak convective support is indicated when few upper-level maxima are present, low-level moisture values are small, and differential temperature and moisture advection is weak. Convective cells that develop within this environment are usually unorganized and dissipate rapidily. In the first three case studies, the intersection of the wind axis with either an upper or lower-level instability axis or centre, revealed the area that supported convective activity later on in the day. However, when prominent temperature and moisture axes are present, convective potential is much higher. Severe weather threat areas were associated with strong differential temperature and moisture advection. In the final seven cases, the positive advection of temperature and moisture decreasing with height was diagnosed in areas where strong upper-level flow was directed normal to the upper-level temperature/moisture axes. Also, quasi-stationary low-level temperature and moisture maxima were depicted below this area of upper-level cooling and drying. Well-organized convective outbreaks, often with

embedded severe weather, developed in these areas in mid-afternoon and continued to re-develop well into the evening.

In these ten examples, the isentropic charts served to delineate the convective threat area and helped to estimate the strength of the storms that can be expected.

"Convective storm type and severity are strongly dependent on the environmental conditions in which the severe storm grows, particularly thermodynamic instability (buoyancy) and vertical wind shear."

Weisman and Klemp (1986)

CHAPTER 6

STATISTICAL ANALYSIS

6.1 Introduction

Although the ten case studies discussed in Chapter 5 demonstrate the application of an isentropic analysis procedure, the operational utility gained from such a small sample is very limited at this stage. A forecaster needs to have confidence in the reliability of these methods based on a larger sample before they will be readily used. To this end, it may be helpful, as a first step, to consider elementary statistics based on June, July, and August data of 1988.

The goals of this statistical analysis are rather modest. It is unreasonable to expect the quantity of data and the accuracy of the analysis used here to reveal adequately the effectiveness of these isentropic

procedures. Rather, it is the goal to provide some broad guidelines that may be used to help forecast lightning and severe weather occurrences using isentropic data.

Section 6.2 examines the efficacy of particular isentropic parameters for diagnosing lightning threat. Section 6.3 considers how the use of isentropic data can lead to the diagnosis of a particular severe weather type, such as tornadoes, large hail, and heavy rain.

6.2 Lightning

All of the 1200 UTC isentropic charts between June 1st and August 31st, 1988, were used in the statistical evaluation of the ability of several parameters to estimate independently the probability that lightning will occur in a certain area. Differential temperature advection, the isentropic wind maximum, the upper and lower-level height and instability centres, and the lower-level moisture centres were all evaluated for this purpose.

Since each of these parameters can be clearly visualized by the quick inspection of the isentropic charts, it was thought worthwhile to determine their individual utility in the forecasting of convective weather. Suppose, for example, that the mere existence of an instability centre depicted on the upper-level potential temperature

surface implied a 95% probability that lightning will occur within the local maximum. This kind of information would be useful to the forecaster who must indicate as best he can the areas of convective threat. He may have either already deduced the area to have high convective potential, in which case this instability centre would support his forecast, or he may have not considered it likely to support convection, in which case the instability centre might make him reconsider his analysis. This field, in a sense, could be used as a check against conventional, convective analysis. Of course, if this instability centre only implied a 25% probability of lightning, then it would not be useful in this regard.

The following table lists the isentropic parameters, the number of times they occurred within the sample period, and the probability that lightning was associated with each parameter.

TABLE 6.1 LIGHTNING STATISTICS

Isentropic Parameter	# of events	% with Lightning
Upper-lvl Height Centre	1	.....100%
Upper-lvl Instability Centre	22	..... 77%
Upper-lvl Saturation Centre	15	..... 73%

Lower-lvl Height Centre	1	.....100%
Lower-lvl Moisture Centre	9	.....78%
Lower-lvl Instability Centre	46	.....72%
Differential Temperature Advection	45	.....86%
Near Upper Level Wind Maximum	80	.....92%

These statistics, though crude, indicate that the above parameter maxima showed some predictive skill in delineating the occurrence of lightning in the summer of 1988. Note that the upper and lower-level height centres were correlated with lightning 100% of the time, but these centres were very rare, each only appearing once in the 92 day period. Probably the most significant statistic is the correlation between lightning and the upper-level wind maximum. A wind maximum was present somewhere in Alberta almost every day during this period, and 92% of the time lightning was recorded somewhere along its axis. Of course, lightning could also have occured elsewhere, in regions remote from these parameter maxima.

These statistics only provide the first step in evaluating the operational usefulness of such isentropic parameters. Not only is a much larger sample required to

increase the confidence of such statistical values, but they should be tested also against an independent data set. Since the sample used here consisted of the only useable summer data available, further statistical evaluations were not possible at this time.

This study has only considered the ability of a single parameter, independent of all others, to alert a forecaster to possible lightning threat. An evaluation of how well a combination of "predictors" could delineate the position of lightning threat should also be considered. For example, if an upper-level instability centre were to coincide with the location of a low-level moisture centre, and both were near the isentropic wind axis, the probability of lightning to occur within the region of superposition would most likely be higher than if these parameters were present alone. An analysis of this kind, however, would involve more complex computational methods, such as conditional probabilities and non-linear regression analysis, which are beyond the scope of these investigations.

6.3 Severe Weather

Seven out of the ten case studies showed how isentropic analysis can help delineate strong, well-organized convective threat areas by using selected isentropic fields for evaluating the pre-convective environment. These severe

storm environments were organized in regions where differential temperature and moisture advection was present near the upper-level wind maximum and the low-level moisture and thermal maxima. It is the goal, here, to go one step further and use the isentropic data for predicting the most likely severe weather event that may occur within the area of potential threat. Again, because of the restricted nature of these investigations, only broad conclusions can be expected.

All of the tornado, large hail, and heavy rain events reported between June and September, 1988, were investigated to determine how they could be differentiated by means of isentropic data. High wind events and reports of funnel clouds not reaching the ground were not used, since they are often associated with other types of convective weather.

6.3.1 Tornadoes

Tornadoes have long eluded the forecast skills of meteorologists. Their size and composition make them one of the most difficult meteorological phenomena to predict. However, with the advent of doppler radar, the "nowcasting" of tornadoes has been much improved. A mesocyclone within a thunderstorm core can now often be detected, providing forecasters with perhaps 20 minutes of lead time before the vortex extends to the ground. The longer-term forecasting

(6-18hrs) of tornadic potential has not improved as quickly. It is the aim here to show how isentropic analysis may reveal tornadic potential several hours in advance.

It is well known that tornadic development critically depends on the environmental wind shear. Strong, veering winds between the ground and the 600mb level have been found associated with tornado development (McGinley, 1986). Since the isentropic height field depicts strong vertical shear in areas where the isobars are tightly packed (strong temperature gradient) it is reasonable to investigate the relationship between the positions of these tight gradients with the tornado reports.

A total of 26 tornadoes were reported during the analysis period, and 25 of these events occured in conjunction with a strong pressure gradient (>200mb/500Km) depicted on the upper-level (308K) height analysis. This kind of correlation suggests that potential for tornadic development is low if a strong thermal gradient is not present on the 1200 UTC upper-height panel. Since these gradients often extend over large bands (as in Figure 5.40), other "predictors" are needed to localize the area of tornado threat further. To this end, the differential temperature and differential moisture fields are used. Ten out of the 15 non-nocturnal (pre-midnight) tornado events that occured in 1988, were reported within the area bounded

by the upper and lower temperature and moisture maxima lines (refer to Section 5.2.10, for applicable case study). It should be noted that these bounded areas are often quite small, typically 100 to 200 kilometers square. As the threat area size decreases, the probability of having an event in the area decreases as well. However, emphasis should be placed on the fact that almost 70% of the tornadoes that were reported between 6:00AM and midnight (local time) during 1988, occured within the area bounded by the four curves up to 18 hours earlier. Lastly, the wind axis can also be used to further reduce the area of tornado threat. Only six of 15 tornadoes occured close to the juxtaposition of the wind axis with the differential temperature and moisture area. This relatively poor result was expected, as the area of threat is now typically very small.

Since these results are based on such a small sample, their statistical value is limited. However, the isentropic data, especially the temperature and moisture fields, tend to show valuable information which may be of great operational use when assessing the threat of tornadoes.

6.3.2 Large Hail

Potential hail size is most often estimated by using a tephigram. The parcel energy method and nomogram developed by Miller (1972) can be used as a "first guess" for assessing maximum hail size. Severe hail events (>20mm diameter) are often associated with the storms that produce tornadoes. Out of the 17 large-hail events recorded between June and September, 1988, only six were not associated with a tornado. Intuitively, the intense updrafts within severe thunderstorms that produce tornadoes will also be apt to produce large hail. Since they both rely on well-organized storm structures to generate these vertical velocities, it is difficult to distinguish a tornado-producing environment from a large-hail-producing environment several hours before convective onset. Essentially, then, the parameters which were used to delineate tornadic threat can also be used to assess the threat of large hail. However, differences in the actual parameter values associated with the tornado and hail events have been found. These "differences" help to discriminate between the two severe weather events.

All of the tornado events (26) and large-hail events (20) that occured between June and September (1988) in Alberta have been compared with the isentropic data. The position of each event was correlated to the moisture,

instability and relative humidity analyzed at that position on the 1200 UTC isentropic charts. The following statistics emerged;

1. a) 90% of the tornado events were associated with moisture values between 90-175 (note that these values are as plotted on the charts i.e. g/Kgx10). These values were derived by adding the lower and upper level moisture values obtained from the moisture panel near each tornado event.
   b) 90% of the hail events were associated with columns having slightly less moisture, in the 85-155(g/Kgx10) range.

2. a) 90% of the tornado events had upper and lower instability values totaling between 90-235(mb).
   b) 90% of the hail events had upper and lower instability totals in the 180-290(mb) range. Note that large hail threat tends to be associated with higher instability values apparent within the pre-convective column. Physically, tornadoes are probably produced within thunderstorms that have higher wind shear than those only producing large hail. The smaller instability values associated with the tornado events suggest, therefore, that the pre-storm tornadic environment has more dynamic than thermodynamic processes active within it, unlike large-hail producing environments.

3. a) 90% of the tornado events were associated with "relative humidity" values between 70-250(mb).
   b) 90% of the relative humidity values corresponding to the hail events had values between 70-250(mb), exactly the same range as the tornado events.

Though these statistics are simple, they tend to show that hail threat is more likely when the instability values analyzed on the lower and upper levels, near the severe weather threat area, combine to totals greater than 235mb. Also, large hail is not as likely when the lower and upper moisture total is greater than 15.5g/Kg. Since the relative humidity associated with the tornado and large hail events had the same range of values, this parameter field is shown not to be as useful for discriminating between these severe weather events.

Before presenting an example, a consideration of the criteria which are associated with heavy rain events is in order.

6.3.3 Heavy Rain

Like tornado and large hail potential, heavy rain is most often associated with strong, well organized storm complexes. Many of the pre-convective conditions that support other severe weather events are similar to those

that can produce severe downpours and flash floods. However, higher moisture content and more saturated air columns within a weaker flow regime often reveal environments that are especially prone to heavy rain fall. It seems reasonable to suggest that the isentropic fields, especially the moisture and "relative humidity" panels, could help to assess these atmospheric conditions.

The following listing summarizes the statistics from all of the heavy rain events (>25mm/hr) that occured in Alberta between June and September (1988).

1. 90% of the events corresponded to moisture (upper plus lower total) values between 10.5-17.5(g/Kg). This range is slightly higher than the hail event range, but close to the tornado values.

2. 90% of the events had instability values (upper plus lower) within the 135-235(mb) range -- again on par with the tornado values, but much less than the instability found associated with the large hail events.

3. 90% of the rain events had "relative humidity" values between 35-120(mb). Compared with either the tornado or hail events, this range indicates a much more saturated environment associated with heavy rain potential.

A "threshold" nomogram, given in Figure 6.1, helps to compare these different ranges of values which are associated with each severe weather type. To illustrate clearly how this nomogram can help depict severe weather types, three examples, each indicating a different type of threat, are considered. For convenience, the final three case studies in Chapter 5 are used.

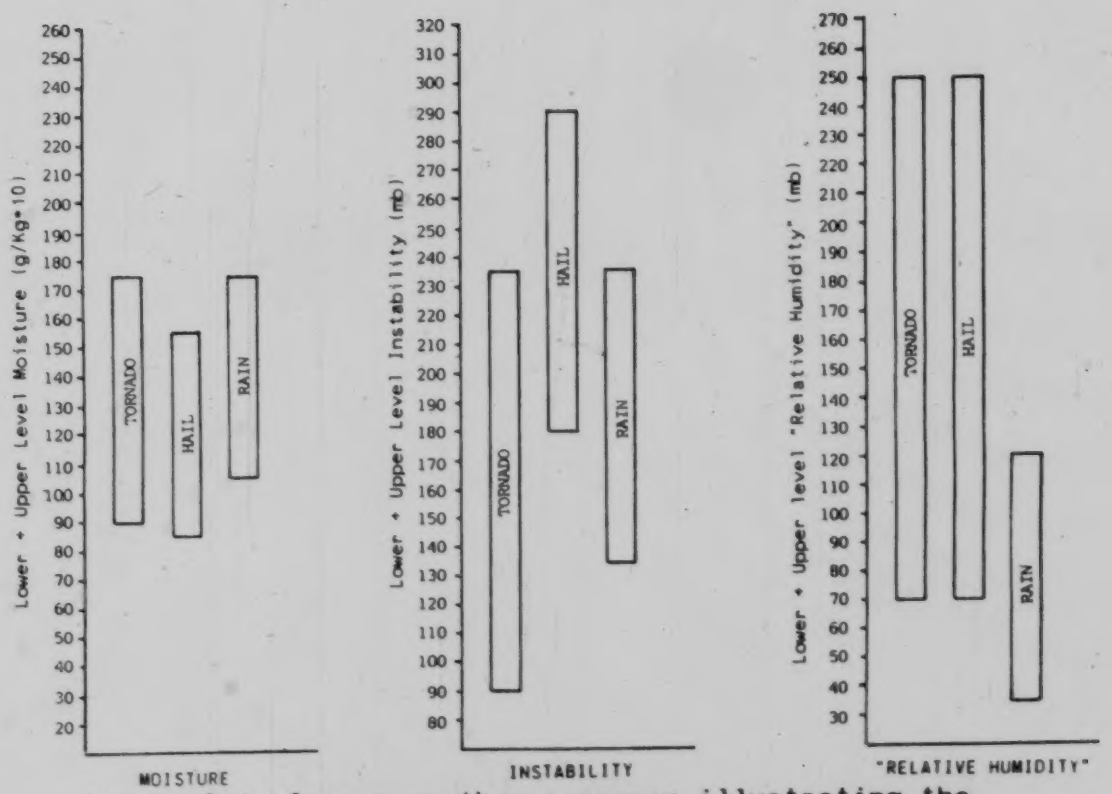

Figure 6.1: Severe weather nomogram illustrating the parameter values associated to the tornado, large hail, and heavy rain events that occurred during June, July, and August, 1988. The boxed area depicts the range containing 90% of the values for each particular severe weather type and isentropic field. Note that the relative humidity values are not in percentages but rather in millibars (as value decreases, relative humidity increases).

6.3.4 04 August 1988

On 04 August at 17:15, 50mm hail (near baseball size) was reported near Barrhead, northeast of Edmonton. The composite analysis in Figure 5.34 delineates the severe convective threat area. The upper and lower potential temperature surfaces are given in Figures 5.31 and 5.32. The following parameter values are present near the threat area;

low level moisture = 80 g/Kgx10
low level instability = 40 mb
low level relative humidity = 100 mb
upper lvl moisture = 60 g/Kgx10
upper lvl instability = 250 mb
upper lvl relative humidity = 150 mb

Therefore;
lower + upper moisture = 140 g/Kgx10
lower + upper instability = 290 mb
lower + upper relative humidity = 250 mb

These last three values can be entered on the threshold nomogram. By doing this, the values for this particular threat area can be compared to the "normal" values for each severe weather type. This heips to diagnose which severe weather event is most likely.

Figure 6.2 clearly compares these values to the "typical" ranges for the tornado, hail and rain events. The dashed line represents the moisture, instability, and relative humidity values for 04 August, 1988, near the threat area. The 140 moisture line intersects all three "boxes", indicating that the moisture near the threat area can support all three severe types. The instability line at 290, however, indicates abnormally high values of instability, only intersecting the top of the hail range. This tends to show that a hail event is likely, since 90% of all the tornado and rain events had instability values much lower. This is not to suggest that a tornado or heavy rain will not occur, but simply that the potential for large hail is highest. Note also that the relative humidity value of 250 far exceeds the "normal" for heavy rain events, further indicating that a heavy rain event is not likely near the threat area.

To summarize, the isentropic data tend to indicate that out of the three severe-weather types of interest here, a large hail event is most probable, due to the very high instability and low relative humidity values near the threat area.

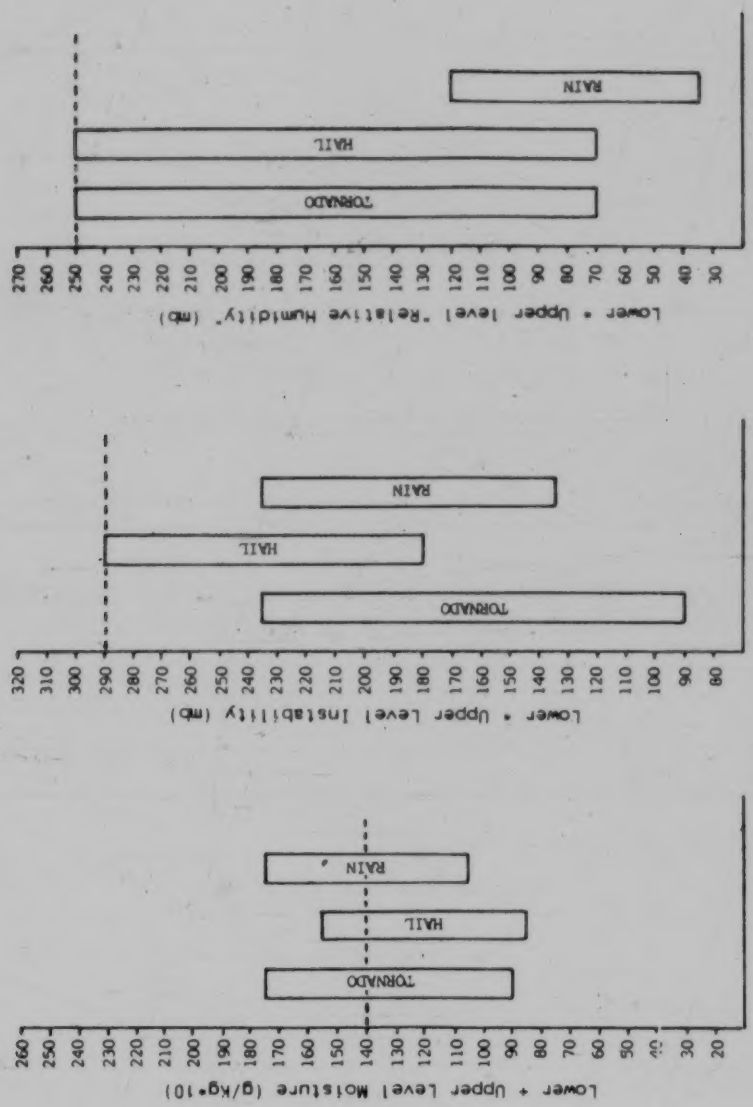

Figure 6.2: As in Figure 6.1. Dashed line represents parameter values depicted at 1200 UTC, 04 August, 1988, in the Edmonton region.

6.3.5 16 August 1988

At about 17:30 MDT, a thunderstorm developed southwest of Calgary. An hour later, some parts of the city were flooded as the storm passed over, giving up to 31mm to some localities. Figures 5.35 through 5.39 illustrate the conditions that developed that morning. The severe-threat area was delineated in the Calgary and Red Deer regions (refer to composite chart, Figure 5.38). By closer inspection of the isentropic data, the following values within the threat region (specifically near Calgary) can be obtained;

lower + upper moisture = 75 + 35 = 110 g/Kgx10

lower + upper instability = 100 + 110 = 210 mb

lower + upper relative humidity = 30 + 35 = 65 mb

Referring to the "threshold nomogram" in Figure 6.3, the dashed line denotes these values. By inspection, this line again intersects all three moisture boxes, not isolating any severe weather type. The instability value of 210 also intersects each threshold range. However, the abnormally low relative humidity value of 65 indicates a nearly saturated column in the area and only intersects the rain box. This suggests that the threat area has heavy rain

potential. Based on these statistics, the occurrence of large hail or tornadic activity is possible but not as likely.

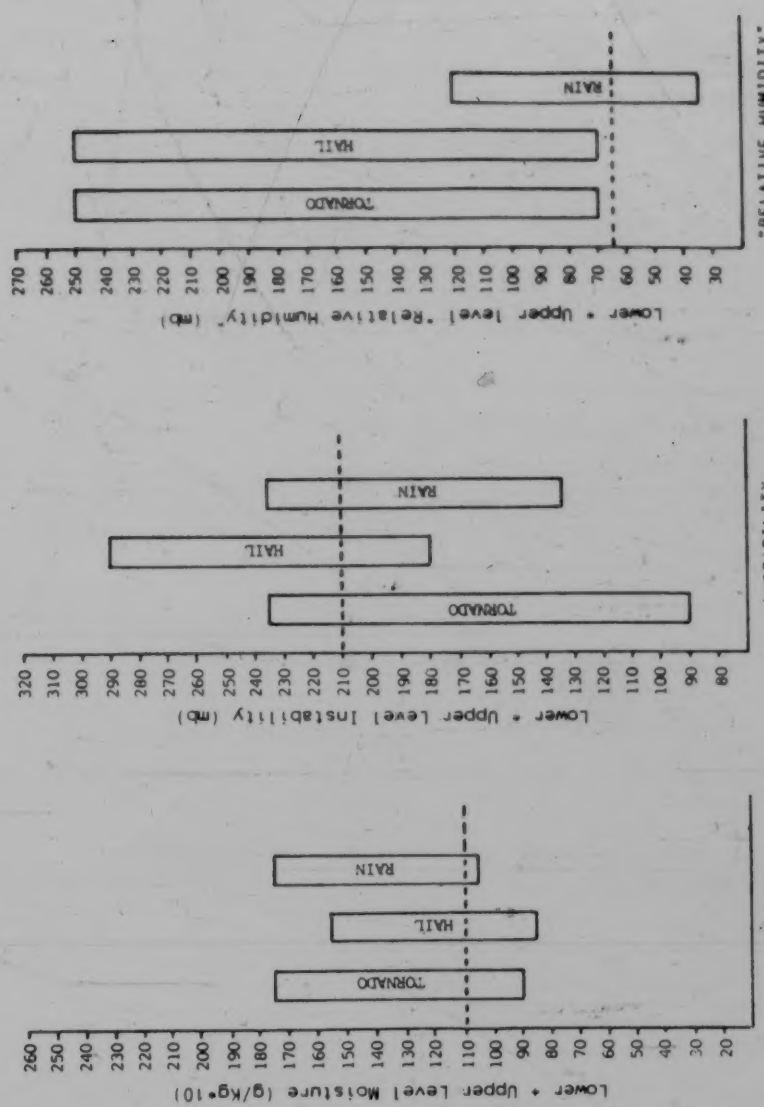

Figure 6.3: As in Figure 6.1. Dashed line represents parameter values depicted at 1200 UTC, 16 August, 1988, in the Calgary region.

6.3.6 29 August 1988

On this day, a tornado (F1) touched down near Fort Vermilion in the High Level region at about 22:30 (MDT). Section 5.2.10 discuses the conditions that help to determine the area of severe weather threat. The following values are obtained by inspecting the upper and lower (298K) analyses near the threat area;

lower + upper moisture = 105 + 55 = 160 g/Kgx10
lower + upper instability = 50 + 150 = 200 mb
lower + upper relative humidity = 90 + 90 = 180 mb

Apart from the strong upper-level height gradient, the strong wind axis, and the area of differential temperature and moisture advection in the High Level region, the severe weather nomogram helps to depict the potential for tornadic development.

The dashed line in Figure 6.4 represents the values near the threat region. The moisture total of 160 tends to show that either a tornado or heavy rain event is likely, since 90% of the large hail events correspond to an upper and lower moisture total less than 155. The instability total of 200 intersects all three ranges, indicating that the instability near the area can support either event. Finally, the relative humidity total of 180 suggests a

tornado or large hail event as being most likely. The rain threshold range is much lower, indicating that, statistically, the threat environment is too dry to support heavy rain fall. The only severe weather type common to all three criteria was the tornado event.

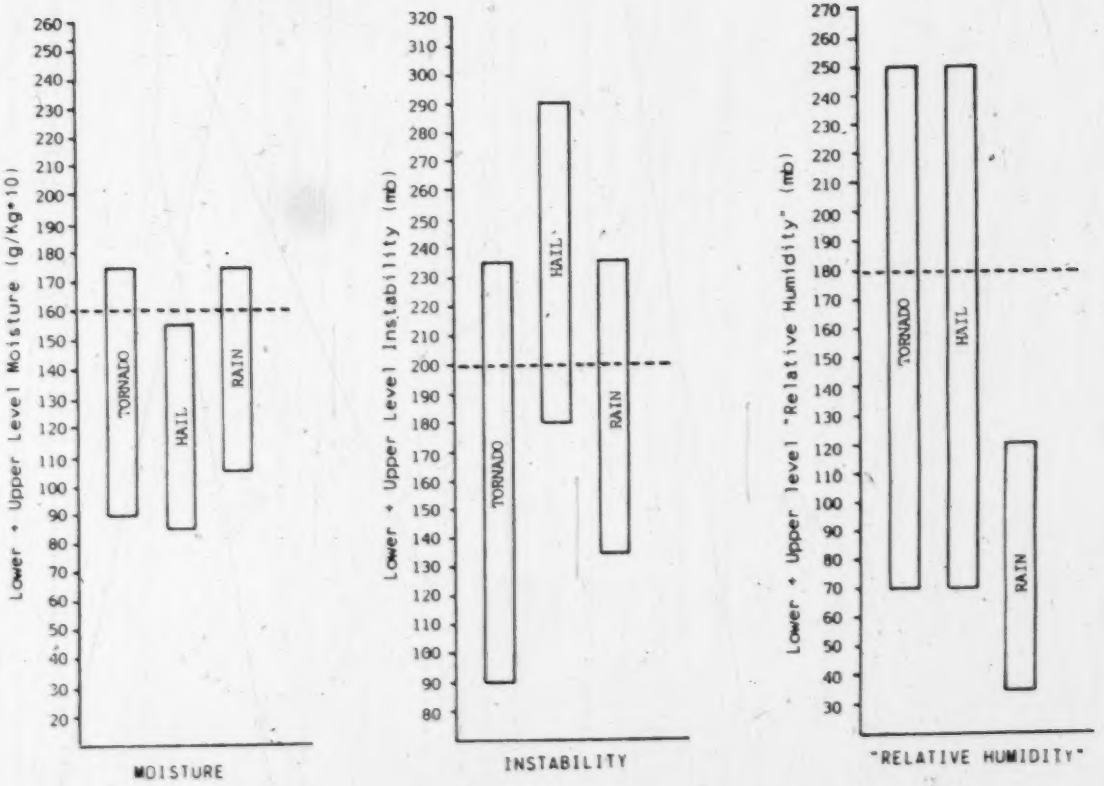

Figure 6.4: As in Figure 6.1. Dashed line represents parameter values depicted at 1200 UTC, 29 August, 1988, in the High Level region.

6.4 Summary

The analysis of isentropic data has shown to be of use for assessing lightning potential and for discriminating between severe weather types.

It was found that nine times out of ten, either differential temperature advection or an isentropic wind axis will have lightning associated with it. Also, about eight out of ten times, lightning was found within an upper instability centre or near a lower-level moisture centre. These parameters are easily analysed on the 1200 UTC isentropic charts which make them useful as a quick check against other convective forecasting guides. However, the operational useability of these "probabilities" is limited. If another data set were available, these values could be tested, and a better evaluation of their efficacy for forecasting lightning could then be made.

The severe weather events (tornado, large hail, heavy rain) of 1988 were all evaluated and found to have different parameter values associated with each. Notably, the instability values corresponding to the large hail events were most often much higher than those associated with the tornado and heavy rain events. Also, a distinct difference between the relative humidity values associated with heavy rain, from either the tornado or large hail events, was

clearly apparent. These differences in "threshold" values help to delineate severe weather types. The three examples considered here illustrate this methodology, by showing how a nomogram can be used to isolated the potential for a particular severe weather type. Large-hail potential was singled out by the existence of abnormally high instability values. A heavy rain fall was "predicted" due to abnormally low values shown on the relative humidity panel. Finally, tornadic potential was found to be high when high values of moisture and "relative humidity" were present along with strong differential advection of temperature and moisture.

The practical value of these methods are not unexpected, as the fields used reveal important atmospheric conditions upon which severe weather types depend. If these methods were implemented operationally, they could be constantly tested against independent data, promising a more accurate assessment of how well they stand up to the rigors of severe weather forecasting.

"Experienced forecasters and analysts, however, who had become familiar with the isentropic chart generally felt, and still feel, that a long step backwards was taken when the isentropic analysis was abandoned."

Oliver, V.J. and M.B. Oliver (1951)

CHAPTER 7

CONCLUSIONS AND FUTURE WORK

7.1 Conclusions

The main objective of this study was to assess the ability of isentropic analysis to diagnose convective weather in Alberta. Case studies and elementary statistical analysis were used to this end.

Ten case studies were chosen to detail ten different convective environments. The following conclusions can be drawn from this sample:

1. a) Environments with weak convective potential are associated with poorly organized parameter maxima. In three cases, the support for weak convection was depicted by the intersection of an instability axis or centre with the upper-level wind maximum.

b) Strong or severe convective potential was indicated when high amplitude, well-defined thermal and moisture axes were present. The threat area was marked out in regions where the upper level temperature and moisture axes were located downstream of the low-level temperature/moisture maxima. The area of severe convective threat was found to be where the isentropic wind maximum intersected the area bounded by well-organized atmospheric parameters. It is in such regions that the strongest differential temperature and moisture advection is taking place, increasing the potential and latent instability already present in the convectively unstable environment.

c) The strength and organization of convection was also found to be related to the moisture concentration on the lower-level surface. Moisture values less than 8.0 g/Kg tended to support only weak convective cells, while environments with greater than 8.0 g/Kg often

experienced more intense, well-organized convective outbreaks, especially if the convection developed near a low-level moisture centre.

Limited by the sample size, these "conclusions" are very broad, only providing general guidelines that help to assess convective potential and affirm the usefulness of these charts. To further these initiatives, a statistical analysis based on three months of isentropic data was carried out. The following results help to quantify the merits of the procedure and increase user confidence in the charts:

2. a) Several isentropic maxima were independently tested to determine how each correlated with lightning occurring up to 18 hours after analysis time. The following parameters had higher than 70% success rates in predicting lightning activity: upper-level instability centres, upper-level height centres, low-level instability centres, low-level height centres, and low-level moisture centres. Also, the upper level wind axis had lightning recorded somewhere along its length over 90% of the time. Finally, differential temperature advection had a 86% probability of predicting the position of lightning strikes. These statistics tend to show that many isentropic

parameters, easily discernable by simple inspection of these charts, can alert the forecaster of convective threat.

b) The potential for either a tornado, large hail, or heavy rain event, was assessed using a nomogram that classifies severe weather types. Three examples were shown to illustrate how isentropic data could distinguish between different severe weather events. A large-hail event was predicted when very high instability values were present in the severe threat area. The potential for a heavy rain event was indicated when relative humidity within the convective environment was abnormally high. Warnings of severe storms with tornadic potential may perhaps be issued more than 15 hours before touchdown in cases with high moisture and low relative humidity within the threat area. These areas of tornado threat also had tight isobar gradients, strong differential temperature and moisture advection, and strong wind axes associated with them.

These supplementary conclusions (2b) are least significant in terms of statistical value since only a very small, non-independent sample was used as a test reference. However, these may be potentially the most important results, since minimal research has been done and little

success has been achieved at forecasting severe weather types in the past. It would be remarkable for a single analysis to reveal not only the severe convective threat area, but also estimate the type of severe weather that may be expected from severe storms six to 18 hours before convective onset. Isentropic analysis has shown encouraging results in this regard.

In the following section, suggestions are made that would extend the work done. It is hoped that these suggestions, in conjunction with this work, will lead to the operational implementation of isentropic analysis at Canadian Weather Centres.

7.2 Future Work

The following list outlines key areas where further investigations would be worthwhile:

1. a) Obtain more severe weather data for input into the nomogram statistics. This would increase confidence limits in the parameter ranges associated with each severe weather type.
   b) Test the nomogram against an independent data set to improve and confirm the procedure's ability to diagnose severe weather types.

2. Use the isentropic convective forecasting techniques outlined in the case studies on a daily basis. This may be difficult, because of the time constraints placed on the operational forecasters. However, when the procedures discussed here were developed, particular attention was paid to the analysis time required. The analysis of the charts and drawing of the composite chart can be done within five minutes. A compromise may be made by consulting the analysis only on days in which severe weather is likely.

3. Evaluate the "false alarm" ratio. How often does convection, particularly severe convection, not occur when severe weather threat is forecast using these techniques?

4. Use non-linear regression methods to obtain the "best" model for convective threat diagnosis. A very large sample would be needed to determine the "significance" of each "predictor." A predictand, possibly lightning intensity or hail size, would then depend only on the "significant" isentropic parameters.

5. Conditional probabilities using several parameters may be useful to indicate the potential for convective weather. For example, if parameter A intersected with parameter D and F, what would be the probability of lightning near this intersection.

6. Use isentropic data to estimate maximum precipitation potential. Develop a "precipitation" nomogram relating moisture and relative humidity values to maximum precipitation amounts.

7. Exploit the ability of isentropic analysis to diagnose weaker condensation procesess, such as fog or persistent low-level stratus.

8. Test the merits of isentropic analysis in other parts of the country. It may be found that similar procedures can be used to diagnose pre-convective threat areas, but threshold values may be different because of climatic and topographical variations.

9. Determine the utility of isentropic charts for diagnosing winter weather. It seems reasonable that heavy snowfall threat could be assessed using a similar analysis procedure, since instability and moisture drive strong winter convection as well.

7.3 Final Remarks

It was not the purpose of this study to suggest that isentropic charts and techniques are superior to the conventional isobaric analyses currently used to forecast convective weather. Rather, they should be considered as a useful supplement to the current convective forecasting methods, since they seem particularly well suited to aid in the pre-convective diagnosis of environments with severe weather potential. No single analysis chart or coordinate system is able to depict the atmosphere perfectly, but isentropic analysis helps to enlighten the intricacies of the atmosphere from a different perspective.

It is hoped that the work presented here will stimulate further research, and lead to a resurgence of isentropic analysis, once considered a tremendous asset to weather forecasters.

BIBLIOGRAPHY

Berry, F.A., E. Bollay and N.R. Byers, 1945: *Handbook of Meteorology*. New York, McGraw-Hill, 848-857.

Bleck, R., 1973: Numerical Forecasting Experiments Based on the Conservation of Potential Vorticity on Isentropic Surfaces. *J. Appl. Meteor.*, Vol. 12, 737-752.

Bleck, R., 1974: Short Range Prediction in Isentropic Coordinates with Filtered and Unfiltered Numerical Models. *Mon. Wea. Rev.*, Vol. 102, 813-829.

Bluestein, H.B., E.W. McCaul, Jr., G.P. Byrd and G.R. Woodall, 1988: Mobile Sounding Observations of a Tornadic Storm Near the Dryline: The Canadian, Texas Storm of 7 May 1986. *Mon. Wea. Rev.*, Vol. 116, 1790-1804.

Byers, H.R., 1938: On the Thermodynamic Interpretation of Isentropic Charts. *Mon. Wea. Rev.*, Vol. 66, 63-68.

Cahir J.J., J.M. Norman, W.D. Lottes and J.A. Toth, 1976: New Tools for Forecasters: Real-time Cross Sections Produced in the Field. *Bull. Amer. Meteor. Soc.*, Vol. 57, 1426-1433.

Carlson, T.N., 1980: Airflow Through Midlatitude Cyclones and the Comma Cloud Pattern. *Mon. Wea. Rev.*, Vol. 108, 1498-1509.

Carlson, T.N., H.A. Anthes, M. Schwartz, S.G. Benjamin, and D.G. Baldwin, 1980: Analysis and Prediction of Severe Storms Environment. *Bull. Amer. Meteor. Soc.*, Vol. 61. 1018-1032.

Carlson, T.N. and F.H. Ludlam, 1968: Conditions for the Occurrence of Severe Local Storms. *Tellus*, Vol. 20, 203-226.

Danielsen, E.F., 1961: Trajectories: Isobaric, Isentropic and Actual. *J. Meteor.*, Vol. 18, 479-496.

Doswell, C.A., 1986: Short-Range Forecasting. Mesoscale Meteorology and Forecasting, Edited by P.S. Ray, *Amer. Meteor. Soc.*, Boston, 1986.

Emanuel, K.A., 1988: Observational Evidence of Slantwise Convective Adjustment. *Mon. Wea. Rev.*, Vol. 116, 1805-1816.

Environment Canada, 1982: *Summer Severe Weather Correspondence Course*, AES, Training Branch, Downsview, Ontario.

Epstein, E.S., 1988: Long-Range Weather Prediction: Limits of Predictability and Beyond. *Wea. and Forecasting*, Vol. 3, 69-75.

Fuelberg, H.E. and G.J. Jedlovec, 1982: A Subsynoptic-Scale Kinetic Energy Analysis of the Red River Valley Tornado Outbreak (AVE-SESAME 1), *Mon. Wea. Rev.*, Vol. 12, 2005-2024.

Goodson, R., 1984: *Precipitation Measurements from Satellites*. M.Sc. Thesis, University of Alberta, 1984.

Green, J.S.A., F.H. Ludlam and J.F.R. McIlveen, 1966: Isentropic Relative-Flow Analysis and the Parcel Theory. *Quart. J. Roy. Meteor. Soc.*, Vol. 92, 210-219.

Hoskins, B.J. and I. Draghici, 1977: The Forcing of Ageostrophic Motion According to the Semi-Geostrophic Equations in an Isentropic Coordinate Model. *J. Atmos. Sci.*, Vol. 34, 1859-1867.

Hoskins, B.J., M.E. McIntyre and A.W. Robertson, 1985: On the Use and Significance of Isentropic Potential Vorticity Maps. *Quart. J. Roy. Met. Soc.*, Vol. 3, 877-946.

Hoskins, B.J., I. Draghici and H.C. Davies, 1978: A New Look at the Omega-Equation. *Quart. J. Roy. Meteor. Soc.*, Vol. 104, 31-38.

Iskenderian, H., 1987: Three-Dimensional Airflow and Precipitation Structure in a Nondeepening Cyclone. *Weather and Forecasting*, Vol. 3, 18-32.

McGinley, J., 1986: Nowcasting Mesoscale Phenomena. Mesoscale Meteorology and Forecasting, Edited by P.S. Ray, *Amer. Meteor. Soc.*, Boston, 1986.

Miller, R.C., 1972: Notes on Analysis of Severe Storm Forecasting Procedures of the Air Force Global Weather Central, Air Weather Service Tech. Report 200 (Rev), 102 pp.

Montgomery, R.B., 1937: A Suggested Method for Representing Gradient Flow in Isentropic Surfaces. *Bull. Amer. Meteor. Soc.*, Vol. 18, 210-212.

Moore, J.T., 1985: A Diagnostic, Isentropic Analysis Package for the Short Term Prediction of Severe Convective Threat Areas. *Preprints Fourteenth Conf. on Severe Local Storms*, Saint Louis University, St. Louis, Missouri, Amer. Meteor. Soc., 127-130.

Moore, J.T. and A.Y. Moran, 1984: Mesoscale Analysis of Surface Variables and Stability during the AVE-SESAME 2 Period. Preprints Tenth Conf. Weather Forecasting and Analysis, Clearwater, Flo, *Amer. Meteor. Soc.*, 500-505.

Namias, J., 1939: The Use of Isentropic Analysis in Short Range Forecasting. *J. Aeronaut. Soc.*, Vol. 5, 295-298.

Namias, J., 1940: An Introduction to the Study of Air Mass and Isentropic Analysis. *Amer. Meteor. Soc.*, Milton, Mass., 141 pp.

Neamtan, S.M., 1944: Pressure Tendencies and Stability Changes in an Isentropic Surface. *Bull. Amer. Meteor. Soc.*, Vol. 25, 127-136.

Oliver, V.J. and M.B. Oliver, 1951: Isentropic Analysis. Compendium of Meteorology, *Amer. Meteor. Soc.*, Boston, Mass., 715-727.

Pauley, R.L. and J.T. Snow, 1988: Speculations on the Kinematics and Dynamics of the 18 July 1986 Minneapolis Tornado. *Preprints Fifteenth Conf. on Severe Local Storms*, 456-459.

Pearson, G.M. and S.R. Blackwell, 1987: Airstream Diagnosis of a Synoptic System. *Second Workshop on Operational Meteorology*, Halifax, N.S., 133-141.

Petersen, R.A. and J.H. Homan, 1989: Short-Range Forecasting and Nowcasting Using a Simple, Isentropic Prediction Model. *Wea. and Forecasting*, Vol. 4, No. 1, 5-23.

Petersen, R.A. and L.W. Uccellini, 1979: The Computation of Isentropic Atmospheric Trajectories Using a Discrete Model Formulation. *Mon. Wea. Rev.*, Vol. 107, 566-574.

Pettenssen, S., 1956: *Weather Analysis and Forecasting*. 2nd ed., Vol. 1. New York, McGraw-Hill, 320-339.

Reap, R.M., 1972: An Operational Three-Dimensional Trajectory Model. *J.Appl. Meteor.*, Vol. 11, 1193-1202.

Rockwood, A.A. and R.A. Maddox, 1988: Mesoscale and Synoptic Scale Interactions Leading to Intense Convection: The Case of 7 June 1982. *Weather and Forecasting*, Vol. 3, 51-68.

Rossby, C.G., 1937a: Isentropic Analysis. *Bull. Amer. Meteor. Soc.*, Vol. 18, 201-209.

Rotunno, R., 1986: Tornadoes and Tornadogenesis. Mesoscale Meteorology and Forecasting, Edited by P.S. Ray, *Amer. Meteor. Soc.*, Boston, 1986.

Schaaf, C.B., J. Wurman and R.M. Banta, 1988: Thunderstorm-Producing Terrain Features. *Bull. Amer. Meteor. Soc.*, Vol. 69, 272-276.

Shaw, Sir N., 1933: *Manual of Meteorology*, Vol. 3, *The Physical Processes of Weather*. Cambridge University Press, 259-266.

Spar, J., 1943: The Correlation Between Specific Humidity and Potential Vorticity in the Atmosphere. *Bull. Amer. Meteor. Soc.*, Vol. 24, 196-200.

Spilhaus, A.F., 1940: The Shear-Stability Ratio Vector and its use in Isentropic Analysis. *Bull. Amer. Meteor. Soc.*, Vol. 21, 239-248.

Starr, V.P., 1940: The Construction of Isentropic Relative Motion Charts. *Bull. Amer. Meteor. Soc.*, Vol. 21, 236-239.

Strong, G.S., 1986: *Synoptic to Mesoscale Dynamics of Severe Thunderstorm Environments: A Diagnostic Study with Forecasting Applications.* Ph.D. Thesis, University of Alberta, 1986.

Trevisan, A., L. Ferranti and P. Malguzzi, 1988: Further Developments of Normal Mode Theory of Lee Cyclogenesis: Isentropic Coordinate Model. *J. Atmos. Sci.*, Vol.45, No.24, 3880-3888.

Wallace, A., 1987: Tracks of the Edmonton Tornado, 31 July 1987, Preliminary Report. *Western Region Technical Note*, Atmospheric Environment Service, Canada, 11 pp.

Weisman, M.L. and J.B. Klemp, 1986: Characteristics of Isolated Convective Storms. Mesoscale Meteorology and Forecasting, Edited by P.S. Ray, *Amer. Meteor. Soc.*, Boston, 1986.

Wilson, L.J., 1981: *Isentropic Analysis - Operational Applications and Interpretation.* Unpublished Training Manual, Atmospheric Environment Service, Downsview, Ont., Feb. 1981.

Wilson, L.J., S. Siok and B. Marois, 1980: Operational Application of Isentropic Analysis to the Diagnosis of Severe Convective Weather Threat Areas. *Preprints Eighth Conf. Weather Forecasting and Analysis*, Denver, Amer. Meteor. Soc., 166-173.

Wyss, J. and K.A. Emanuel, 1988: The Pre-Storm Environment of Midlatitude Prefrontal Squall Lines. *Mon. Wea. Rev.*, Vol. 116, 790-794.

Zwack, P. and M. Kabil, 1988: Estimating Lower Tropospheric Vertical Motion from Surface Pressure and Pressure Tendency Data Alone. *Mon. Wea. Rev.*, Vol. 116, 795-803.

APPENDIX A

Equations of Motion in Isentropic Coordinates

For the sake of ready reference, a brief review of the fundamental equations of motion in isentropic coordinates is in order. A comparison with the equations expressed in isobaric coordinates will reveal significant differences between the two. Set A shows each of the isentropic relations which can be compared to the isobaric form in Set B.

SET A - Isentropic Relations

$$M = c_p T + gz$$ The Montgomery Streamfunction

$$\frac{\partial u}{\partial t} + u\frac{\partial u}{\partial x} + v\frac{\partial u}{\partial y} - fv + \frac{\partial M}{\partial x} = 0$$

$$\frac{\partial v}{\partial t} + u\frac{\partial v}{\partial x} + v\frac{\partial v}{\partial y} + fu + \frac{\partial M}{\partial y} = 0$$ Horizontal Momentum

$$\left(\frac{\partial}{\partial t} + \bar{V}_H \cdot \nabla\right)\frac{\partial p}{\partial \theta} + \frac{\partial p}{\partial \theta}\left(\nabla_\theta \cdot \bar{V}\right) = 0$$ Continuity

$$\frac{dQ}{dt} = c_p \frac{d \ln \theta}{dt}$$ Hydrostatic

$$\frac{\partial M}{\partial \theta} = \frac{c_p T}{\theta} + g\frac{\partial z}{\partial \theta}$$ Thermodynamic Energy

SET B - Isobaric Relations

$$\frac{\partial u}{\partial t} + u\frac{\partial u}{\partial x} + v\frac{\partial u}{\partial y} + \omega\frac{\partial u}{\partial p} - fv + \frac{\partial \phi}{\partial x} = 0$$

$$\frac{\partial v}{\partial t} + u\frac{\partial v}{\partial x} + v\frac{\partial v}{\partial y} + \omega\frac{\partial v}{\partial p} + fu + \frac{\partial \phi}{\partial y} = 0$$

Horizontal Momentum

$$\frac{\partial \omega}{\partial p} + \nabla_p \cdot \bar{V} = 0$$

Continuity

$$\frac{\partial \phi}{\partial p} = -\frac{1}{\rho}$$

Hydrostatic

$$\frac{dQ}{dt} = \frac{c_p}{T}\frac{dT}{dt} - \frac{R}{p}\omega$$

Thermodynamic Energy

At first glance, it may seem as though only the momentum and energy equations are simpler in isentropic coordinate form. However, closer examination reveals that all of the isentropic relations describe the basic atmospheric processes in a simple and convenient form.

The Montgomery Streamfunction is a measure of the thermal and geopotential energy of the atmosphere, quantities which are related through the hydrostatic relation. A contour analysis of the Montgomery function depicts the wind field on an isentropic surface. These "streamlines" are analagous to the geopotential height contours on a constant pressure surface, in that the isentropic wind speed is also inversely proportional to the spacing of the Montgomery contours.

It should be noted that the vertical advection terms are not given explicitly in the isentropic form of the momentum equations. All adiabatic advection, thermal advection and vertical motion is implicity accounted for through the Montgomery function, M. Isentropic surfaces depict the three-dimensional, adiabatic transport of air parcels as long as diabatic effects can be ignored.

The continuity equation appears mathematically complex in isentropic coordinates. However, by rearranging the equation, the atmospheric stability budget is clearly revealed. The equation can be written in the following form;

$$\frac{\partial\left(\frac{\partial p}{\partial \theta}\right)}{\partial t} = - \bar{V}_H \cdot \nabla \left(\frac{\partial p}{\partial \theta}\right) - \nabla_H \bar{V} \left(\frac{\partial p}{\partial \theta}\right)$$

The term on the left hand side indicates the local rate of change of stability, since the stability is defined as the change of pressure with potential temperature, dp/d0. The first term on the right-hand side of the equation denotes the advection of stability. The last term expresses the change of stability generated by the streaching or shrinking of isentropes in the vertical. The local change of stability, is thus due to the advection of stability by the mean flow, and the production of stability by divergence or convergence within an isentropic layer.

In a hydrostatic atmosphere, the distribution of Montgomery potential with respect to potential-temperature is determined by the ratio of temperature over potential-temperature, and how potential-temperature changes with height.

The thermodynamic energy equation is much simpler in isentropic coordinates. It states that diabatic heat exchanges cause isentropic surfaces to propagate through the

atmosphere. For example, adding heat (+ dQ/dt) to a parcel will increase its potential-temperature (+ $d\ln\theta/dt$) and thus force its isentropic surface to dip towards lower potential-temperature values.

This has been a quick treatment of the equations of motion. It is beyond the scope of this text to derive these relations but it is necessary to provide the reader with at least a glance at the origin of the isentropic coordinate system.

APPENDIX B

Isobaric and Surface Analysis Charts

In the following figures, 00 Hour (morning) isobaric and surface analyses corresponding to each of the case studies in Chapter 5 are given (except for 29 August, 1988, as it was not available). Produced by the Canadian Meteorological Centre (CMC), these charts provide the opportunity to compare the isentropic charts to the standard isobaric analyses.

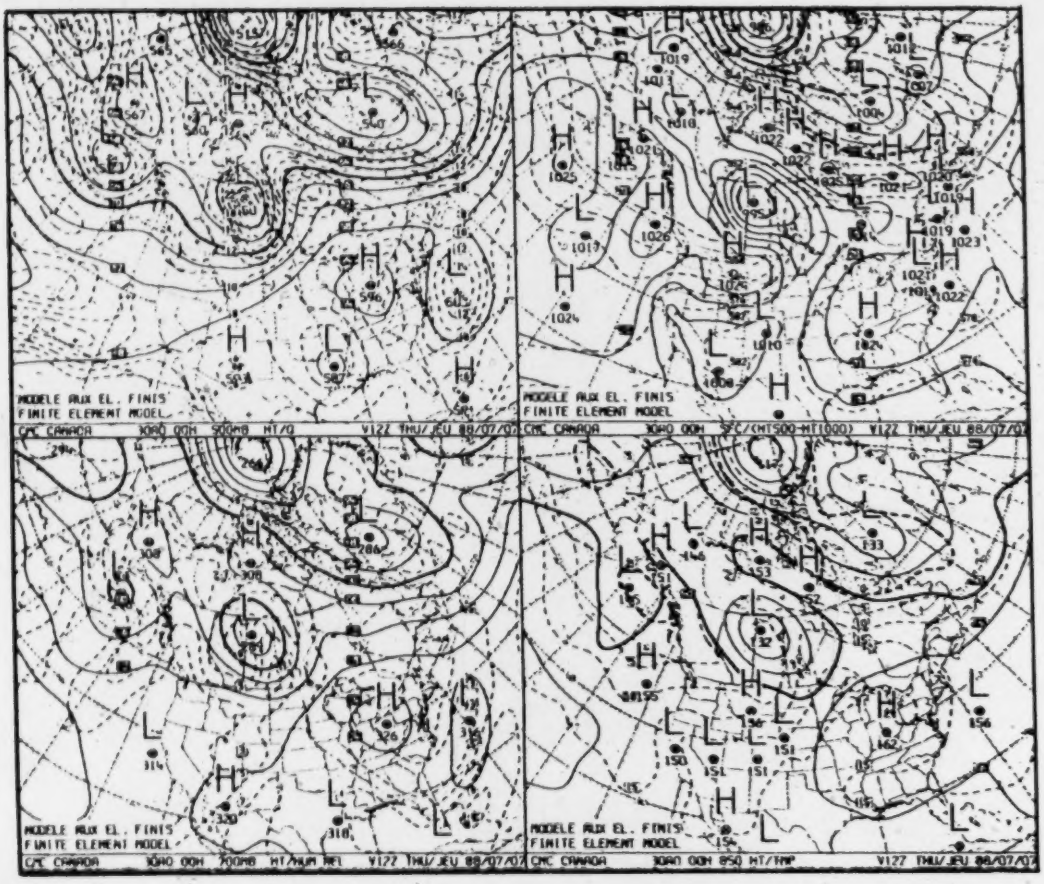

Figure B1: CMC 00 hour analysis (Finite Element Model) of surface, 850mb, 700mb, and 500mb data for 1200 UTC, 07 July, 1988.

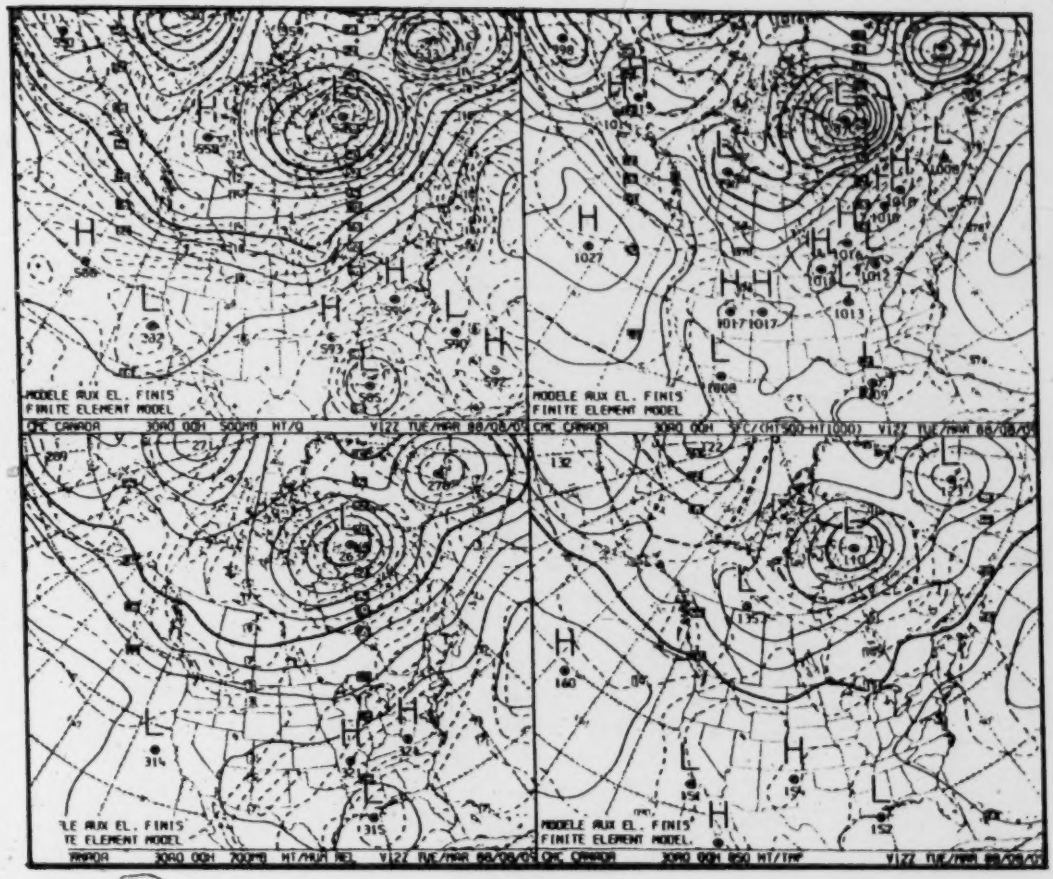

Figure B2: As in Figure B1 except for 09 August, 1988.

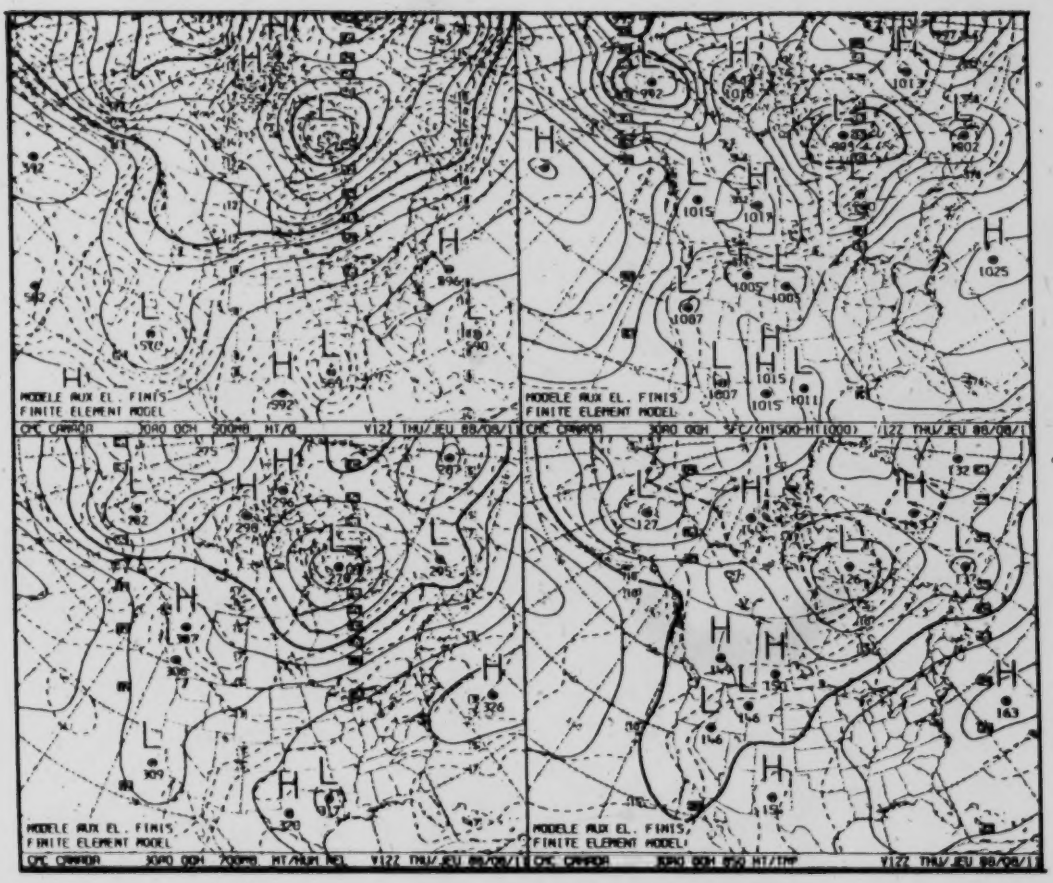

Figure B3: As in Figure B1 except for 11 August, 1988.

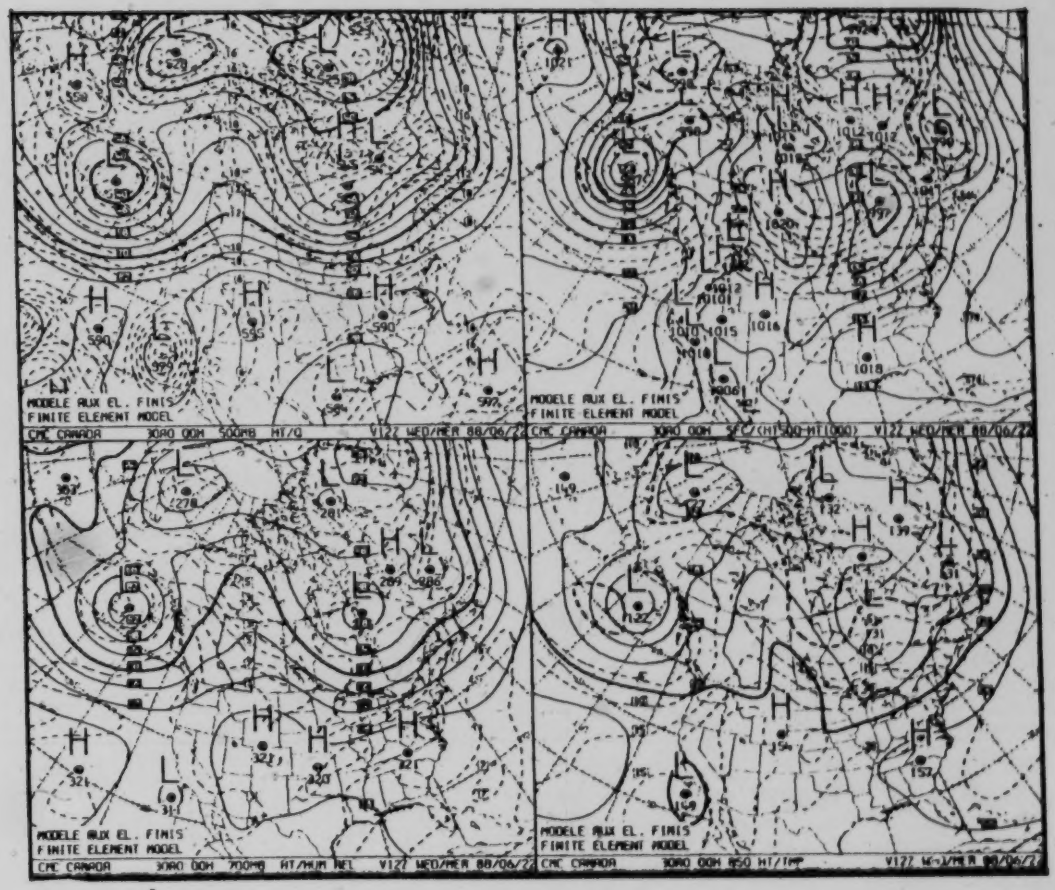

Figure B4: As in Figure B1 except for 22 June, 1988.

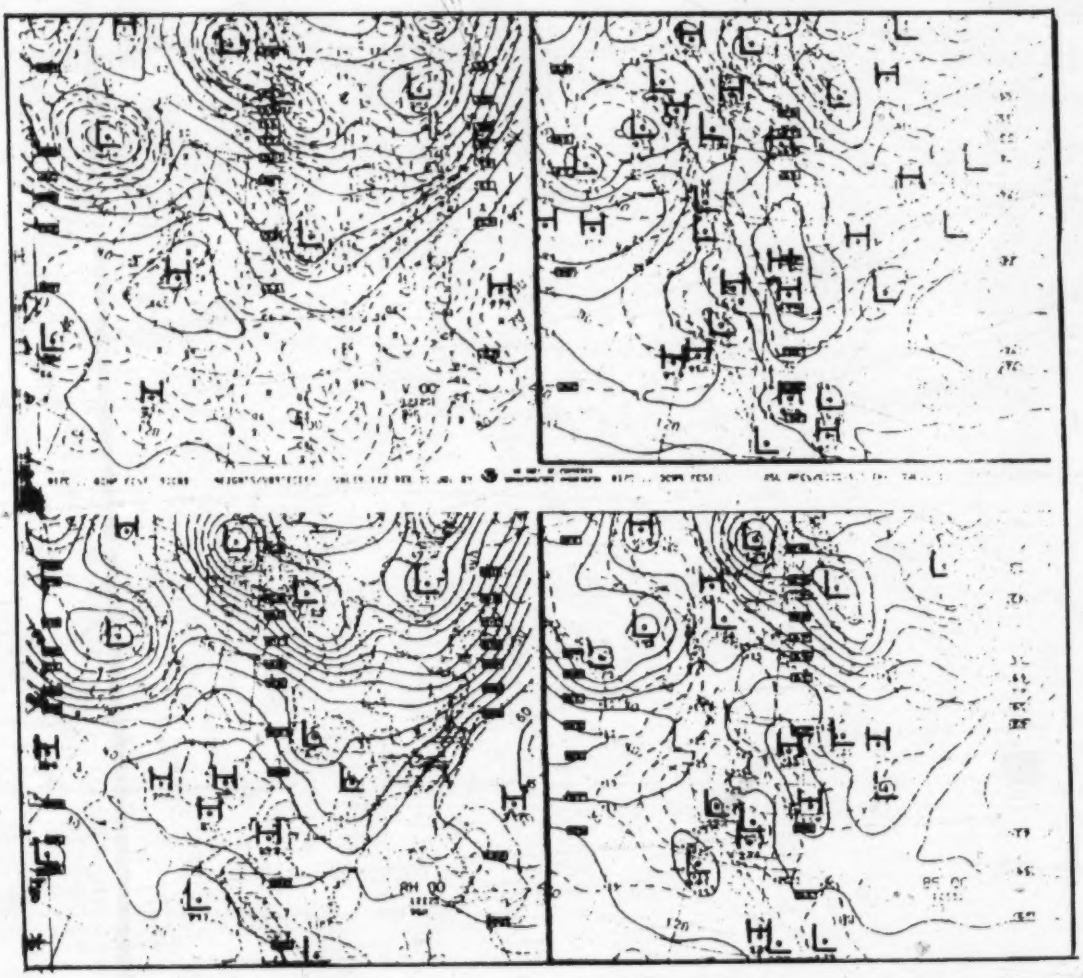

Figure B5: Limited Fine Mesh (LFM) 00 hour objective analysis for 1200 UTC, 20 July, 1988.

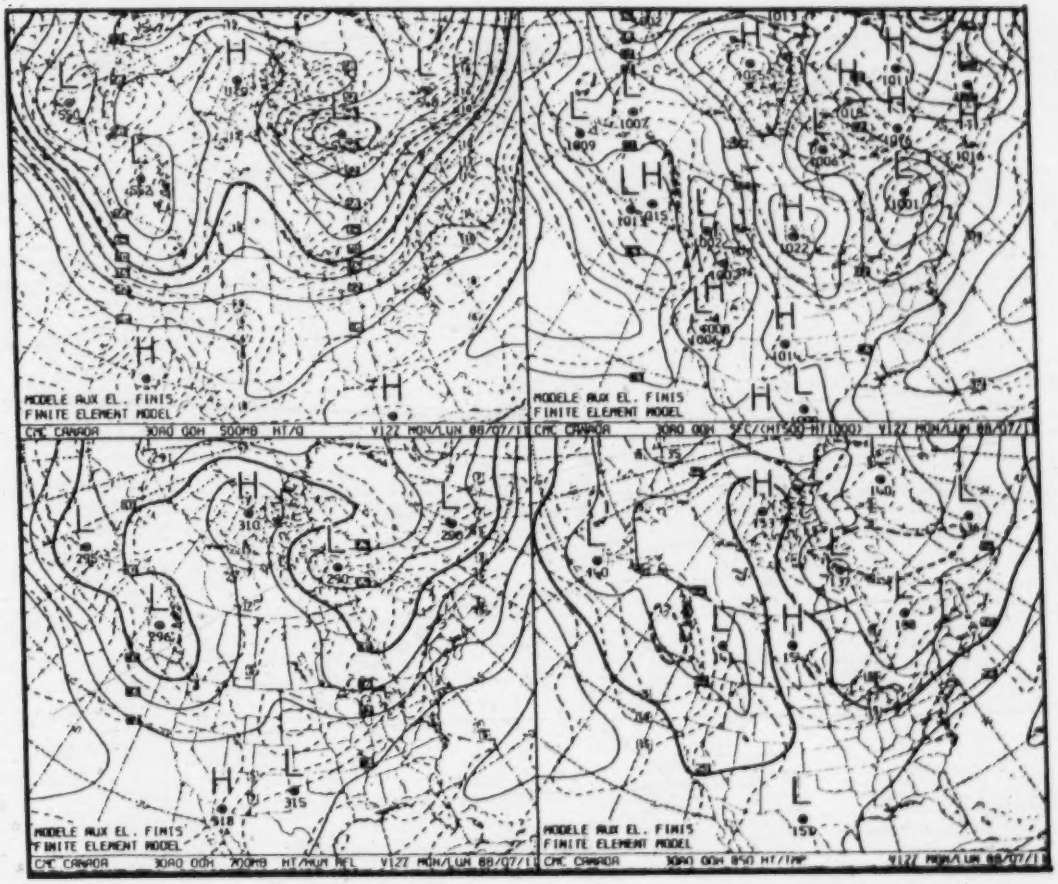

Figure B6: As in Figure B1 except for 11 July, 1988.

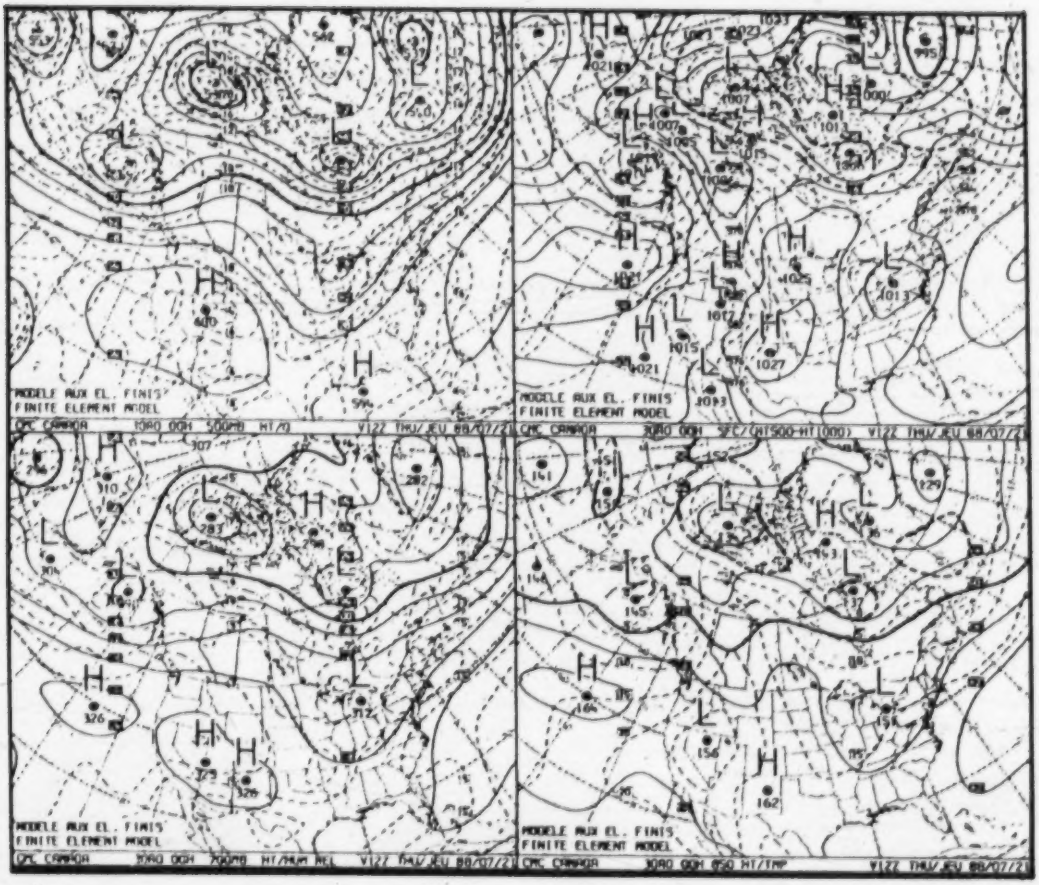

Figure B7: As in Figure B1 except for 21 July, 1988.

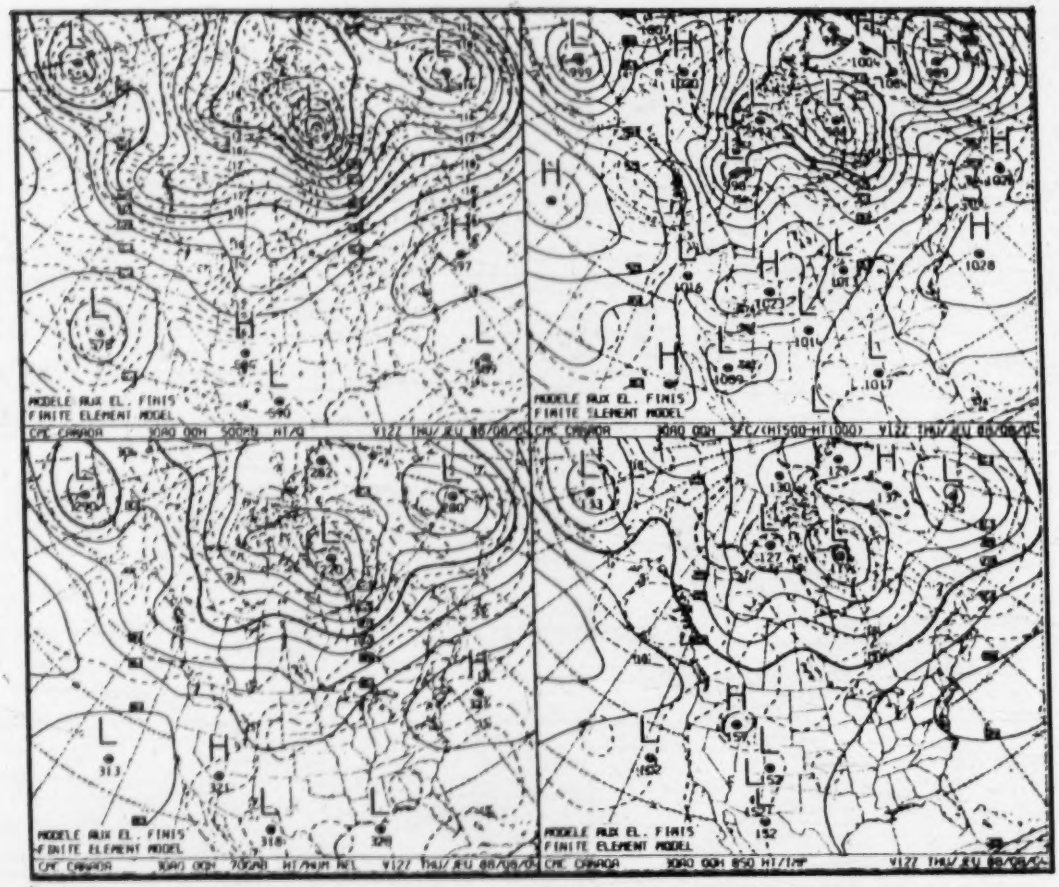

Figure B8: As in Figure B1 except for 04 August, 1988.

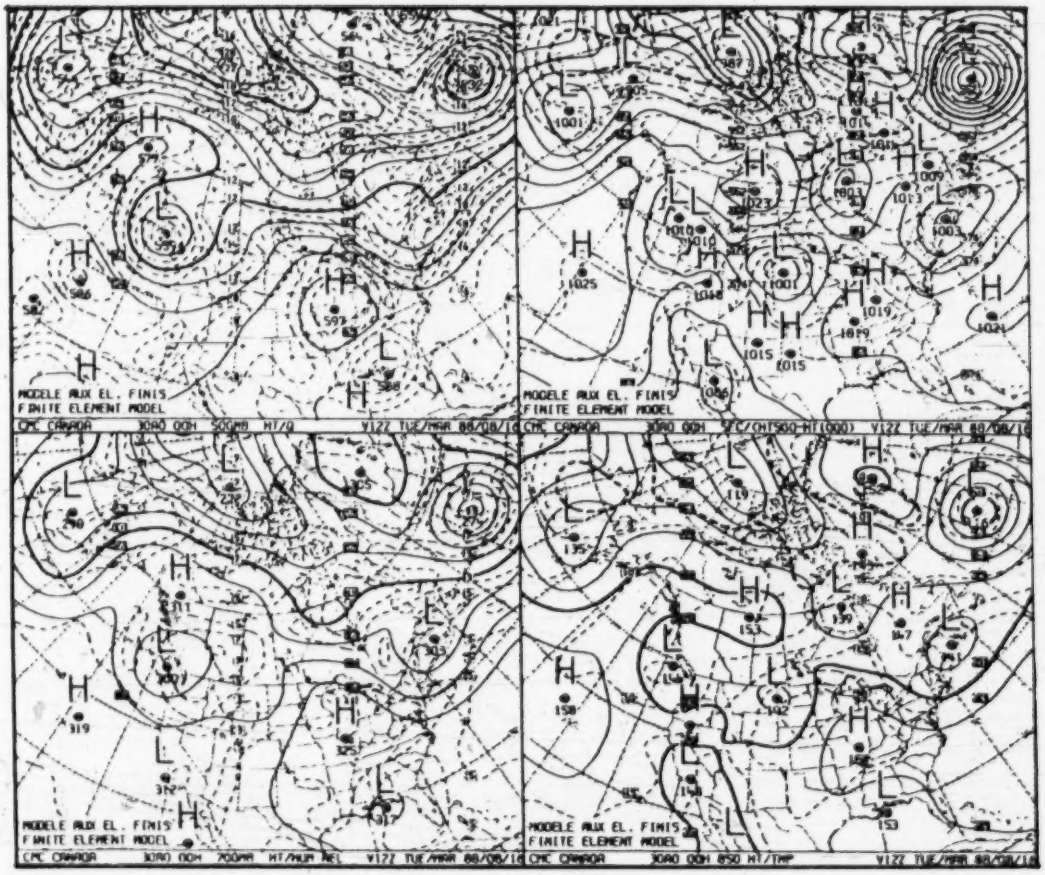

Figure B9: As in Figure B1 except for 16 August, 1988.

APPENDIX C

Cross-section Plots

Selected vertical cross-sections are illustrated. Produced at the Arctic Weather Centre (ARWC), they provide further insight into the vertical structure of the atmosphere. Only a few plots are given as many were unavailable.

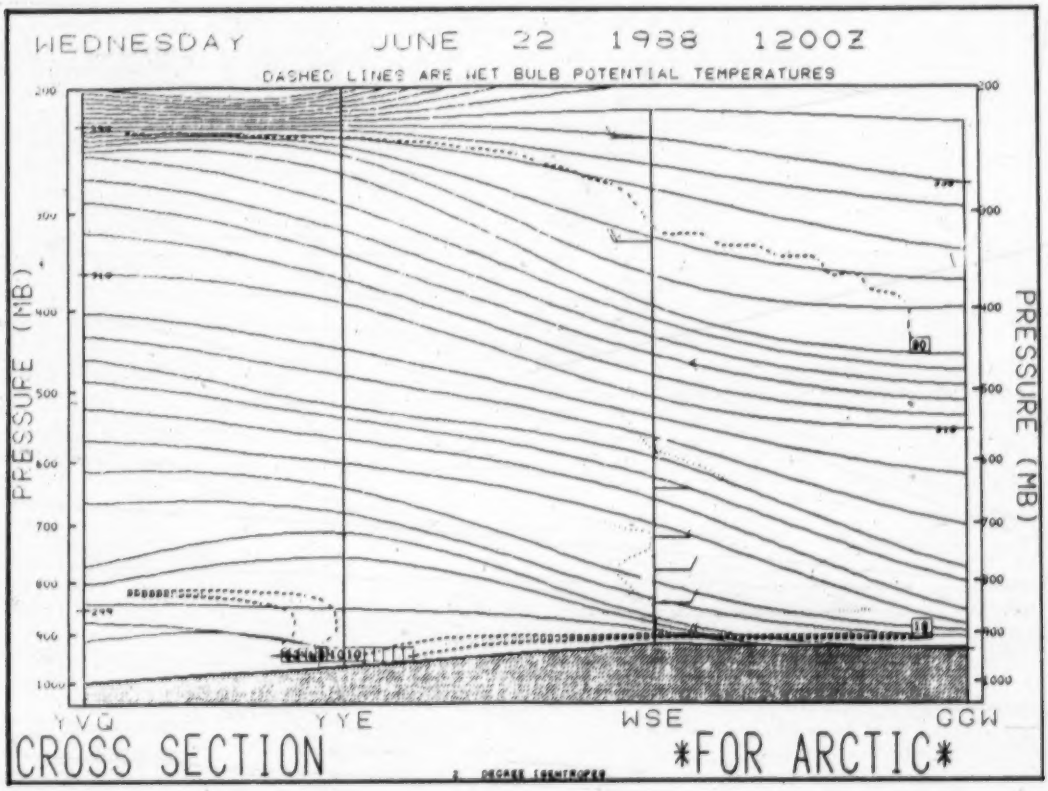

Figure C1: As in Figure 2.5 except for 22 June, 1988. (Corresponds to line drawn on Figure 5.13)

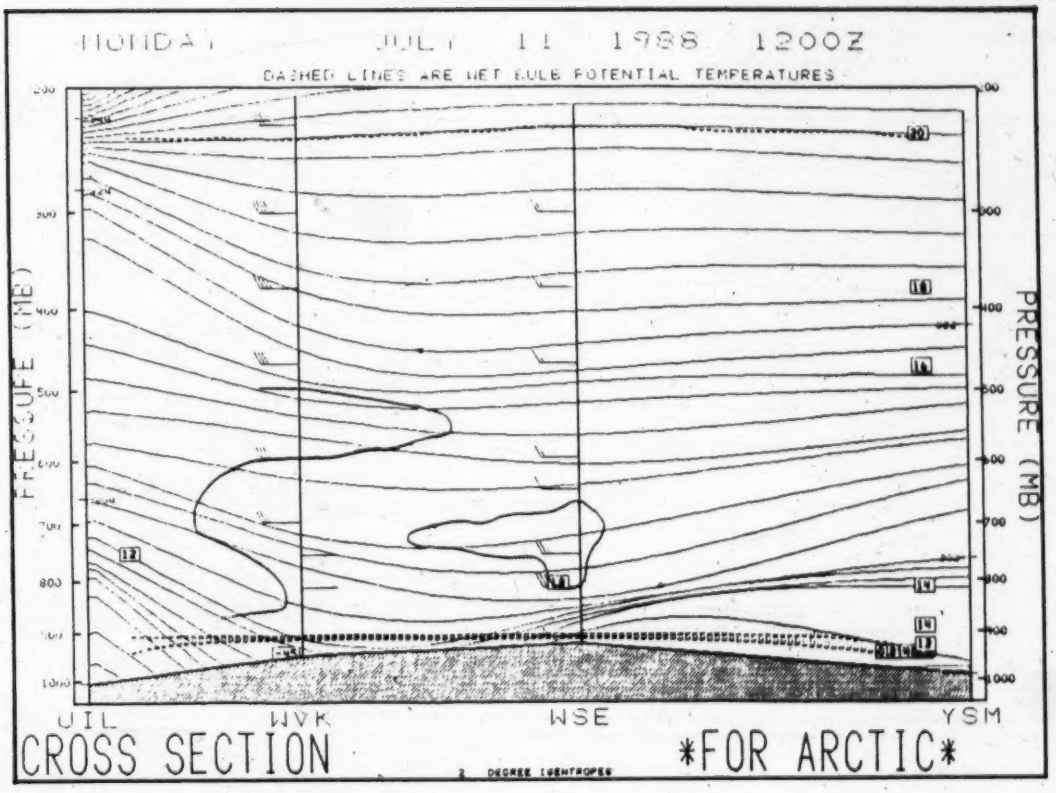

Figure C2: As in Figure 2.5 except for 11 July, 1988.
(Corresponds to line drawn on Figure 5.21)

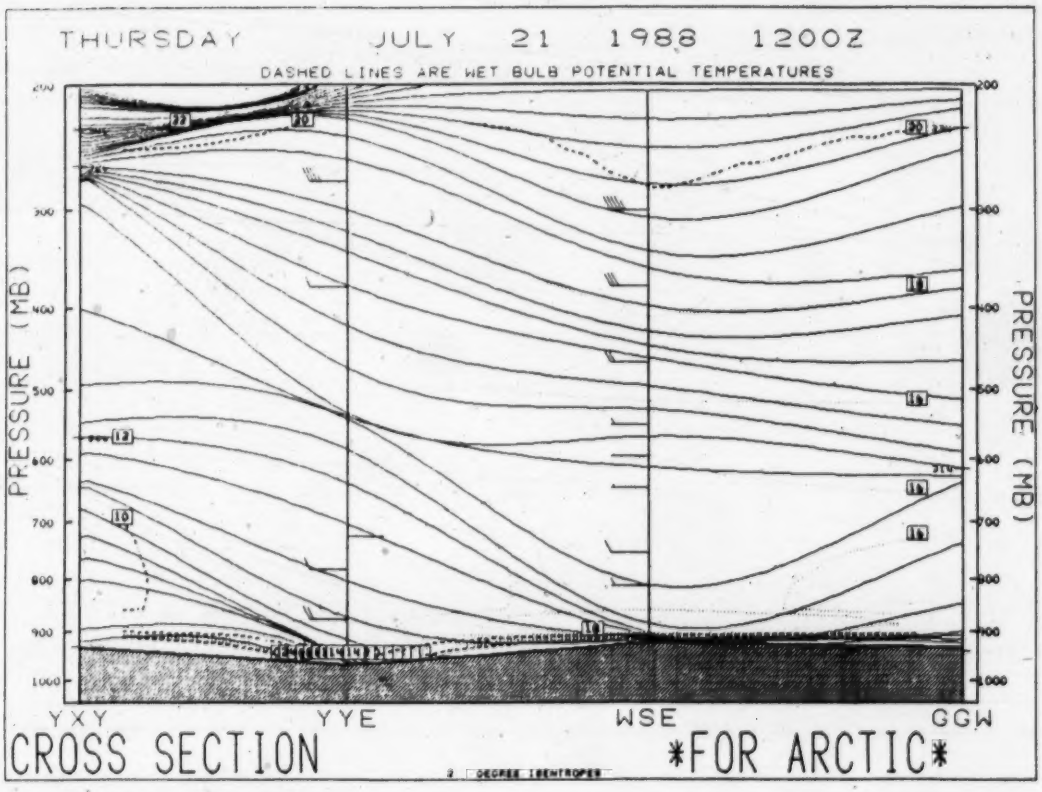

Figure C3: As in Figure 2.5 except for 21 July, 1988.
(Corresponds to line drawn on Figure 5.26)

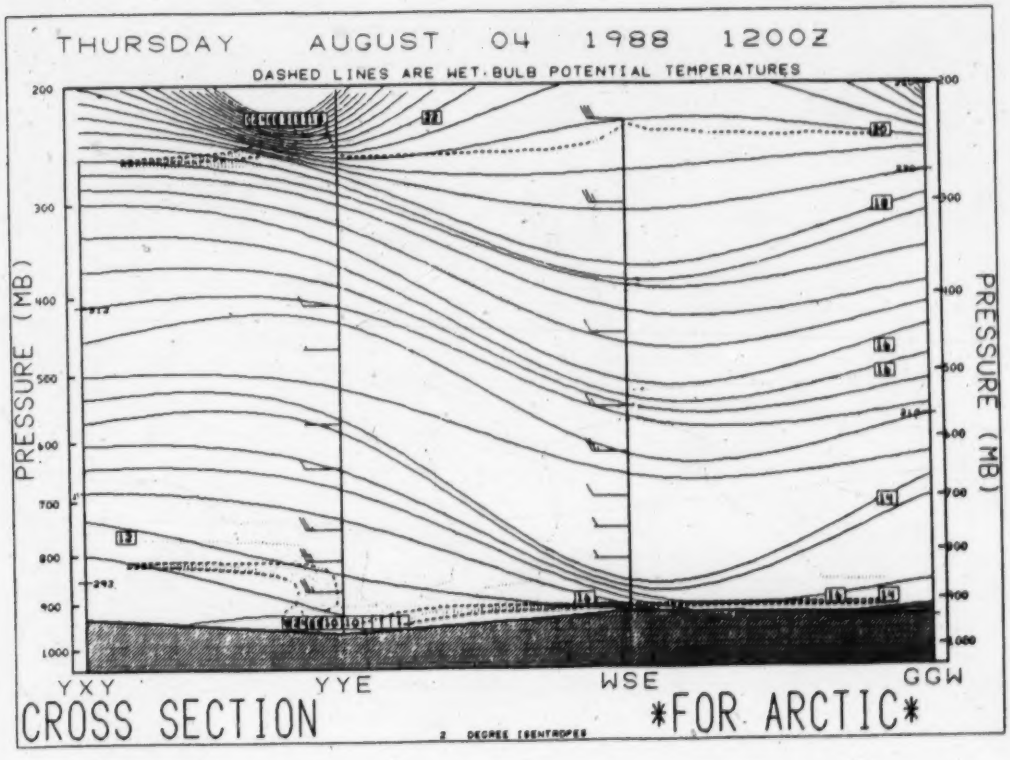

Figure C4: As in Figure 2.5 except for 04 August, 1988.
(Corresponds to line drawn on Figure 5.32)

APPENDIX D

Alberta Forecast Regions

Figure D1: The Alberta forecast regions.